



Tomografia por Micro-ondas

Imagens através de Micro-ondas de campo próximo

2012 – 2022

Uma História com mais de 10 anos de pesquisas...

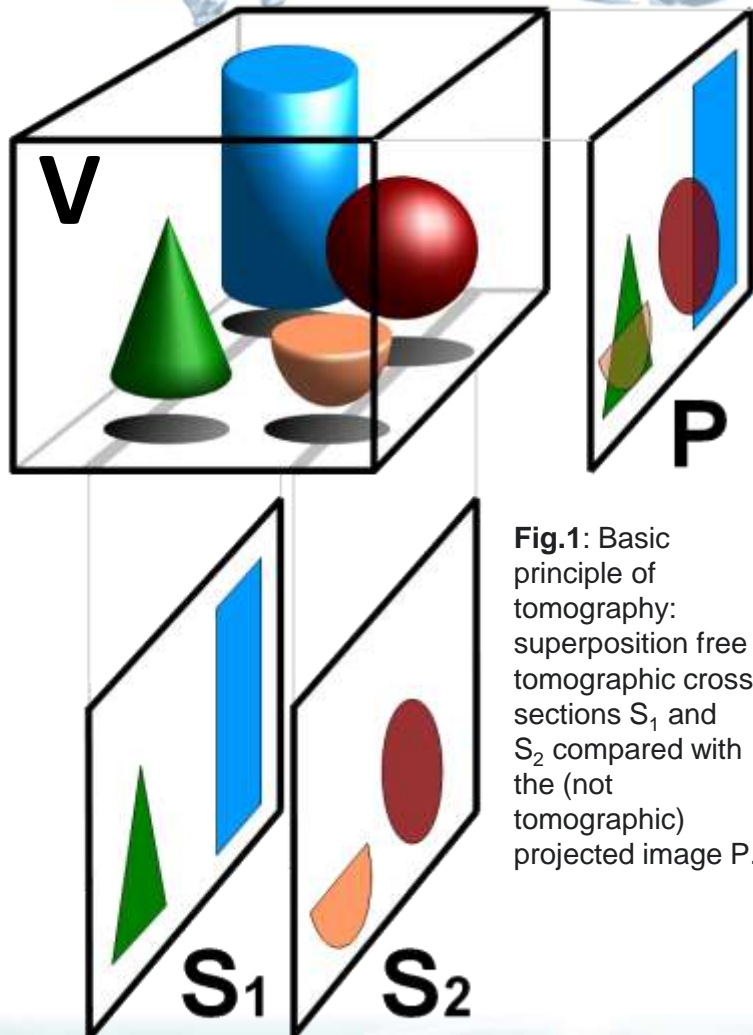
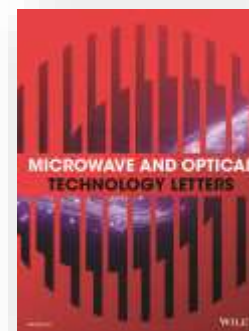
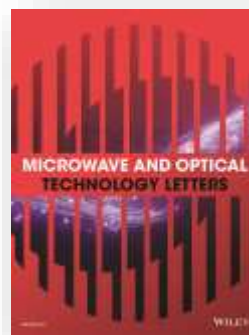


Fig.1: Basic principle of tomography: superposition free tomographic cross sections S_1 and S_2 compared with the (not tomographic) projected image P.

https://en.wikipedia.org/wiki/File:TomographyPrinciple_Illustration.png





Tomografia por Micro-ondas

Imagens através de Micro-ondas de campo próximo

https://en.wikipedia.org/wiki/File:TomographyPrinciple_Illustration.png

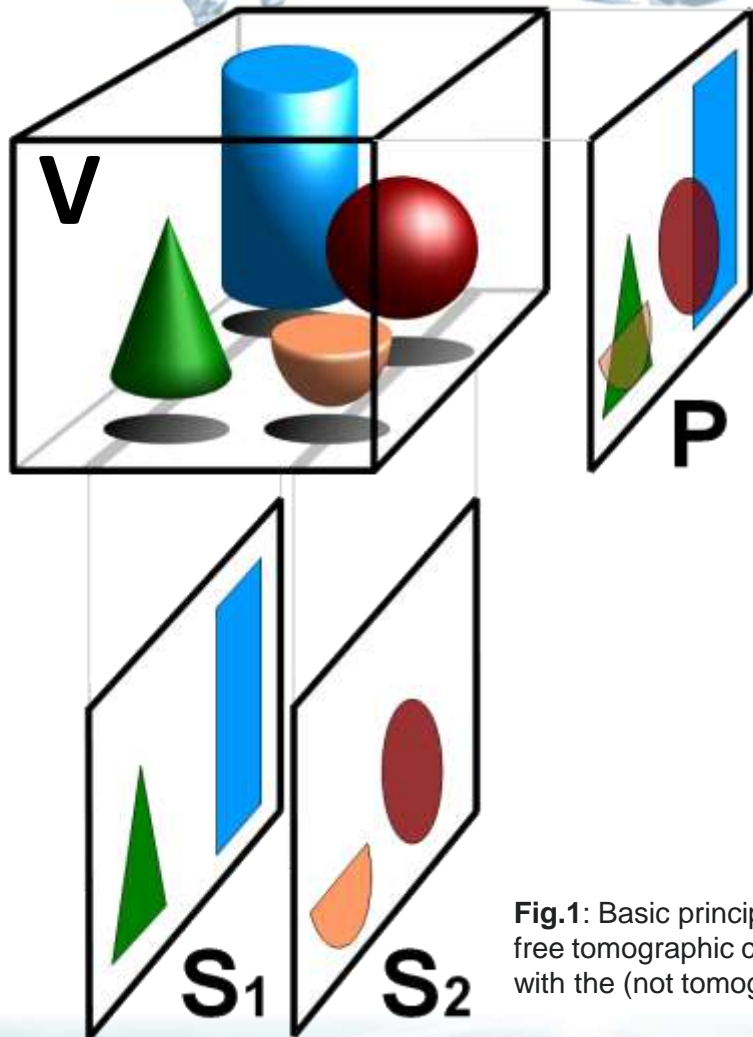
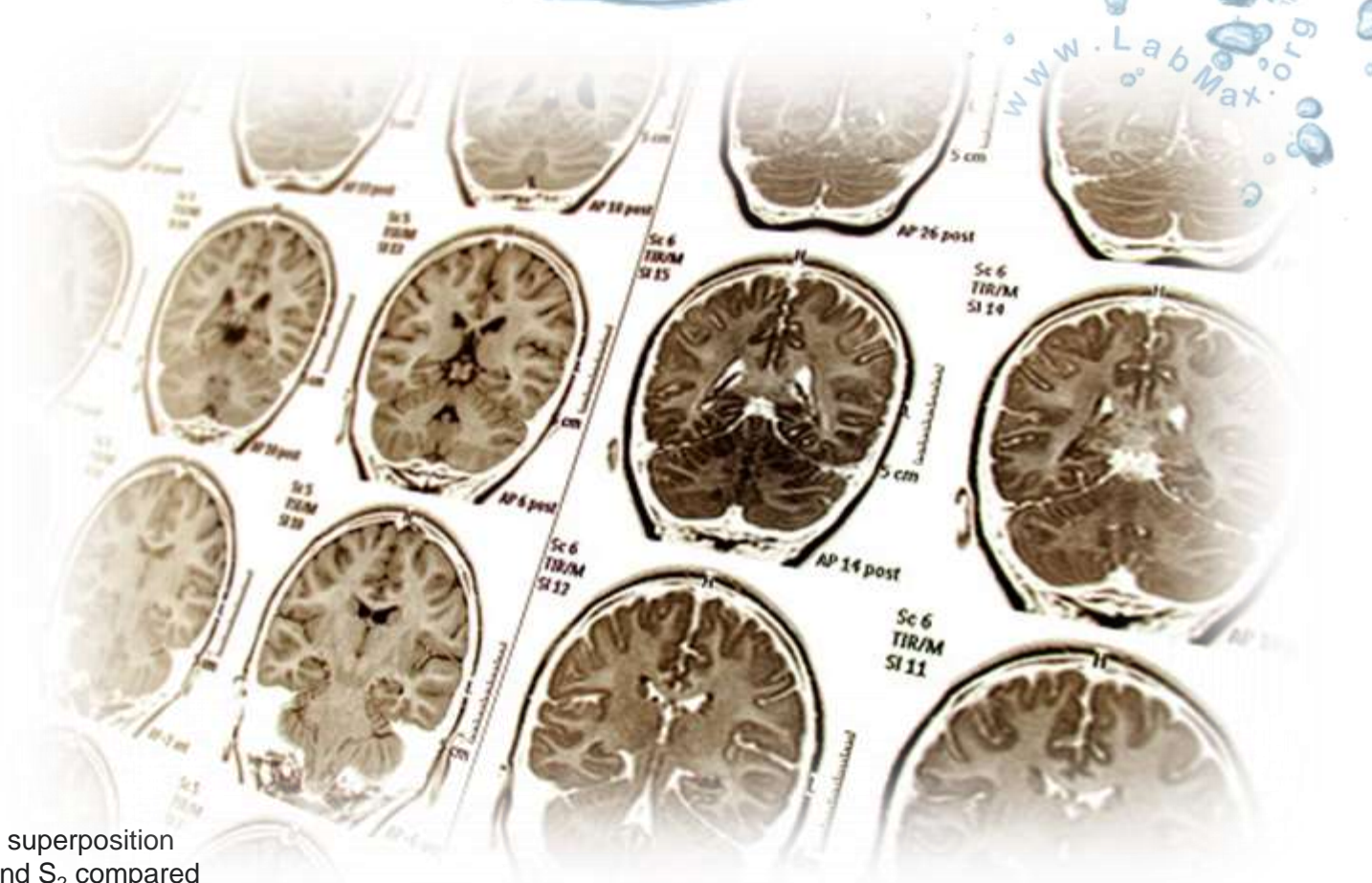


Fig.1: Basic principle of tomography: superposition free tomographic cross sections S_1 and S_2 compared with the (not tomographic) projected image P.





Tomografia por Micro-ondas

Imagens através de Micro-ondas de campo próximo

2012-2015

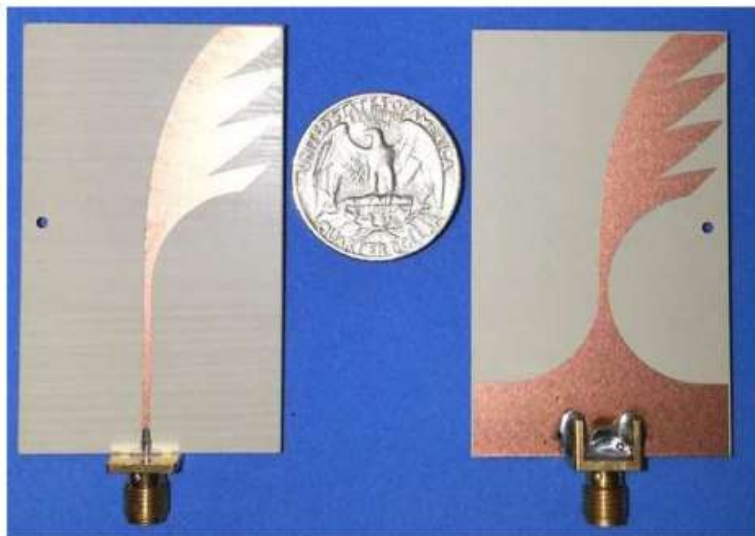
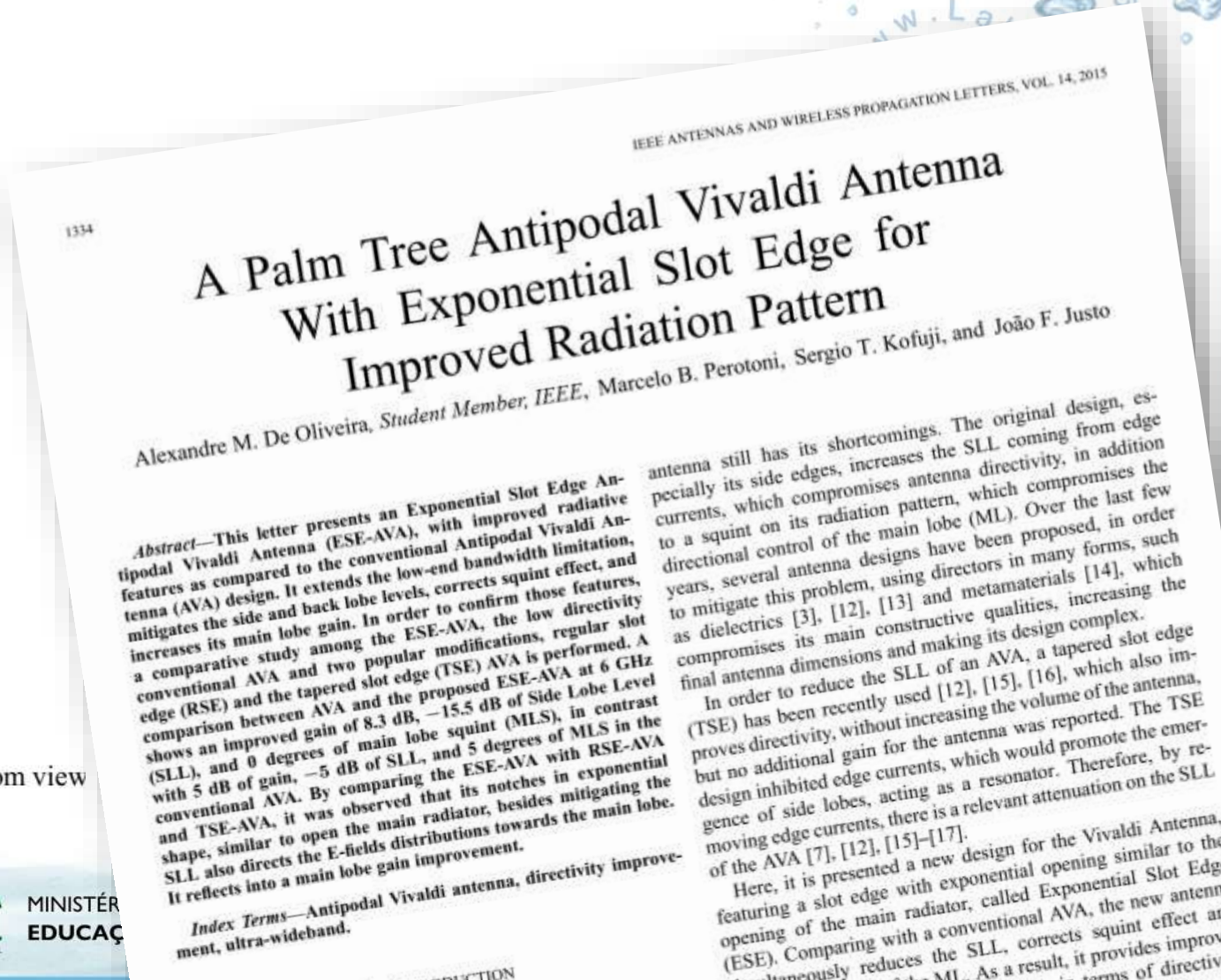


Fig. 2. Fabricated ESE-AVA photograph, top view on the left and bottom view on the right.



A Palm Tree Antipodal Vivaldi Antenna With Exponential Slot Edge for Improved Radiation Pattern
 Alexandre M. De Oliveira, *Student Member, IEEE*, Marcelo B. Perotoni, Sergio T. Kofuji, and João F. Justo

Abstract—This letter presents an Exponential Slot Edge Antipodal Vivaldi Antenna (ESE-AVA), with improved radiative features as compared to the conventional Antipodal Vivaldi Antenna (AVA) design. It extends the low-end bandwidth limitation, mitigates the side and back lobe levels, corrects squint effect, and increases its main lobe gain. In order to confirm those features, a comparative study among the ESE-AVA, the low directivity conventional AVA and two popular modifications, regular slot edge (RSE) and the tapered slot edge (TSE) AVA is performed. A comparison between AVA and the proposed ESE-AVA at 6 GHz shows an improved gain of 8.3 dB, -15.5 dB of Side Lobe Level (SLL), and 0 degrees of main lobe squint (MLS), in contrast with 5 dB of gain, -5 dB of SLL, and 5 degrees of MLS in the conventional AVA. By comparing the ESE-AVA with RSE-AVA and TSE-AVA, it was observed that its notches in exponential shape, similar to open the main radiator, besides mitigating the SLL also directs the E-fields distributions towards the main lobe. It reflects into a main lobe gain improvement.

Index Terms—Antipodal Vivaldi antenna, directivity improvement, ultra-wideband.

antenna still has its shortcomings. The original design, especially its side edges, increases the SLL coming from edge currents, which compromises antenna directivity, in addition to a squint on its radiation pattern, which compromises the directional control of the main lobe (ML). Over the last few years, several antenna designs have been proposed, in order to mitigate this problem, using directors in many forms, such as dielectrics [3], [12], [13] and metamaterials [14], which compromises its main constructive qualities, increasing the final antenna dimensions and making its design complex. In order to reduce the SLL of an AVA, a tapered slot edge (TSE) has been recently used [12], [15], [16], which also improves directivity, without increasing the volume of the antenna, but no additional gain for the antenna was reported. The TSE design inhibited edge currents, which would promote the emergence of side lobes, acting as a resonator. Therefore, by removing edge currents, there is a relevant attenuation on the SLL of the AVA [7], [12], [15]–[17].

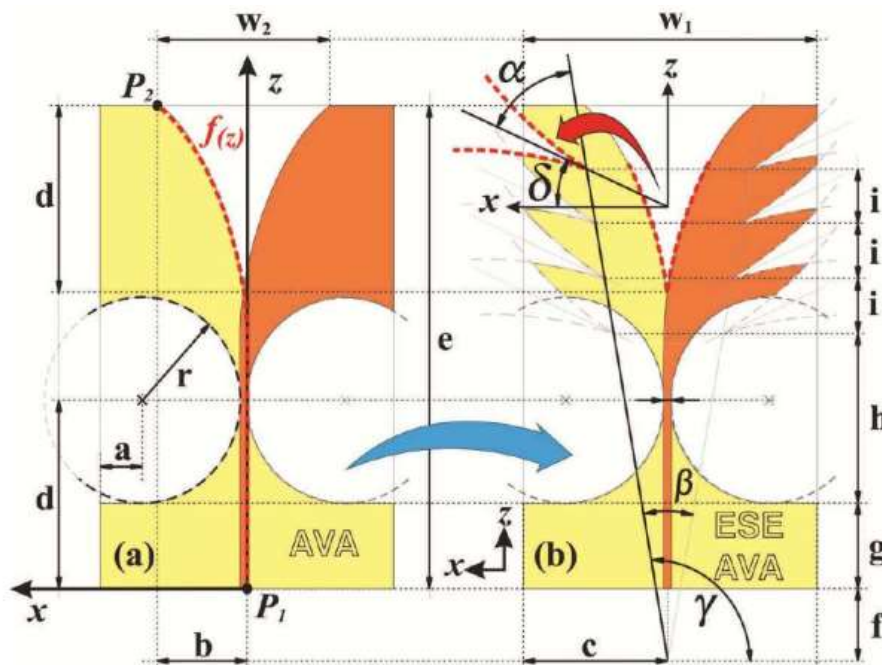
Here, it is presented a new design for the Vivaldi Antenna, featuring a slot edge with exponential opening similar to the opening of the main radiator, called Exponential Slot Edge (ESE). Comparing with a conventional AVA, the new antenna (ESE) simultaneously reduces the SLL, corrects squint effect and improves the ML. As a result, it provides improvement in terms of directivity



Tomografia por Micro-ondas

Imagens através de Micro-ondas de campo próximo

www.LabMax.org



$$f(z) = c_1 e^{Rz} + c_2 \quad (1)$$

$$c_1 = \frac{x_2 - x_1}{e^{Rz_2} - e^{Rz_1}} \quad (2)$$

$$c_2 = \frac{x_2 e^{Rz_2} x_1 e^{Rz_1}}{e^{Rz_2} e^{Rz_1}} \quad (3)$$

Fig. 1. Design and antenna parameters in xz-plane: (a) reference AVA. (b) proposed ESE-AVA.

2012-2015





Tomografia por Micro-ondas

Imagens através de Micro-ondas de campo próximo

www.LabMax.org

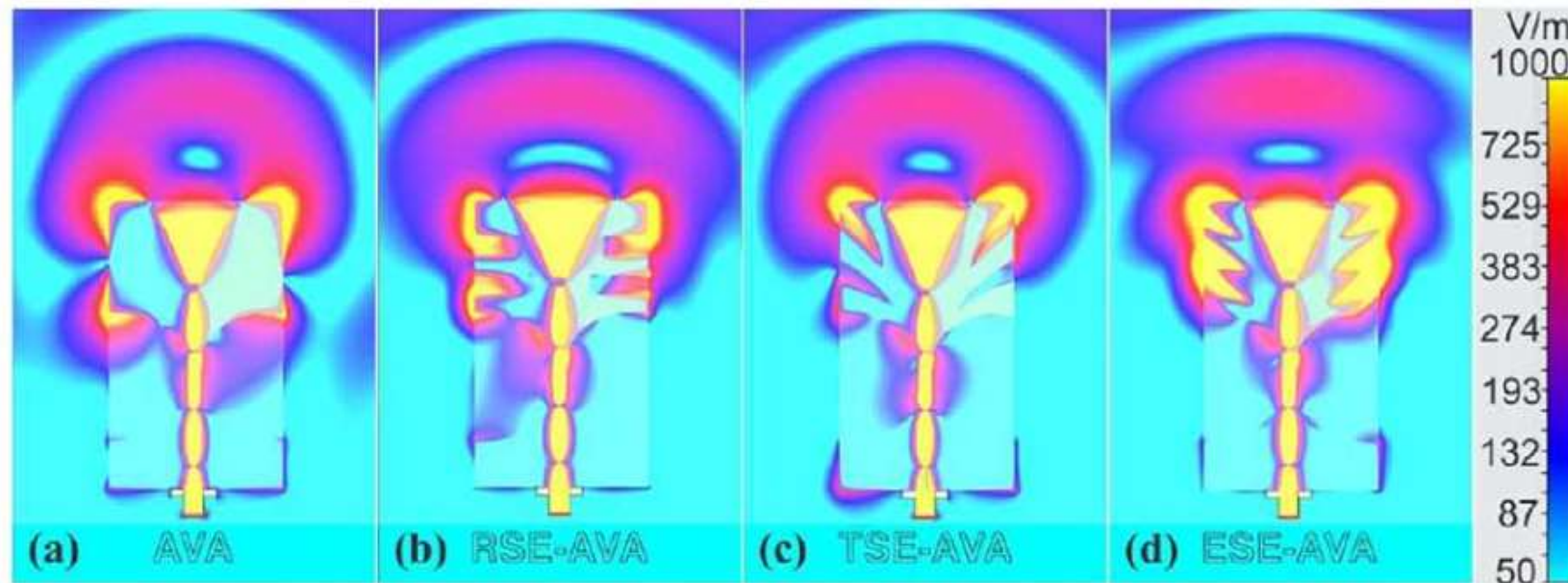
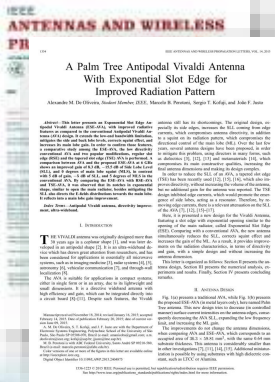


Fig. 9. E-field distribution in xz-plane at 6 GHz for (a) AVA, (b) RSE-AVA, (c) TSE-AVA, and (d) ESE-AVA at 6 GHz.

2012-2015





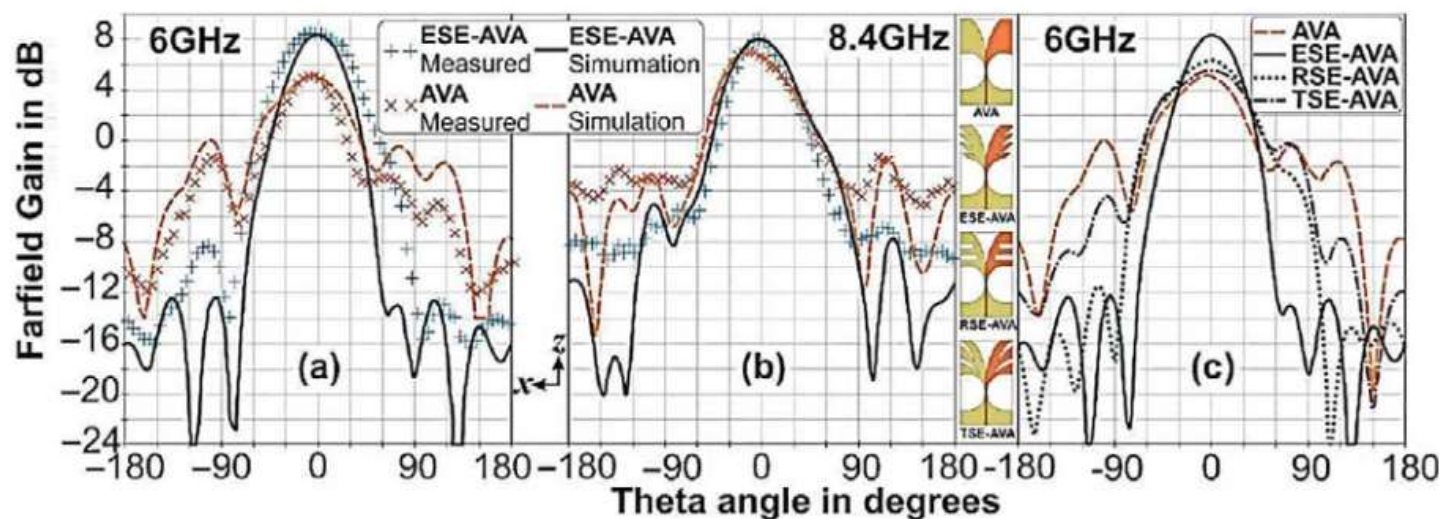
Fomento a Pesquisa PRP do
 IFSP via Edital n.º 823/2018



Tomografia por Micro-ondas

Imagens através de Micro-ondas de campo próximo

www.LabMax.org



2012-2015



Fig. 10. Measured and simulated radiation pattern at (a) 6 and (b) 8.4 GHz of the AVA and ESE-AVA. (c) Simulated radiation pattern at 6 GHz of the AVA (dashed-line), ESE-AVA (solid-line), RSE-AVA (dotted-line), and TSE-AVA (dotdashed-line).



Instituto Federal de São Paulo
Laboratório Maxwell
 Micro-ondas e Eletromagnetismo Aplicado
 Certificado CNPq n° 5.497.663.866.471.659



LittleMax
 e a luta contra o Câncer
 Cerebral Infantil

Fomento a Pesquisa PRP do
 IFSP via Edital n° 823/2018



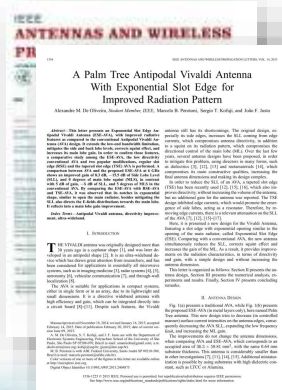
Academia Cearense
 de Matemática - ACM

Tomografia por Micro-ondas

Imagens através de Micro-ondas de campo próximo

www.LabMax.org

2012-2015

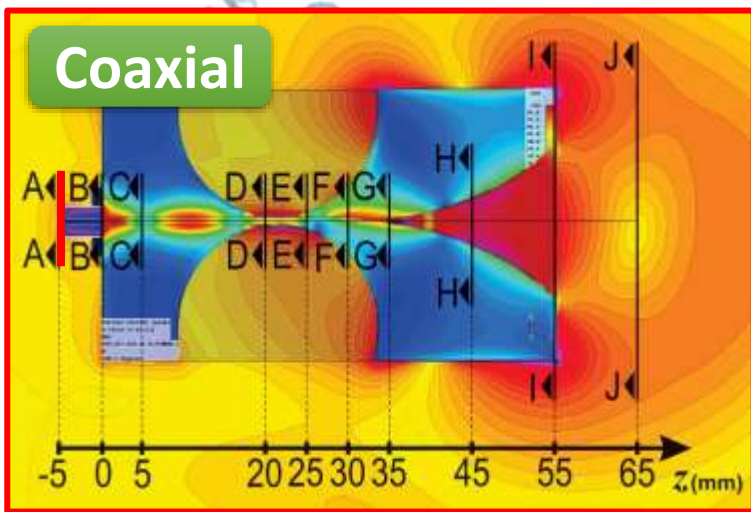


Dr. Alexandre Manicoba de Oliveira
amanicoba@ifsp.edu.br



Tomografia por Micro-ondas

Imagens através de Micro-ondas de campo próximo

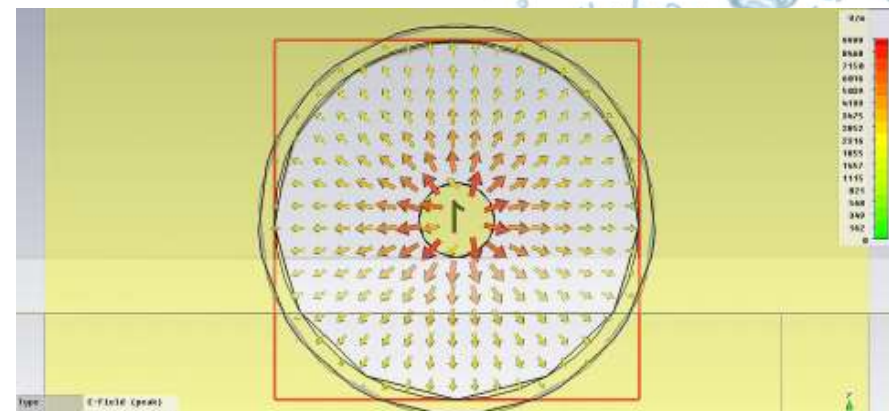


2012-2015

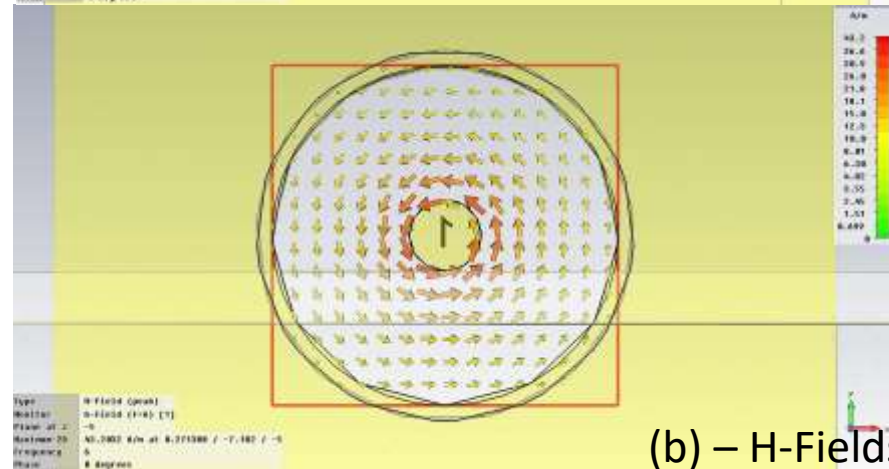


Nessas condições as equações de Maxwell usadas são:

$$\begin{cases} \nabla \cdot \vec{E} = \rho / \epsilon_r \\ \nabla \times \vec{E} = -\partial \vec{B} / \partial t \\ \nabla \cdot \vec{B} = 0 \\ \nabla \times \vec{B} = \mu_r \vec{J}_T \end{cases}$$



(a) – E-Fields

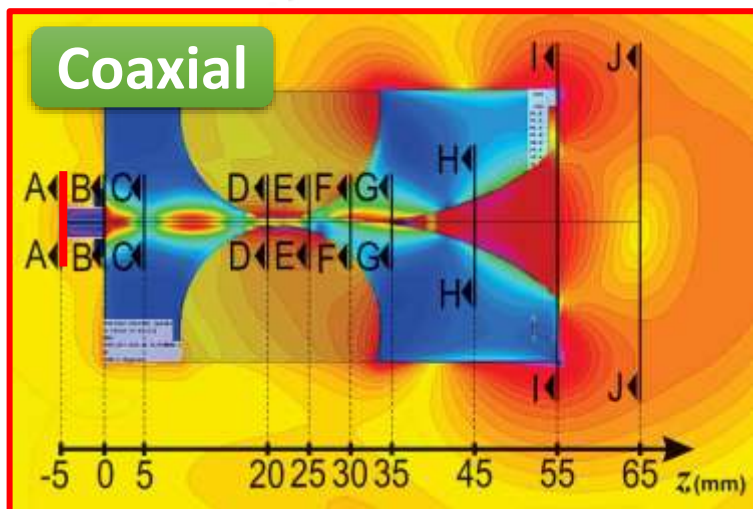


(b) – H-Fields



Tomografia por Micro-ondas

Imagens através de Micro-ondas de campo próximo

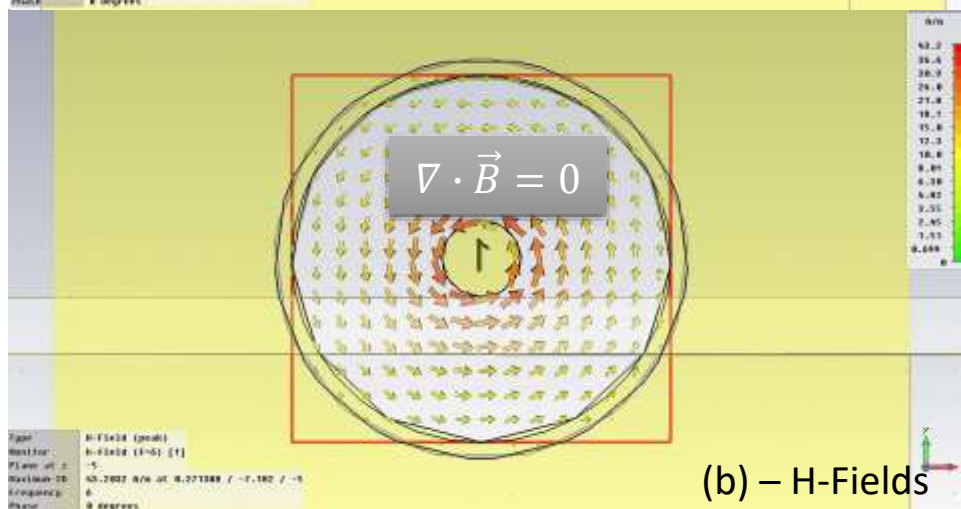
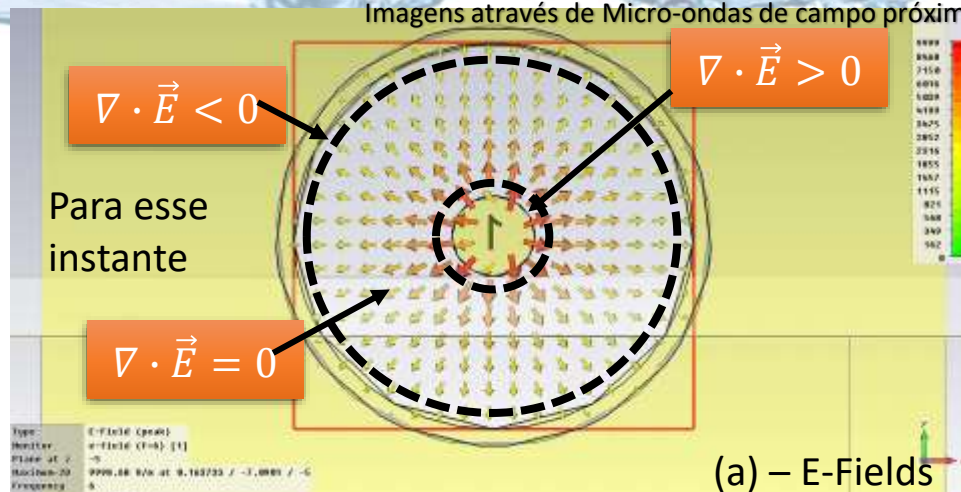


2012-2015



Nessas condições as equações de Maxwell usadas são:

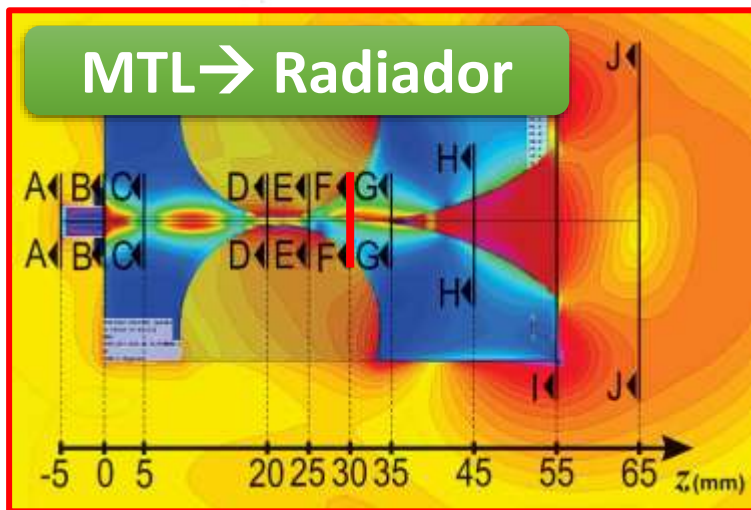
$$\begin{cases} \nabla \cdot \vec{E} = \rho / \epsilon_r \\ \nabla \times \vec{E} = -\partial \vec{B} / \partial t \\ \nabla \cdot \vec{B} = 0 \\ \nabla \times \vec{B} = \mu_r \vec{J}_T \end{cases}$$





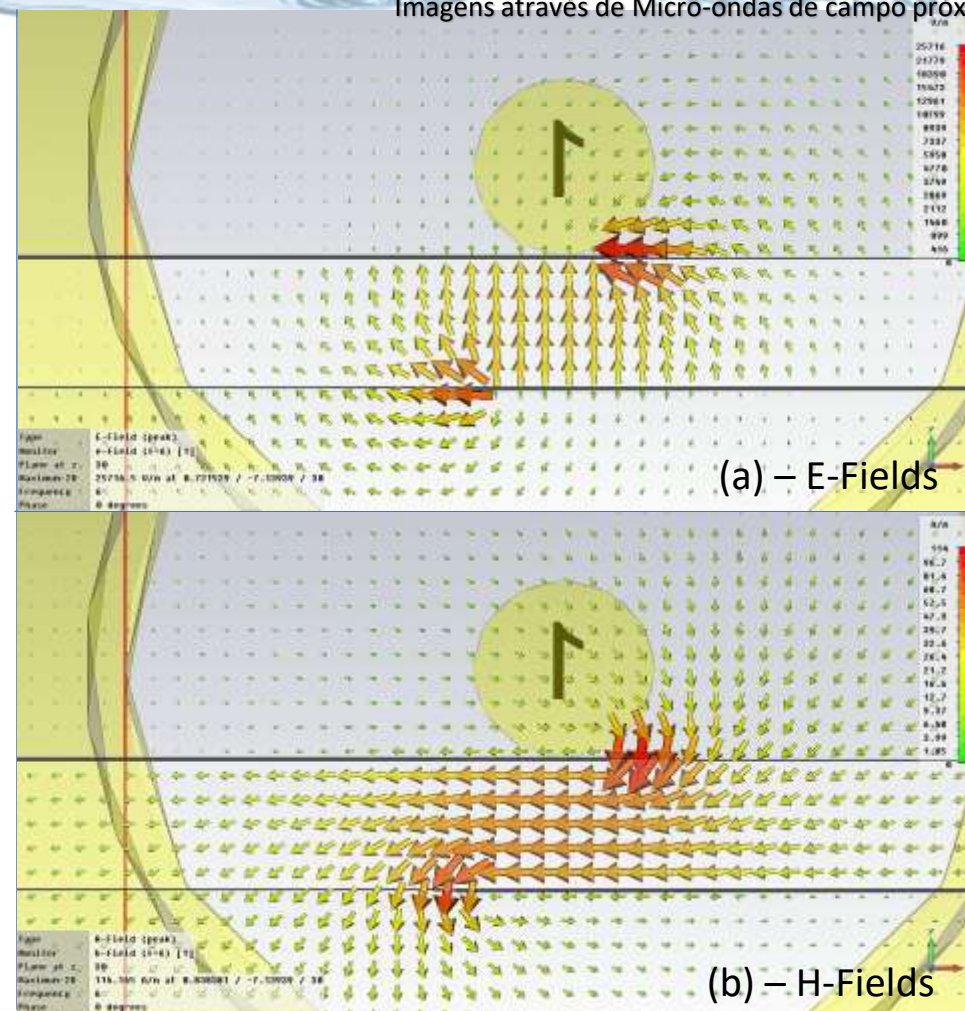
Tomografia por Micro-ondas

Imagens através de Micro-ondas de campo próximo



Nessas condições as equações de Maxwell usadas são:

$$\begin{cases} \nabla \cdot \vec{E} = \rho / \epsilon_{eff} \\ \nabla \times \vec{E} = -\partial \vec{B} / \partial t \\ \nabla \cdot \vec{B} = 0 \\ \nabla \times \vec{B} = \mu_{eff} \vec{J}_T \end{cases}$$



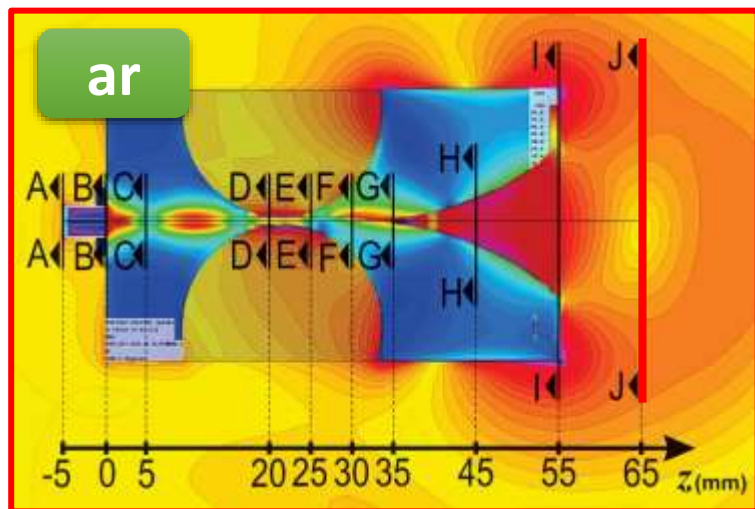
2012-2015





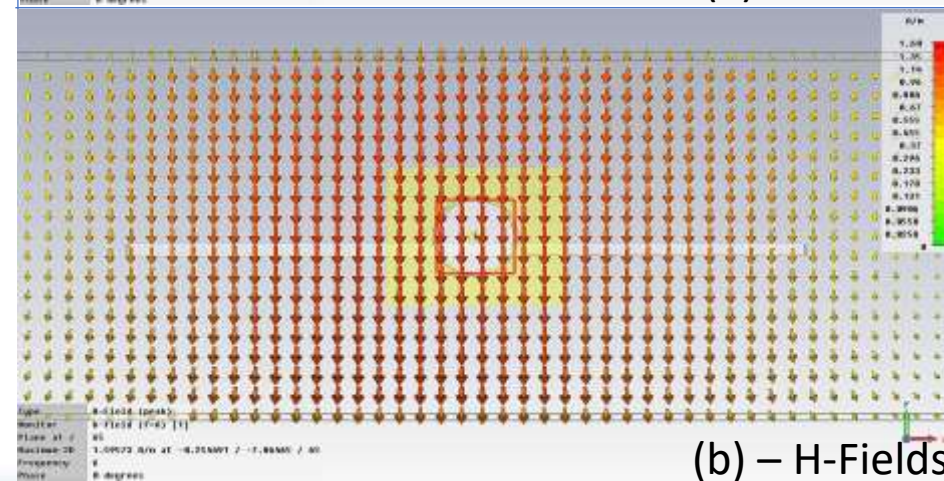
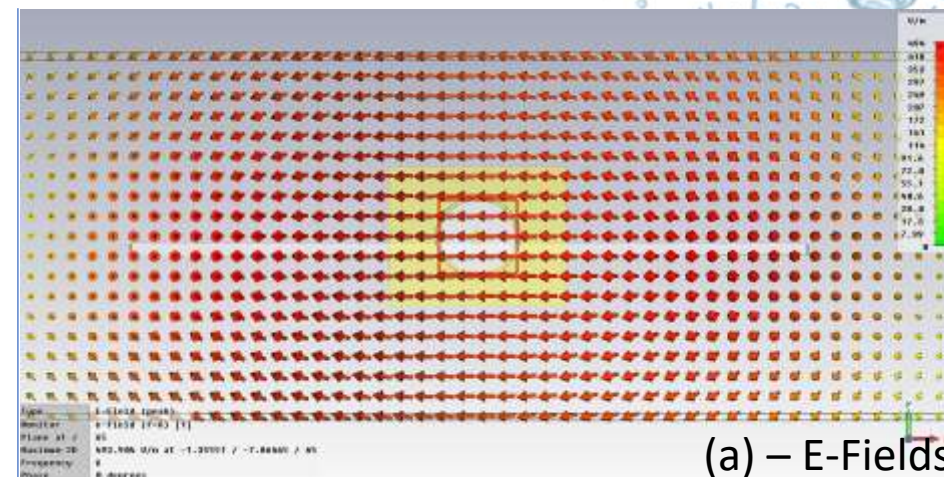
Tomografia por Micro-ondas

Imagens através de Micro-ondas de campo próximo



Nessas condições as equações de Maxwell usadas são:

$$\begin{cases} \nabla \cdot \vec{D} \rightarrow 0 \\ \nabla \times \vec{E} = -\partial \vec{B} / \partial t \\ \nabla \cdot \vec{B} = 0 \\ \nabla \times \vec{H} = \partial \vec{D} / \partial t \end{cases}$$



2012-2015



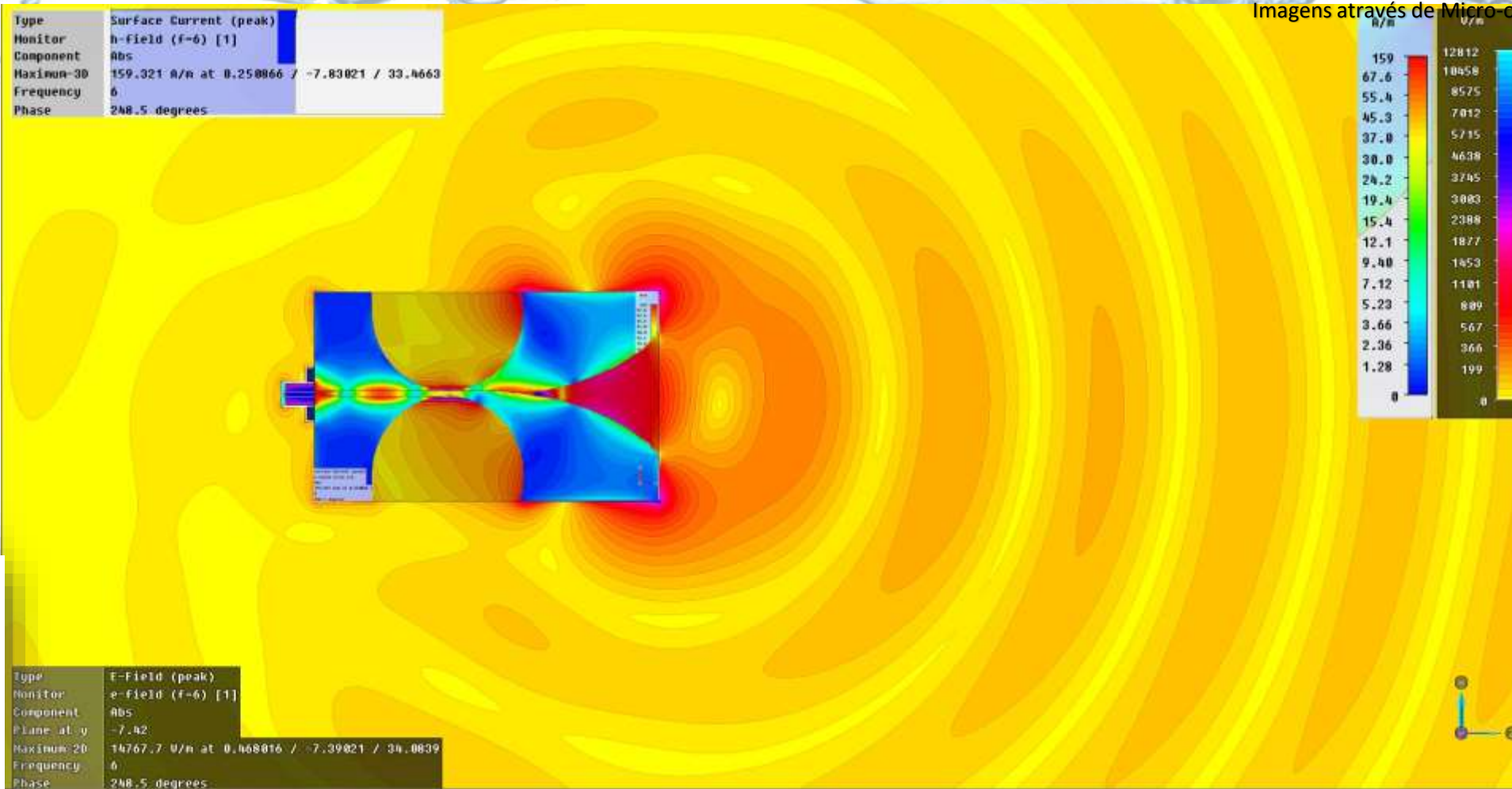


Fomento a Pesquisa PRP do
 IFSP via Edital n.º 823/2018



Tomografia por Micro-ondas

Imagens através de Micro-ondas de campo próximo



2012-2015





Tomografia por Micro-ondas

Imagens através de Micro-ondas de campo próximo



O espaço ao redor da antena é dividido em:

2012-2015





Tomografia por Micro-ondas

Imagens através de Micro-ondas de campo próximo



2012-2015



O espaço ao redor da antena é dividido em:
Região Reativa de campo próximo;



Tomografia por Micro-ondas

Imagens através de Micro-ondas de campo próximo



2012-2015



O espaço ao redor da antena é dividido em:
 Região Reativa de campo próximo;
Região Radiante de campo próximo (Fresnel);



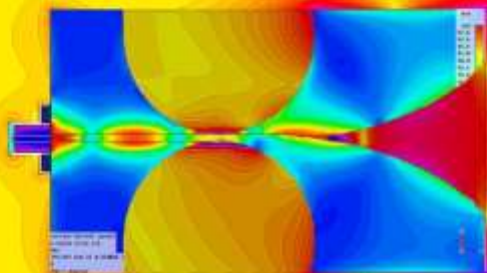
Fomento a Pesquisa PRP do
 IFSP via Edital n.º 823/2018



Tomografia por Micro-ondas

Imagens através de Micro-ondas de campo próximo

Type	Surface Current (peak)
Monitor	h-Field (f-6) [1]
Component	Abs
Maximum-3D	159.321 A/n at 0.250866 / -7.83021 / 33.4663
Frequency	6
Phase	248.5 degrees



2012-2015



O espaço ao redor da antena é dividido em:
 Região Reativa de campo próximo;
 Região Radiante de campo próximo (Fresnel);
 Região de Campo distante (Fraunhofer).

Type	E-Field (Peak)
Monitor	h-Field (f-6) [1]
Component	Abs
Plane at y	-7.42
Maximum	14767.7 A/n at 0.46806 / -7.7321 / 34.0839
Frequency	6
Phase	248.5 degrees

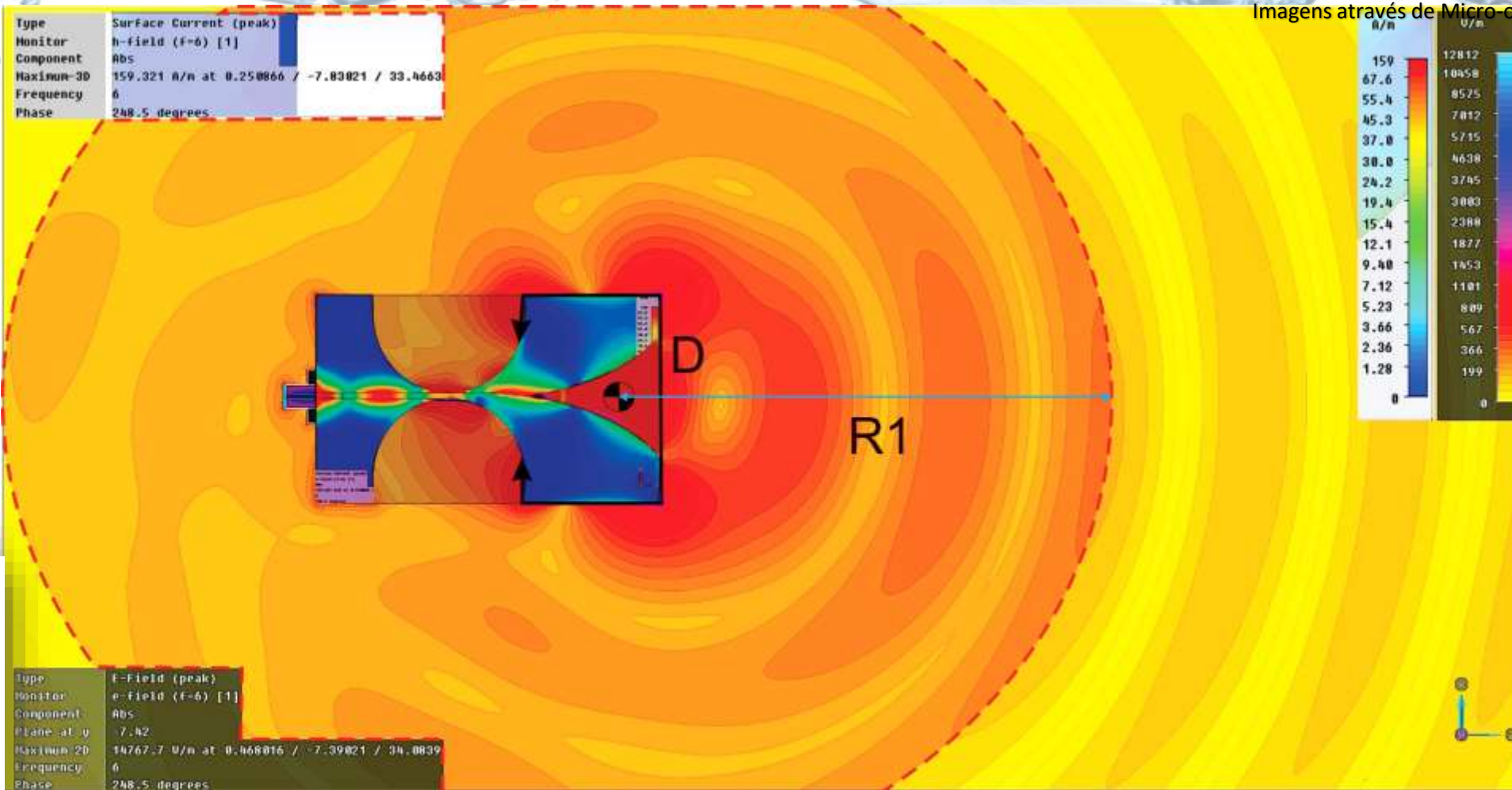


Fomento a Pesquisa PRP do
 IFSP via Edital n°. 823/2018



Tomografia por Micro-ondas

Imagens através de Micro-ondas de campo próximo



2012-2015



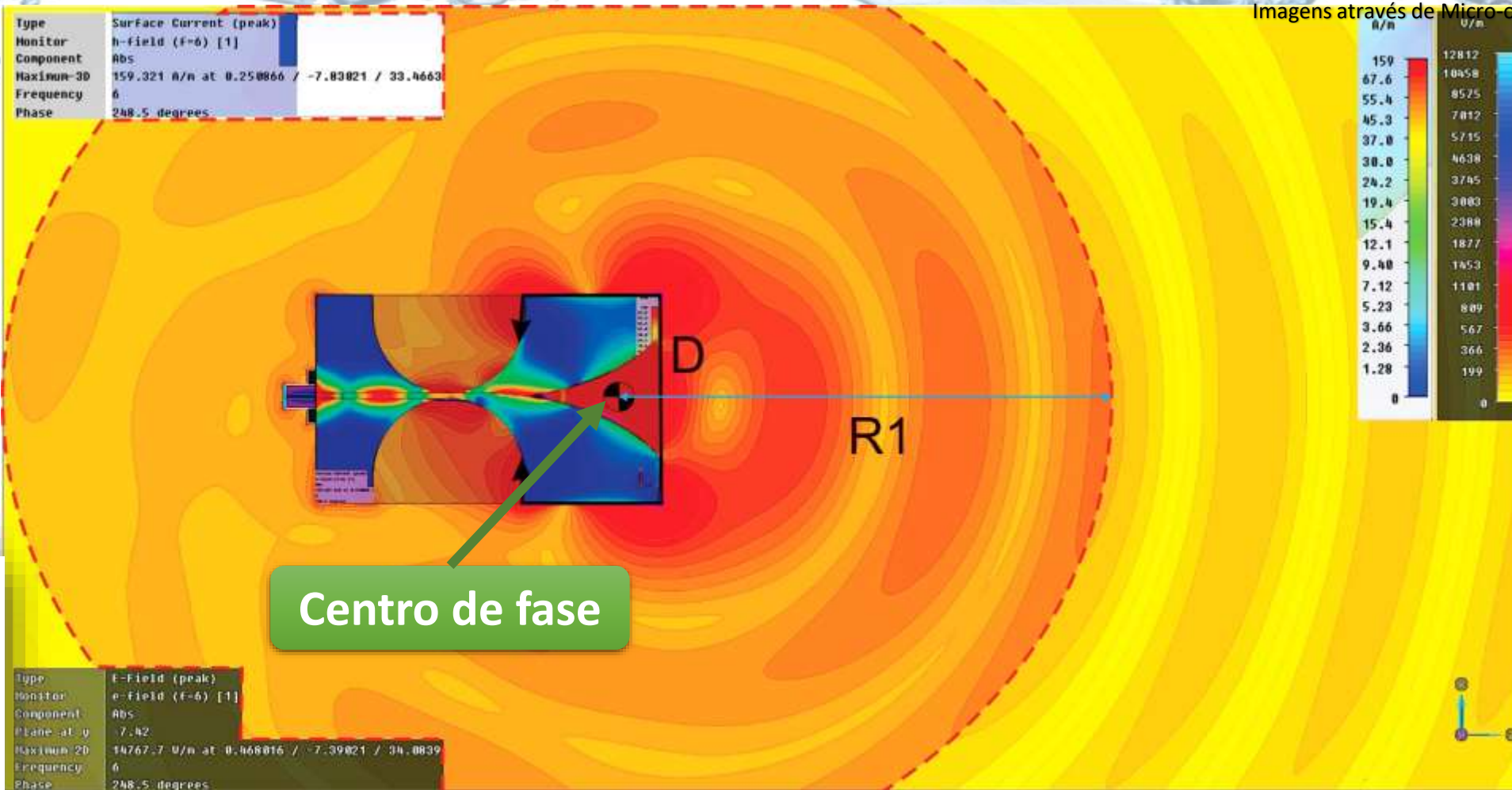


Fomento a Pesquisa PRP do
 IFSP via Edital n.º 823/2018



Tomografia por Micro-ondas

Imagens através de Micro-ondas de campo próximo



2012-2015



Centro de fase

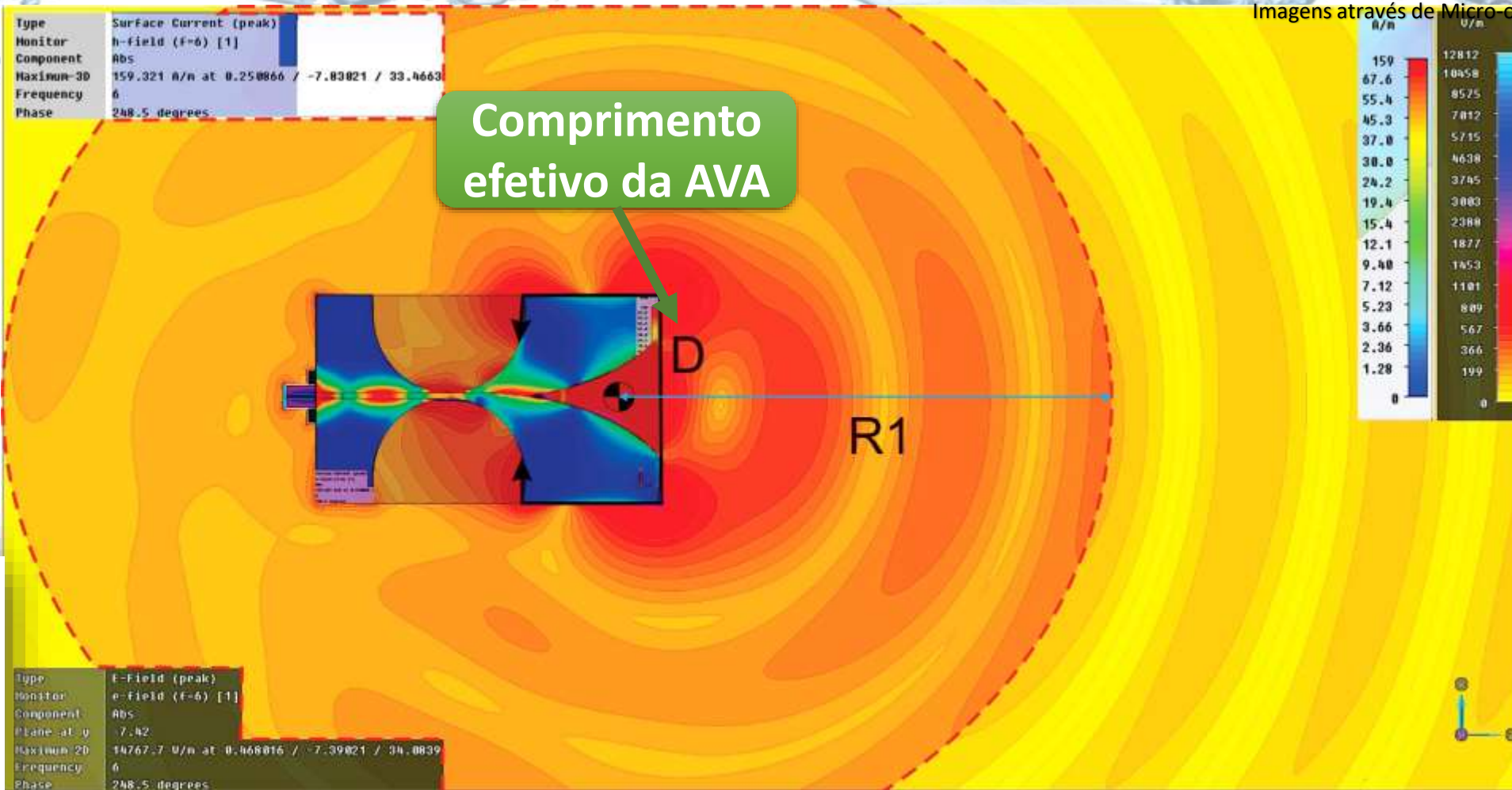


Fomento a Pesquisa PRP do
 IFSP via Edital n.º 823/2018



Tomografia por Micro-ondas

Imagens através de Micro-ondas de campo próximo



2012-2015



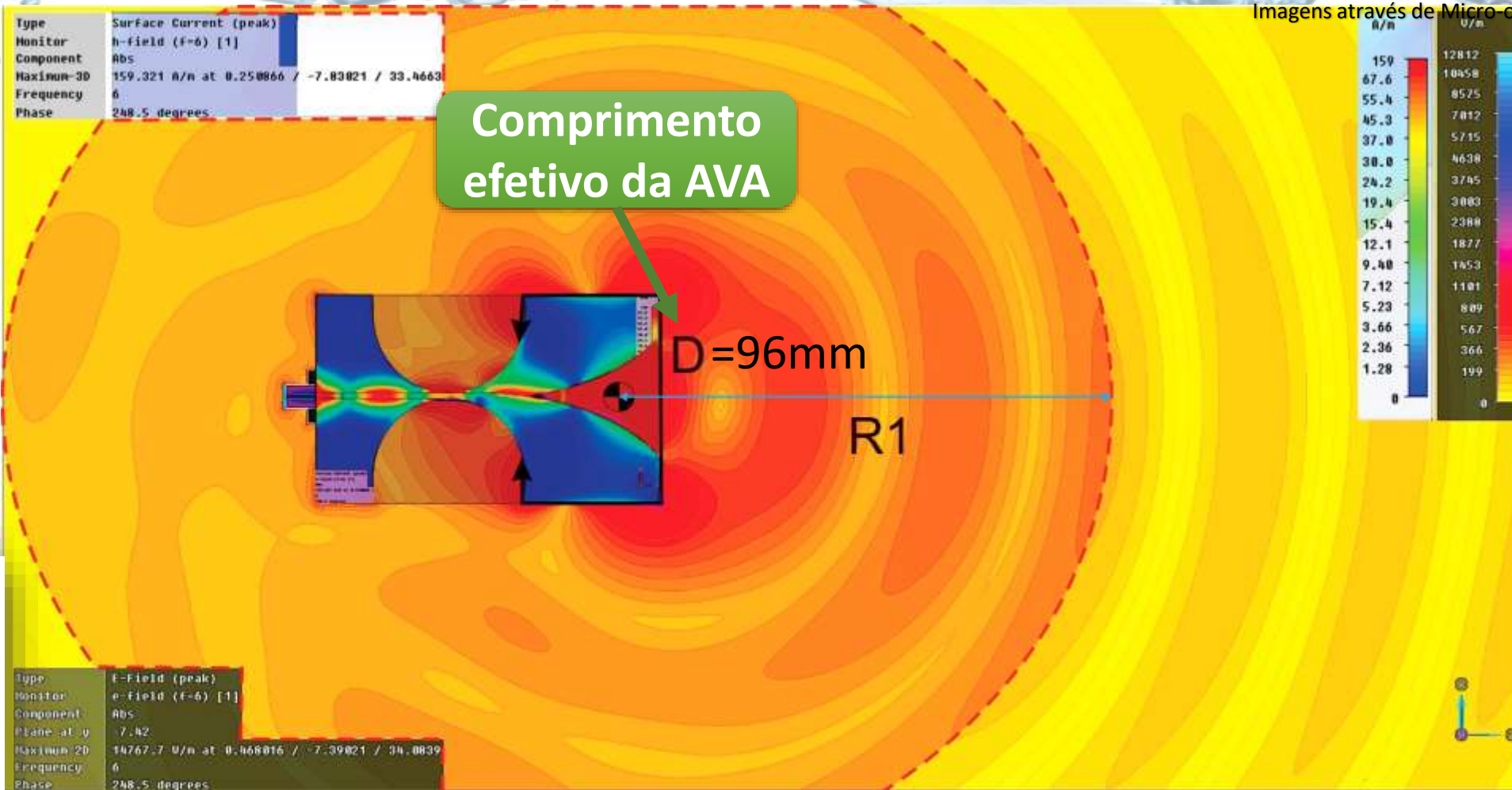


Fomento a Pesquisa PRP do
 IFSP via Edital n.º 823/2018



Tomografia por Micro-ondas

Imagens através de Micro-ondas de campo próximo



2012-2015





Fomento a Pesquisa PRP do
 IFSP via Edital n.º 823/2018



Tomografia por Micro-ondas

Imagens através de Micro-ondas de campo próximo

Type	Surface Current (peak)
Monitor	h-field (F=6) [1]
Component	Abs
Maximum 3D	159.321 A/m at 0.250866 / -7.83821 / 33.4663
Frequency	6
Phase	248.5 degrees

Type	E-Field (peak)
Monitor	e-Field (F=6) [1]
Component	Abs
Plane at y	7.42
Maximum 2D	14767.7 V/m at 0.468816 / -7.39821 / 34.8839
Frequency	6
Phase	248.5 degrees

Distância do
 CF e o limite
 superior da
 região reativa

D=96mm

R1



2012-2015



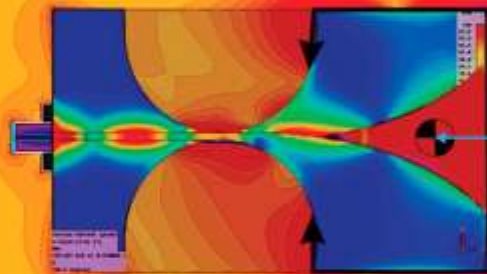


Tomografia por Micro-ondas

Imagens através de Micro-ondas de campo próximo

Type	Surface Current (peak)
Monitor	h-field (F=6) [1]
Component	Abs
Maximum 3D	159.321 A/m at 0.250866 / -7.83821 / 33.4663
Frequency	6
Phase	248.5 degrees

Type	E-Field (peak)
Monitor	e-Field (F=6) [1]
Component	Abs
Plane at y	7.42
Maximum 2D	14767.7 V/m at 0.468816 / -7.39821 / 34.8839
Frequency	6
Phase	248.5 degrees



D=96mm

Distância do
 CF e o limite
 superior da
 região reativa

$$R1 = 0,62 \sqrt{D^3 / \lambda}$$

(BALANIS, 2008)



2012-2015





Fomento a Pesquisa PRP do
 IFSP via Edital n.º 823/2018



Tomografia por Micro-ondas

Imagens através de Micro-ondas de campo próximo

Type	Surface Current (peak)
Monitor	h-field (F=6) [1]
Component	Abs
Maximum 3D	159.321 A/m at 0.250866 / -7.83821 / 33.4663
Frequency	6
Phase	248.5 degrees

Type	E-Field (peak)
Monitor	e-Field (F=6) [1]
Component	Abs
Plane at y	7.42
Maximum 2D	14767 V/m at 0.468816 / -7.39821 / 34.8839
Frequency	6
Phase	248.5 degrees

Distância do
 CF e o limite
 superior da
 região reativa

D=96mm

$$R1 = 0,62 \sqrt{D^3 / \lambda}$$

como $f = 6GHz$



2012-2015





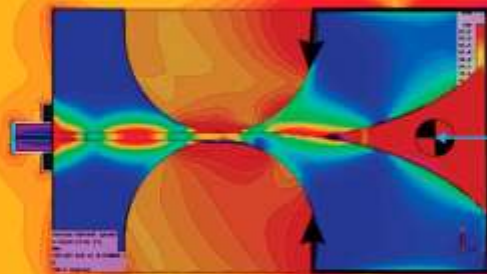
Tomografia por Micro-ondas

Imagens através de Micro-ondas de campo próximo

Type	Surface Current (peak)
Monitor	h-field (F=6) [1]
Component	Abs
Maximum 3D	159.321 A/m at 0.250866 / -7.83821 / 33.4663
Frequency	6
Phase	248.5 degrees

Type	E-Field (peak)
Monitor	e-Field (F=6) [1]
Component	Abs
Plane at y	7.42
Maximum 2D	14767 V/m at 0.468816 / -7.39821 / 34.8839
Frequency	6
Phase	248.5 degrees

Distância do
 CF e o limite
 superior da
 região reativa



D=96mm

$$R1 = 0,62 \sqrt{D^3 / \lambda}$$

como $f = 6GHz$ teremos: $\lambda = \frac{1}{f \sqrt{\epsilon_0 \mu_0}}$



2012-2015



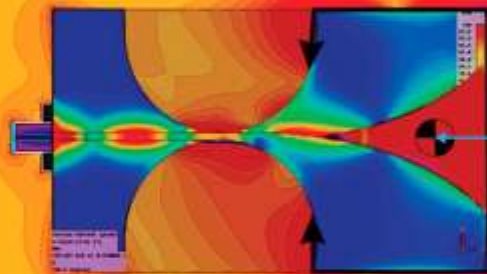


Tomografia por Micro-ondas

Imagens através de Micro-ondas de campo próximo

Type	Surface Current (peak)
Monitor	h-field (F=6) [1]
Component	Abs
Maximum 3D	159.321 A/m at 0.250866 / -7.83821 / 33.4663
Frequency	6
Phase	248.5 degrees

Distância do
 CF e o limite
 superior da
 região reativa



D=96mm

$$R1 = 0,62 \sqrt{D^3 / \lambda}$$

como $f = 6GHz$ teremos: $\lambda = \frac{1}{f \sqrt{\epsilon_0 \mu_0}} = 50mm$



2012-2015



Type	E-Field (peak)
Monitor	e-Field (F=6) [1]
Component	Abs
Plane at	y
Maximum 2D	14767 V/m at 0.468016 / -7.39021 / 34.0839
Frequency	6
Phase	248.5 degrees

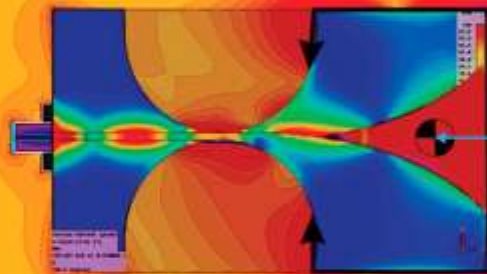


Tomografia por Micro-ondas

Imagens através de Micro-ondas de campo próximo

Type	Surface Current (peak)
Monitor	h-field (F=6) [1]
Component	Abs
Maximum 3D	159.321 A/m at 0.250866 / -7.83821 / 33.4663
Frequency	6
Phase	248.5 degrees

Distância do
 CF e o limite
 superior da
 região reativa



D=96mm

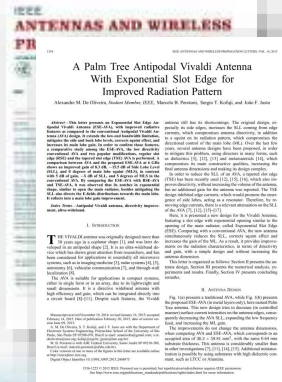
logo:

$$R1 = 0,62 \sqrt{D^3 / \lambda} = 82,5mm$$

como $f = 6GHz$ teremos: $\lambda = \frac{1}{f \sqrt{\epsilon_0 \mu_0}} = 50mm$



2012-2015



Type	E-Field (peak)
Monitor	e-Field (F=6) [1]
Component	Abs
Plane at y	7.42
Maximum 2D	14767 V/m at 0.468016 / -7.39021 / 34.0839
Frequency	6
Phase	248.5 degrees

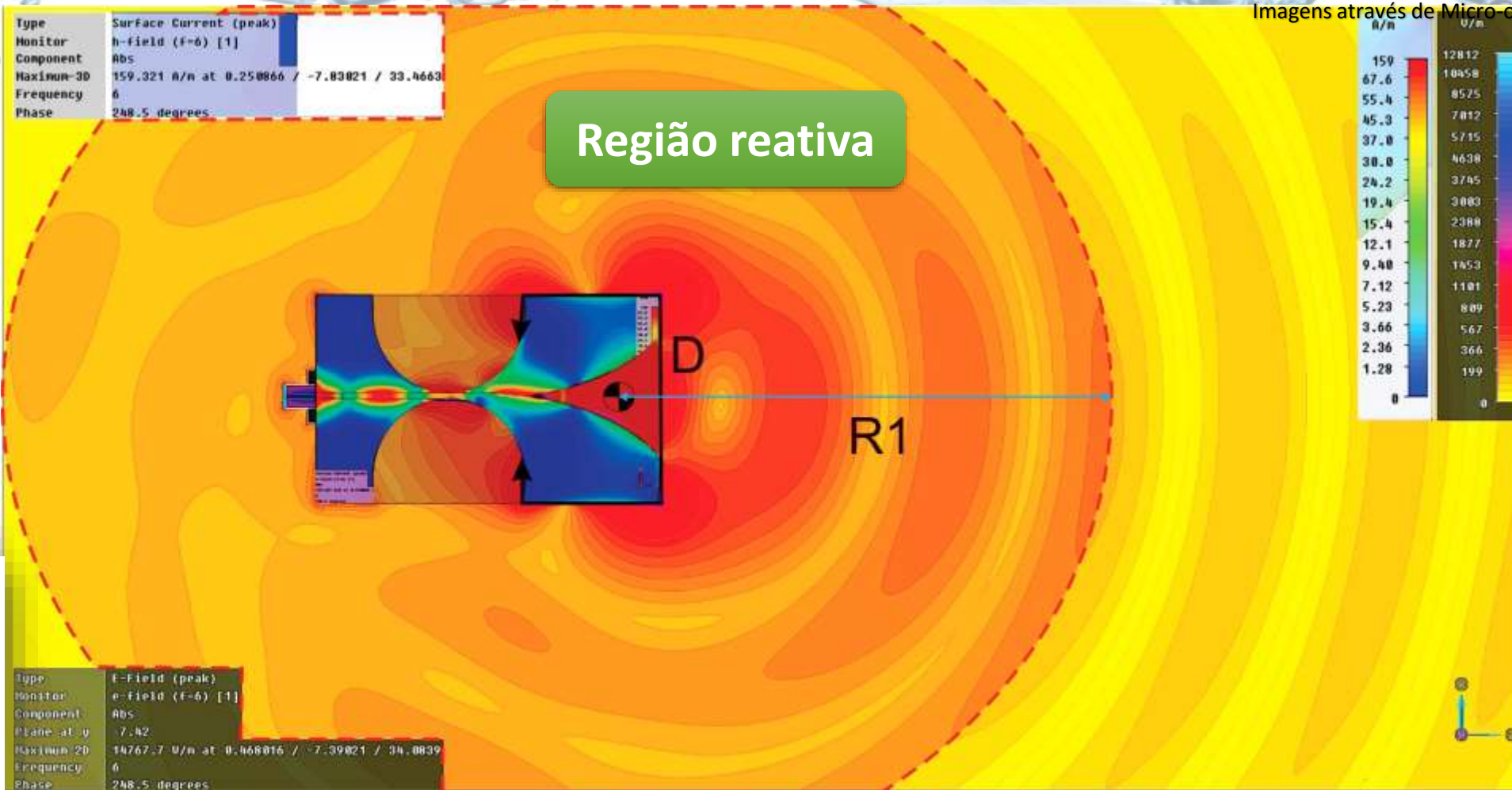


Fomento a Pesquisa PRP do
 IFSP via Edital n.º 823/2018



Tomografia por Micro-ondas

Imagens através de Micro-ondas de campo próximo



2012-2015



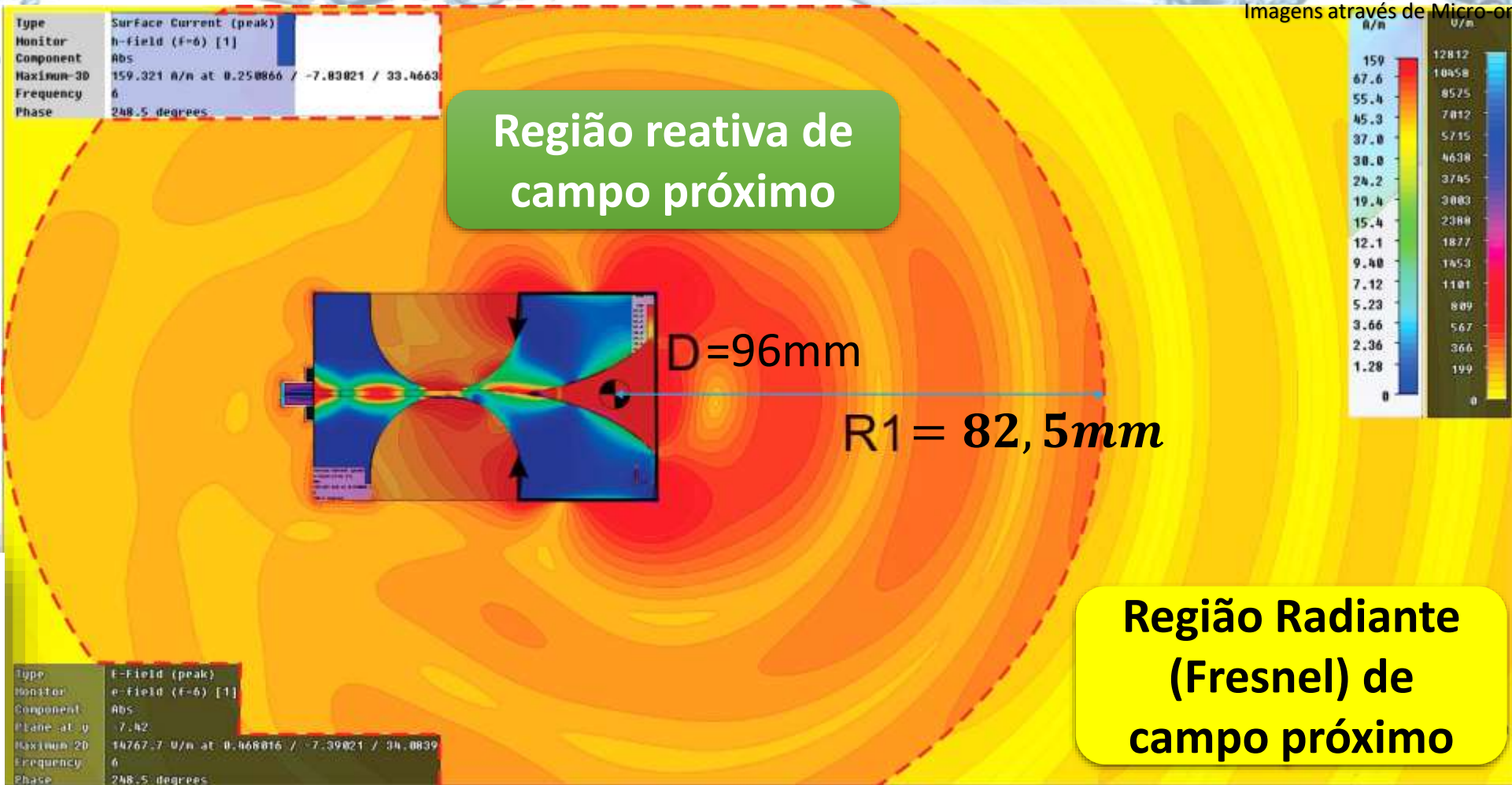


Fomento a Pesquisa PRP do
 IFSP via Edital n°. 823/2018



Tomografia por Micro-ondas

Imagens através de Micro-ondas de campo próximo



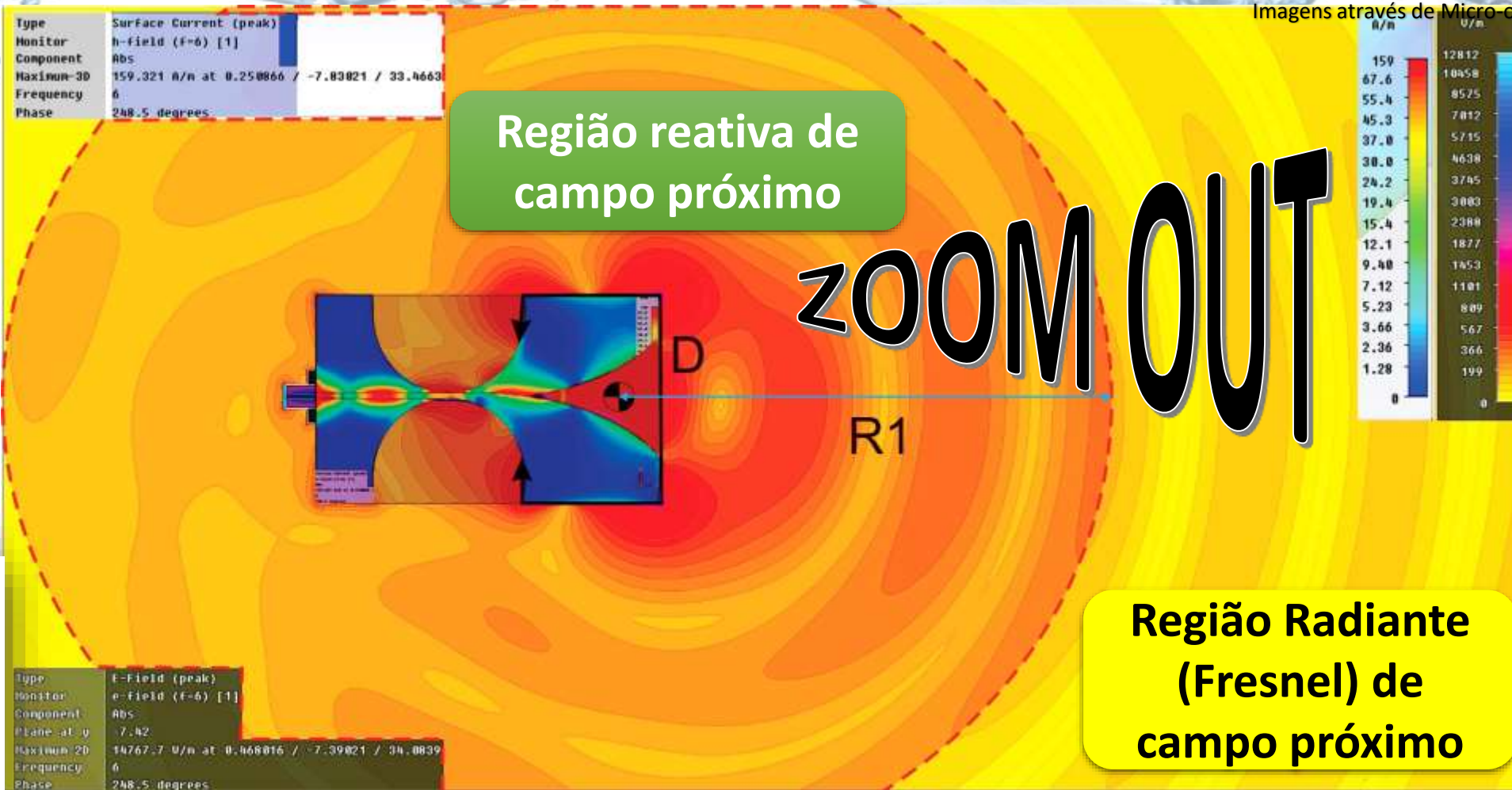
2012-2015





Tomografia por Micro-ondas

Imagens através de Micro-ondas de campo próximo



Região reativa de
 campo próximo

ZOOM OUT

Região Radiante
 (Fresnel) de
 campo próximo

2012-2015

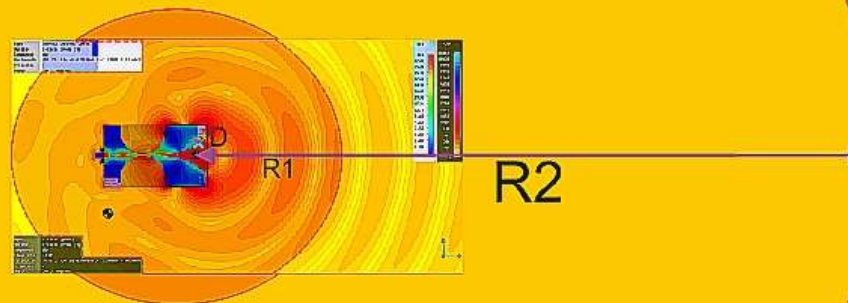


Type	E-Field (peak)
Monitor	e-Field (F=6) [1]
Component	Abs
Plane at y	7.42
Maximum 3D	14767.7 U/m at 0.468016 / -7.39021 / 34.0839
Frequency	6
Phase	248.5 degrees



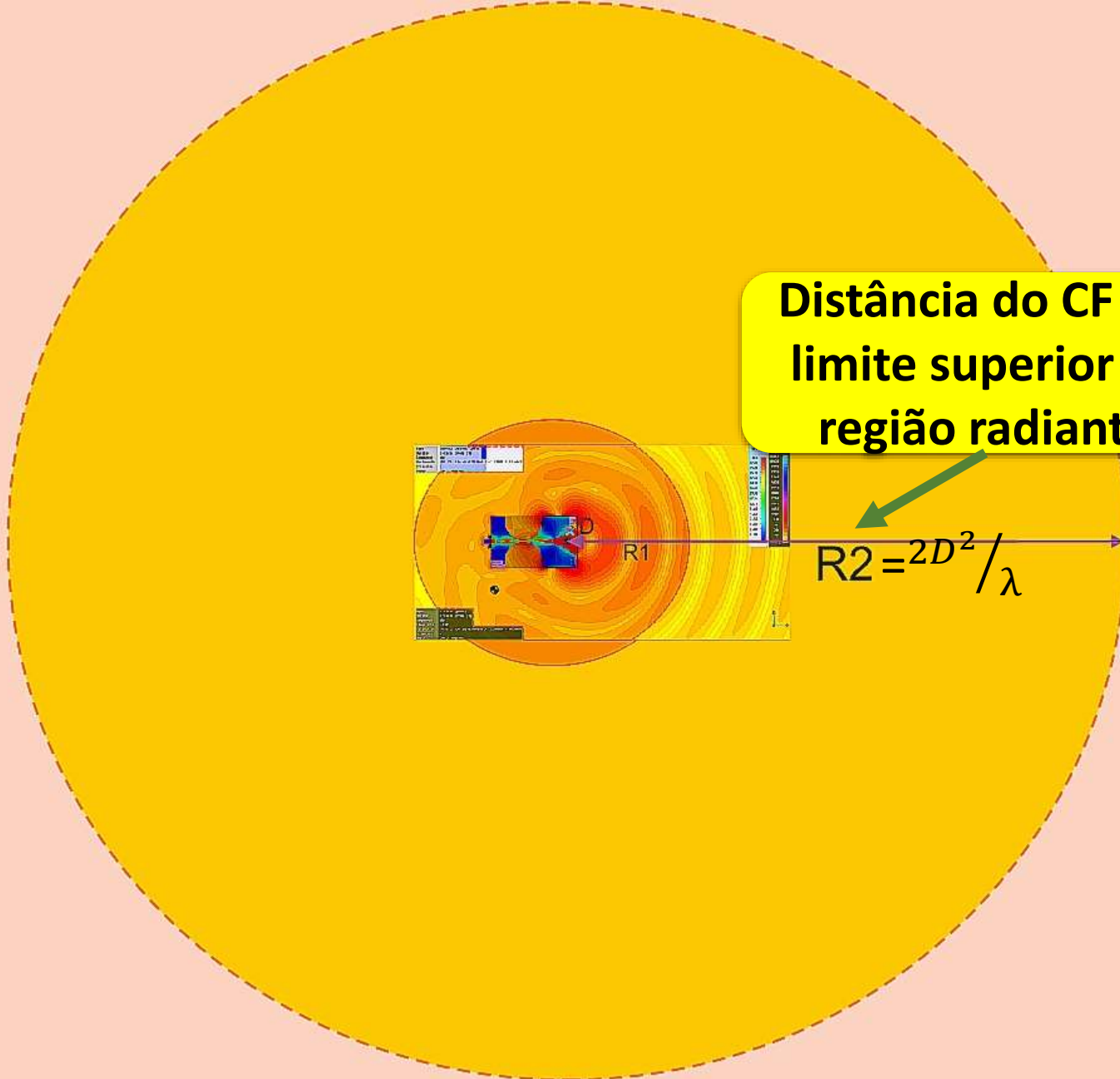
Instituto
Labo
Micro-ondas
Certificado C

ZOOM OUT



2012-2015



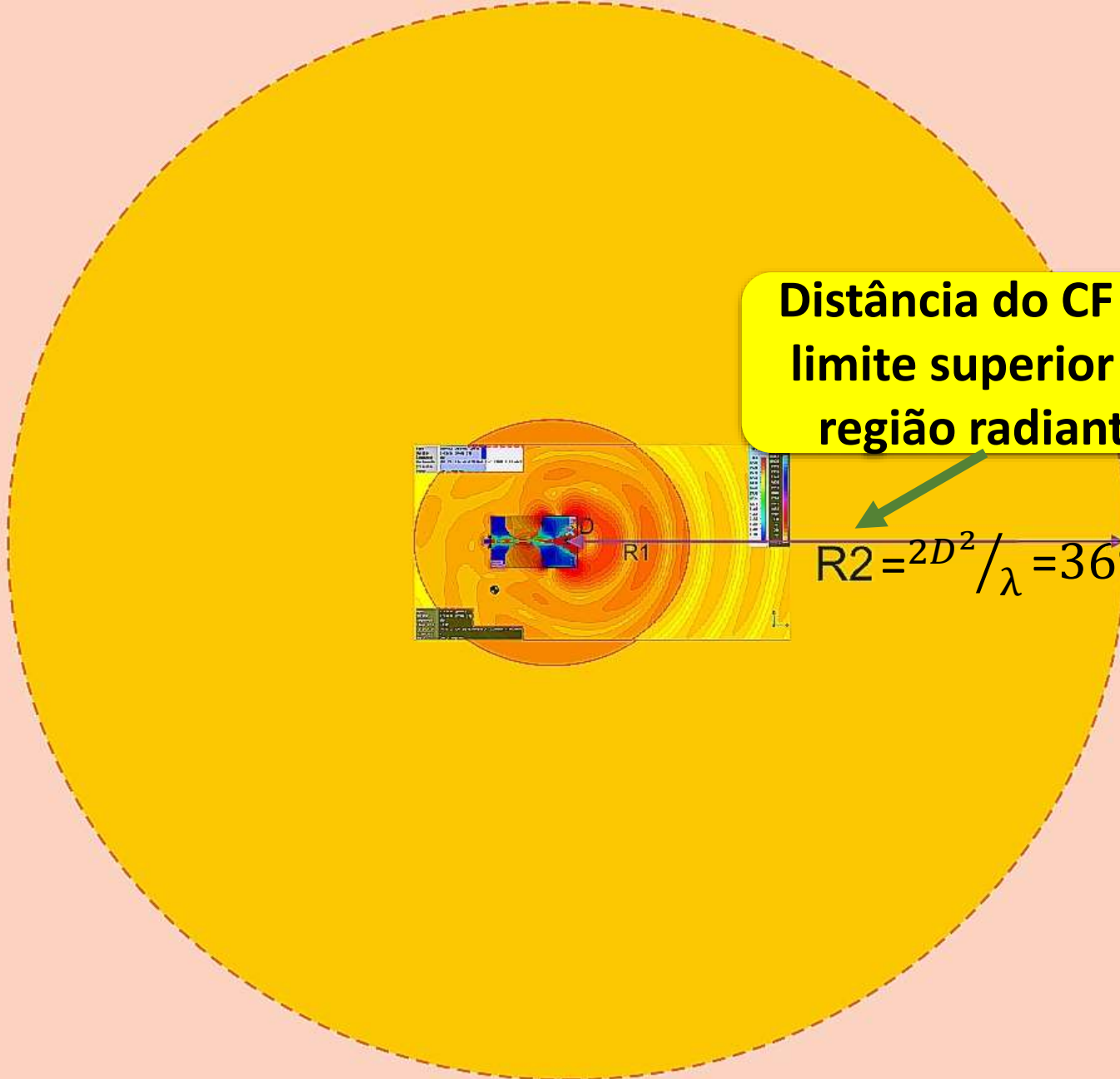


Distância do CF e o limite superior da região radiante

$$R2 = \frac{2D^2}{\lambda}$$

2012-2015

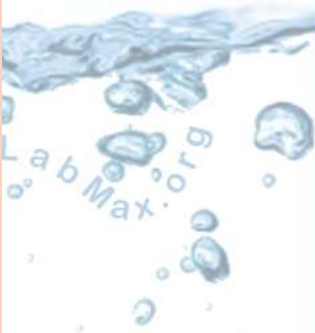




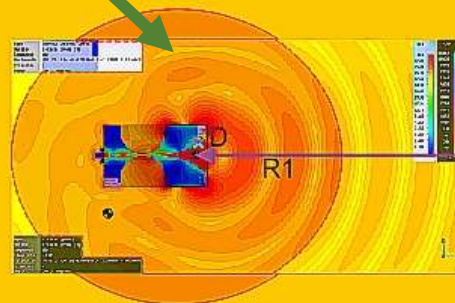
Distância do CF e o limite superior da região radiante

$$R2 = \frac{2D^2}{\lambda} = 369mm$$

2012-2015



Região reativa de campo próximo



$R2=369mm$

Região Radiante (Fresnel) de campo próximo

Região (Fraunhofer) de campo distante

2012-2015





Tomografia por Micro-ondas

Imagens através de Micro-ondas de campo próximo

www.LabMax.org

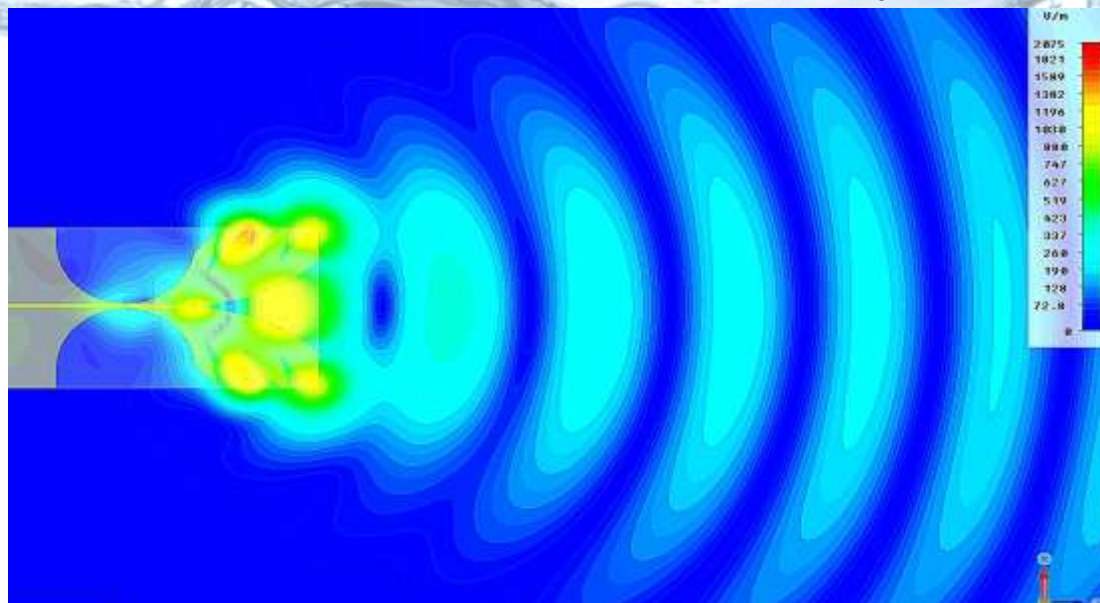


Diagrama de distribuição de campos elétricos no plano x-z, a 6 GHz da Palm Tree AVA-974.

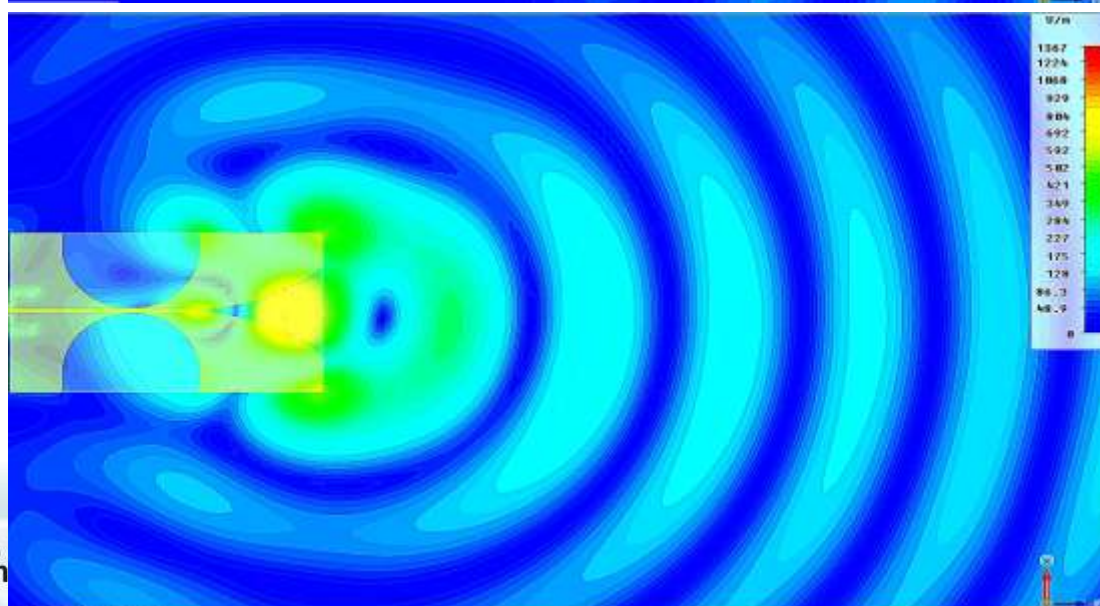
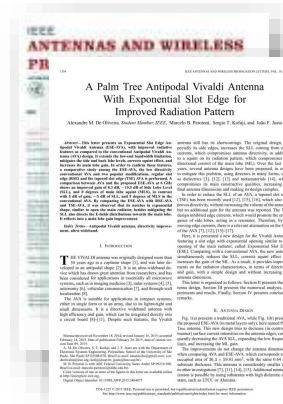


Diagrama de distribuição de campos elétricos no plano x-z, a 6 GHz da AVA-974.

2012-2015





Tomografia por Micro-ondas

Imagens através de Micro-ondas de campo próximo

www.LabMax.org

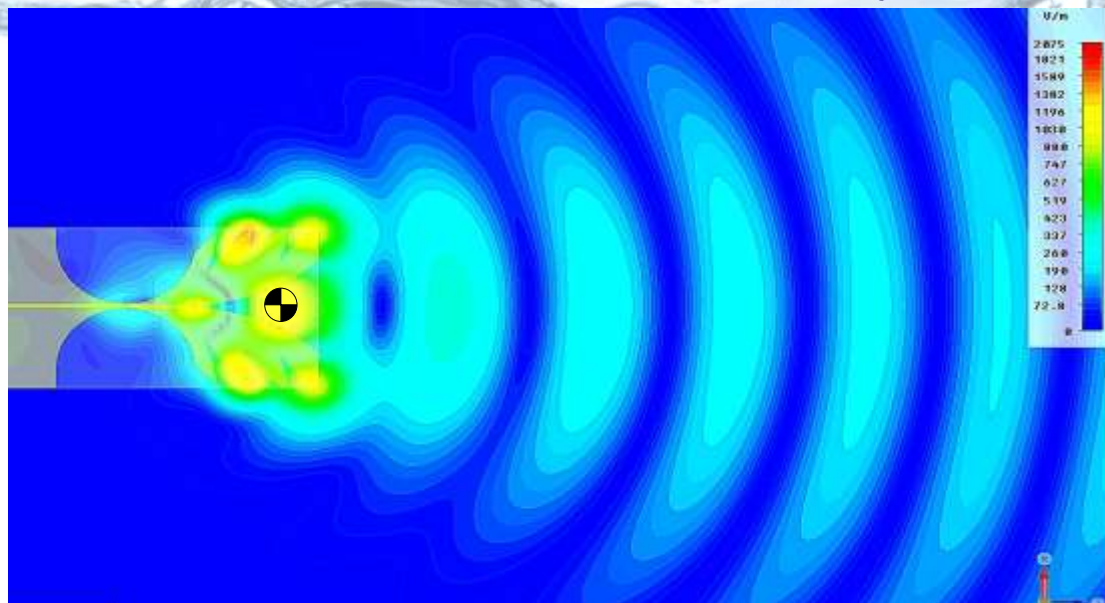


Diagrama de distribuição de campos elétricos no plano x-z, a 6 GHz da Palm Tree AVA-974.

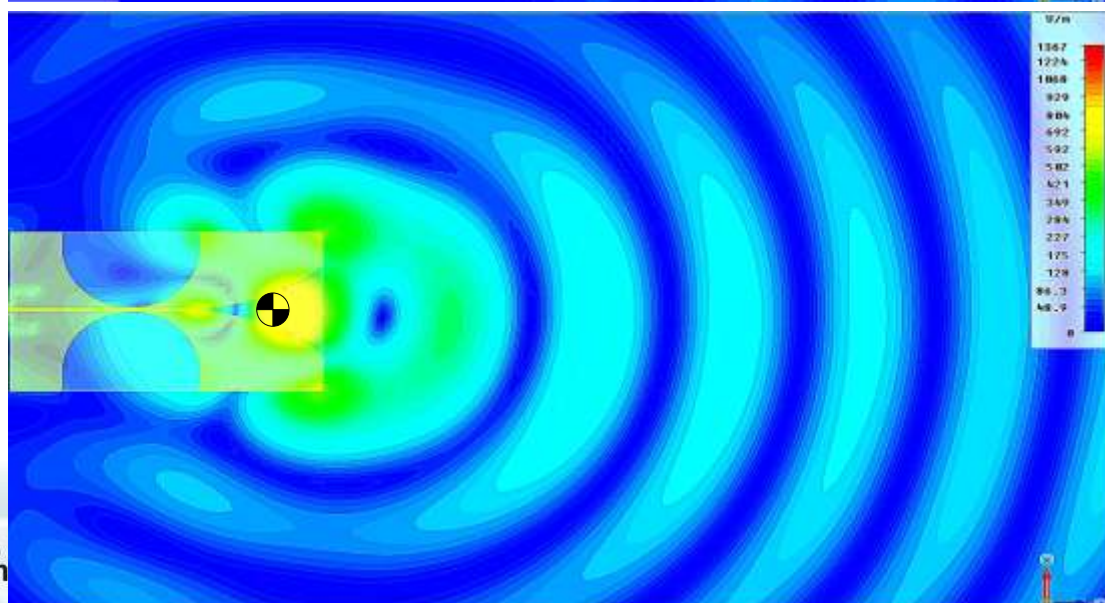


Diagrama de distribuição de campos elétricos no plano x-z, a 6 GHz da AVA-974.

2012-2015





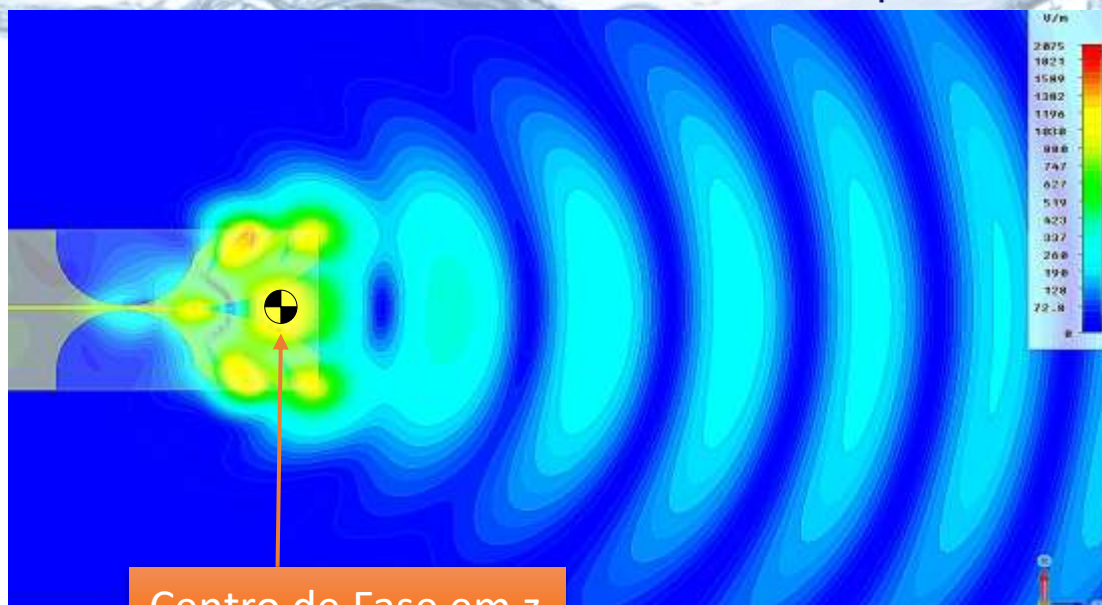
Fomento a Pesquisa PRP do
 IFSP via Edital n.º 823/2018



Tomografia por Micro-ondas

Imagens através de Micro-ondas de campo próximo

www.LabMax.org



Centro de Fase em z

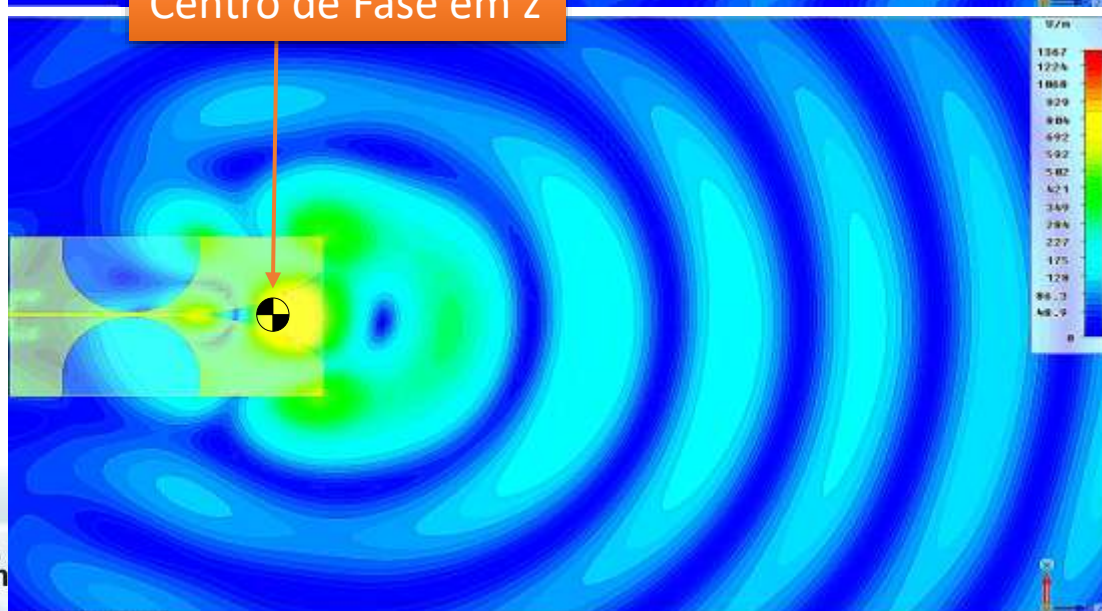


Diagrama de distribuição de campos elétricos no plano x-z, a 6 GHz da Palm Tree AVA-974.

Diagrama de distribuição de campos elétricos no plano x-z, a 6 GHz da AVA-974.

2012-2015





Fomento a Pesquisa PRP do
 IFSP via Edital n.º 823/2018



Tomografia por Micro-ondas

Imagens através de Micro-ondas de campo próximo

www.LabMax.org

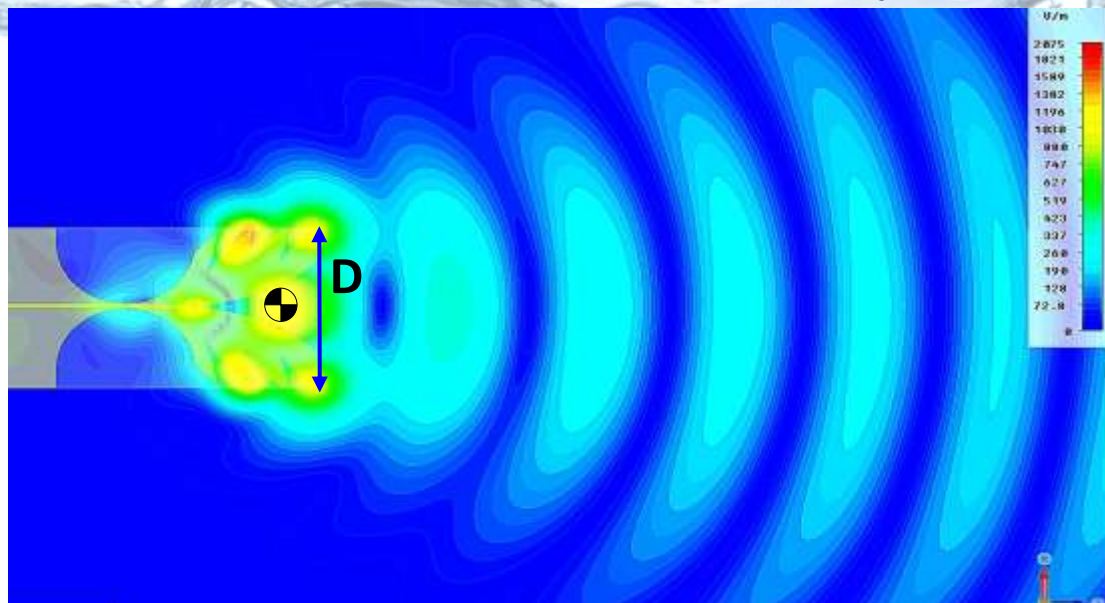


Diagrama de distribuição de campos elétricos no plano x-z, a 6 GHz da Palm Tree AVA-974.

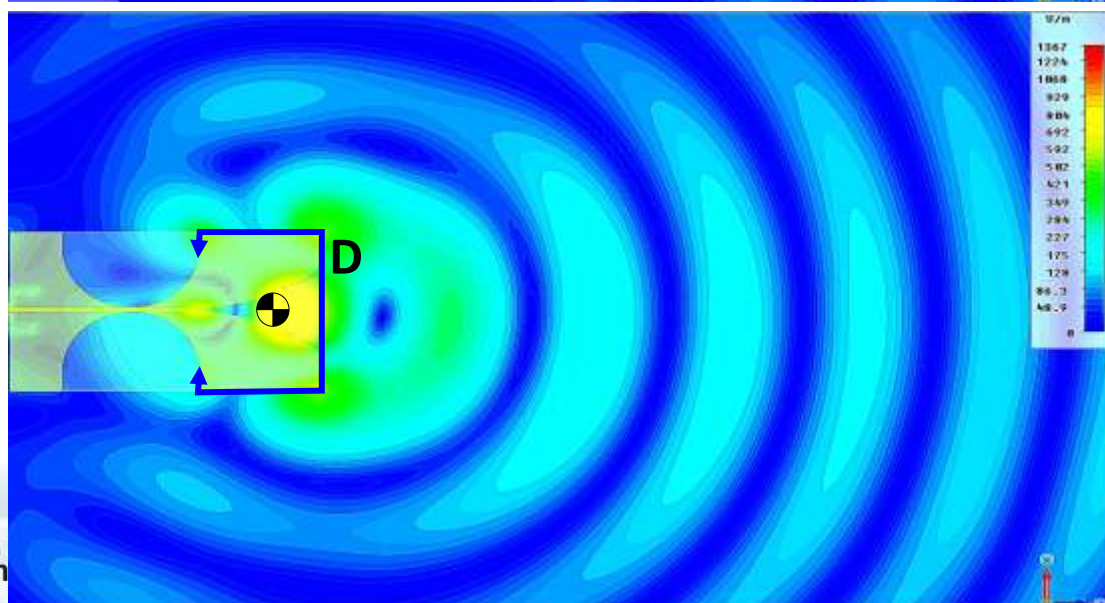


Diagrama de distribuição de campos elétricos no plano x-z, a 6 GHz da AVA-974.

2012-2015





Tomografia por Micro-ondas

Imagens através de Micro-ondas de campo próximo

www.LabMax.org

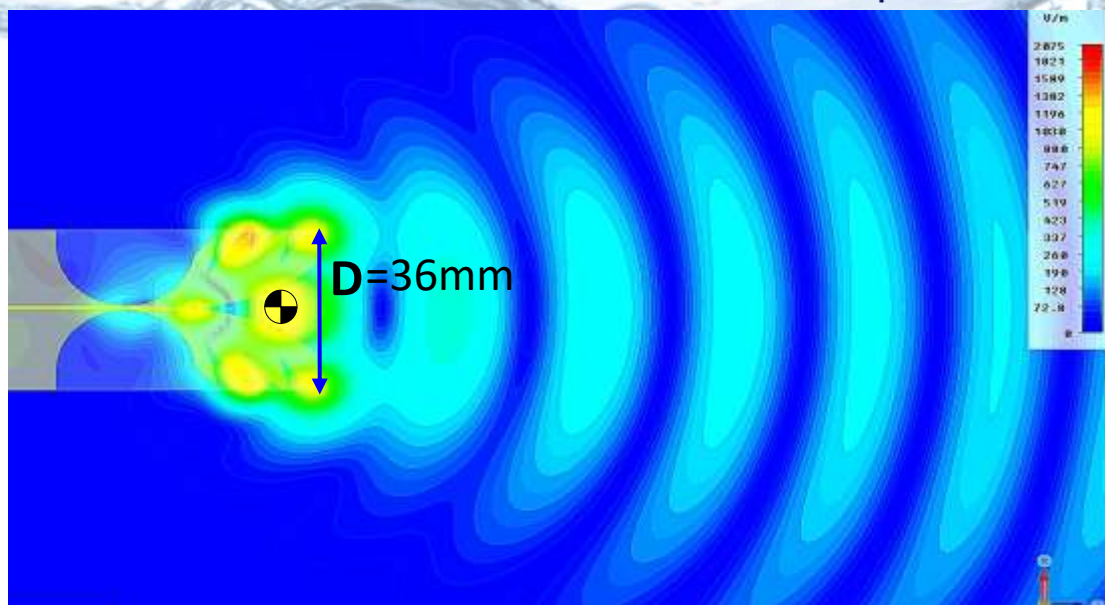


Diagrama de distribuição de campos elétricos no plano x-z, a 6 GHz da Palm Tree AVA-974.

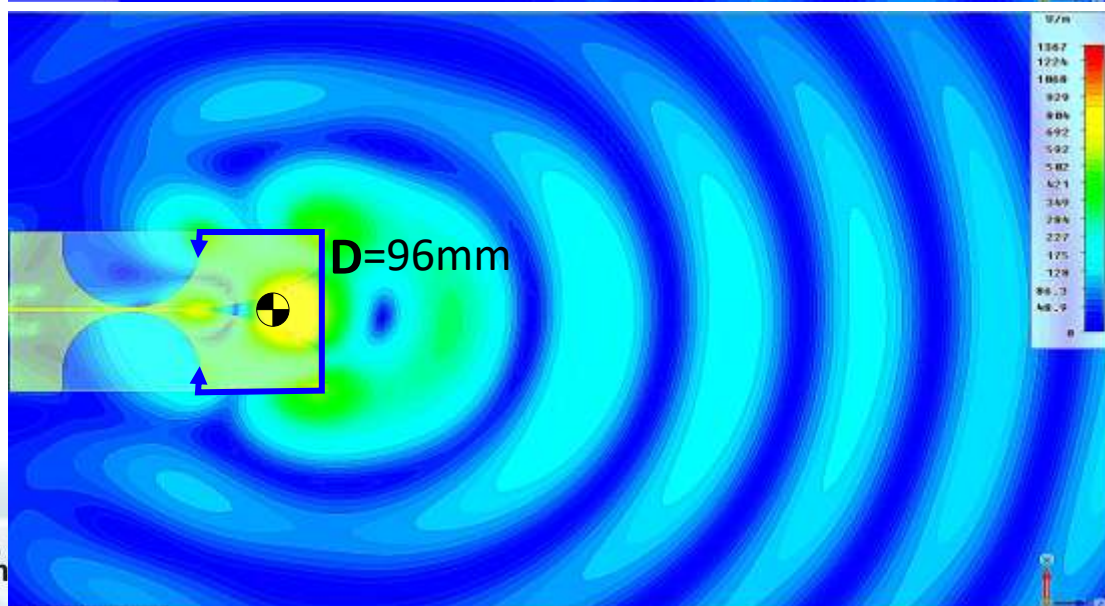


Diagrama de distribuição de campos elétricos no plano x-z, a 6 GHz da AVA-974.

2012-2015





Tomografia por Micro-ondas

Imagens através de Micro-ondas de campo próximo

www.LabMax.org

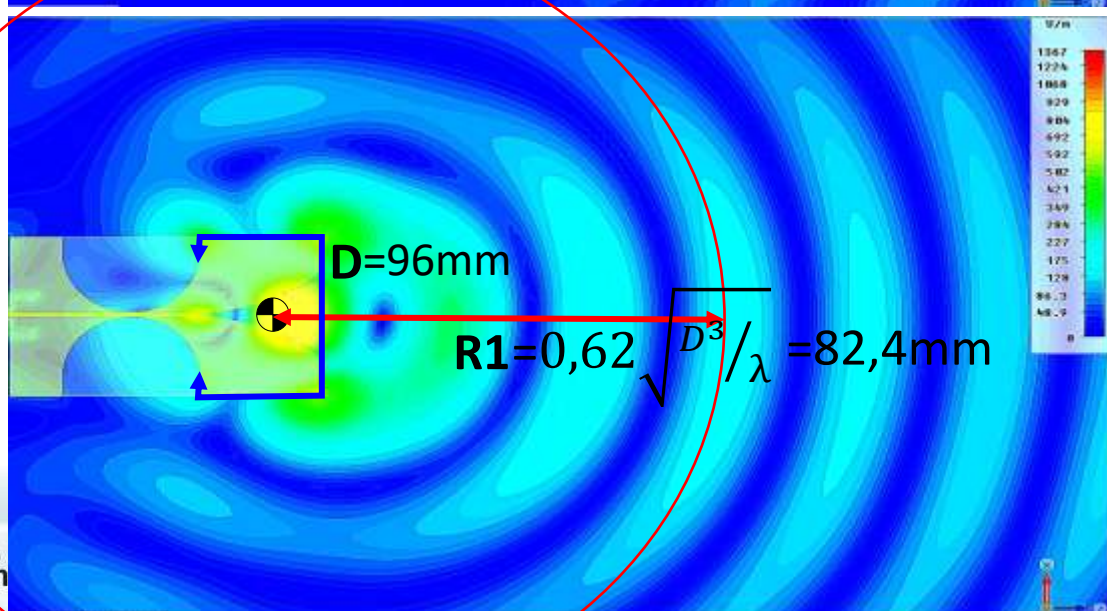
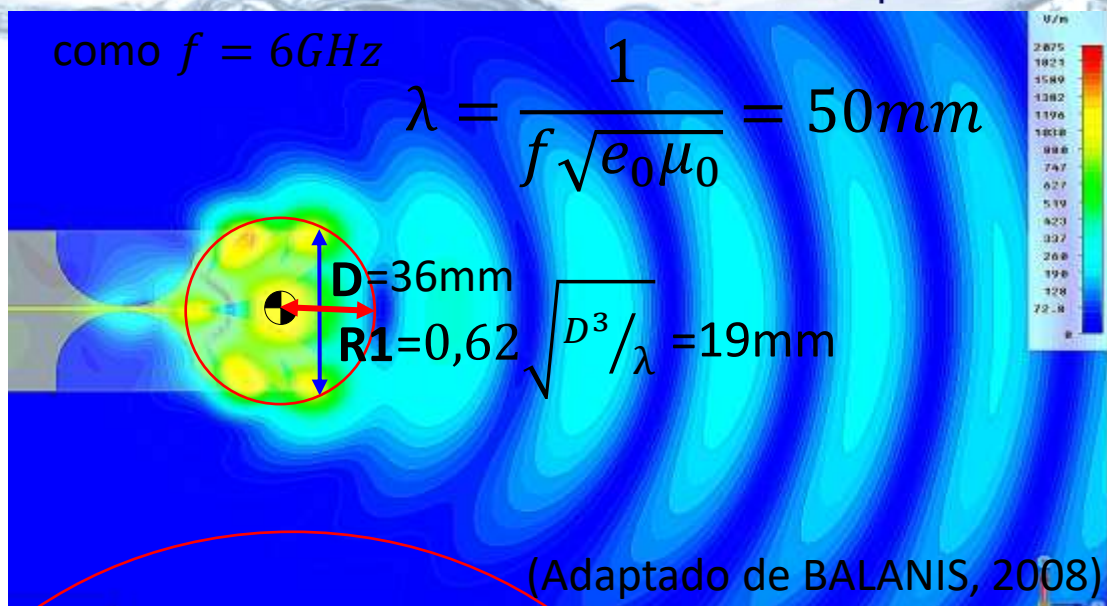


Diagrama de distribuição de campos elétricos no plano x-z, a 6 GHz da Palm Tree AVA-974.

Diagrama de distribuição de campos elétricos no plano x-z, a 6 GHz da AVA-974.

2012-2015





Fomento a Pesquisa PRP do IFSP via Edital nº 823/2018



Tomografia por Micro-ondas

Imagens através de Micro-ondas de campo próximo

www.LabMax.org

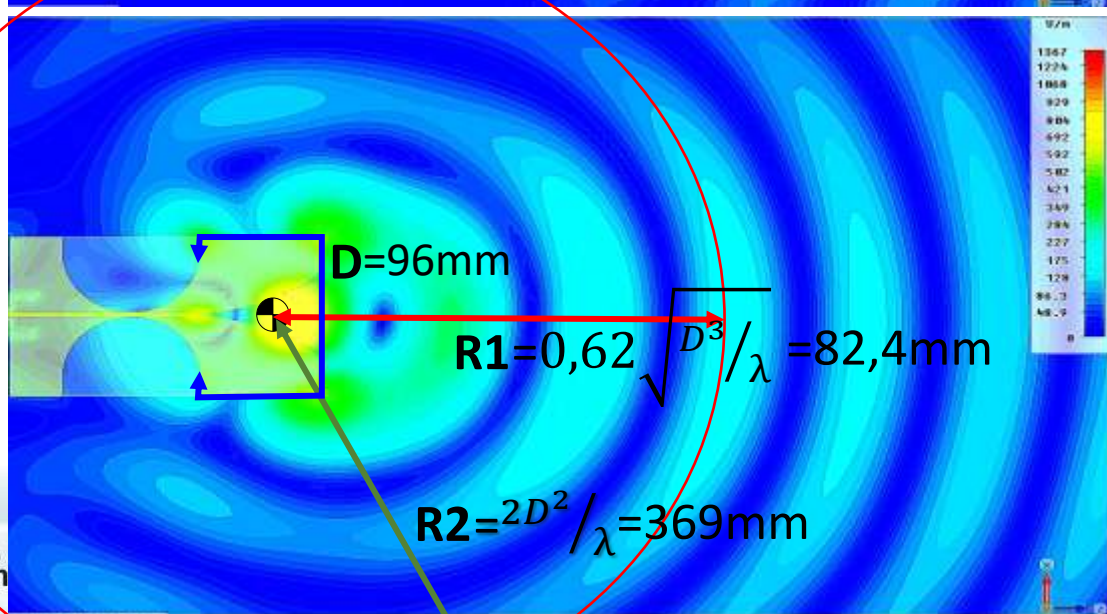
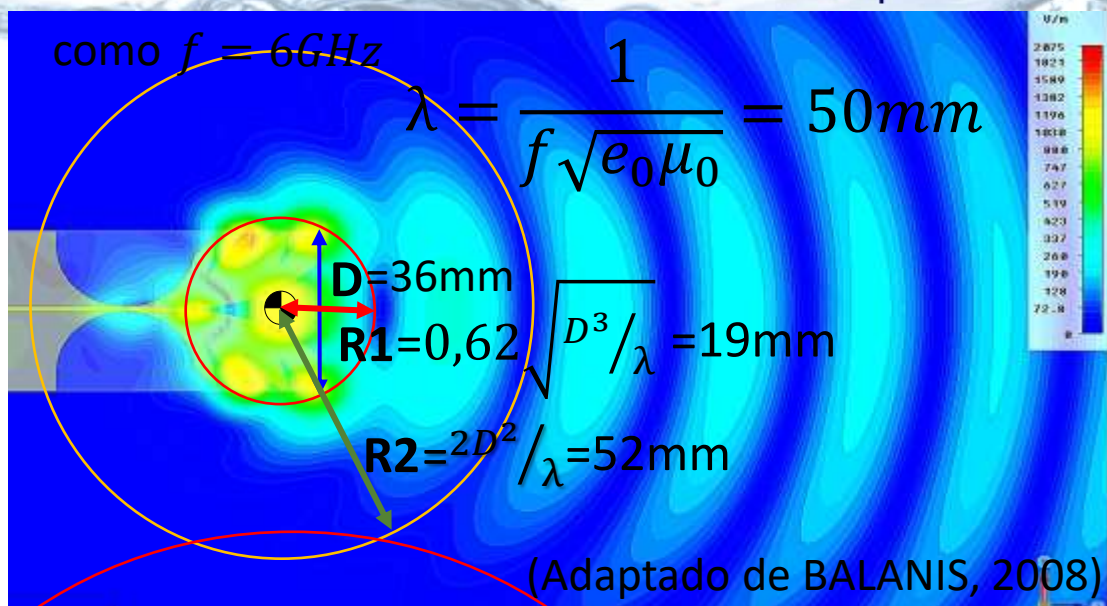


Diagrama de distribuição de campos elétricos no plano x-z, a 6 GHz da Palm Tree AVA-974.

Diagrama de distribuição de campos elétricos no plano x-z, a 6 GHz da AVA-974.

2012-2015





Tomografia por Micro-ondas

Imagens através de Micro-ondas de campo próximo

www.LabMax.org

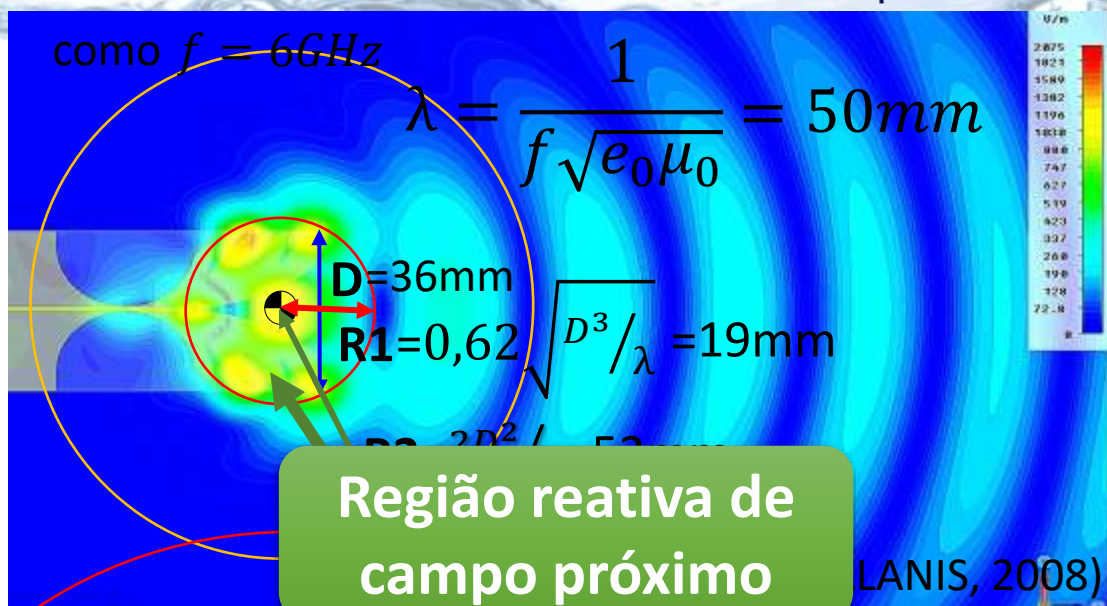


Diagrama de distribuição de campos elétricos no plano x-z, a 6 GHz da Palm Tree AVA-974.

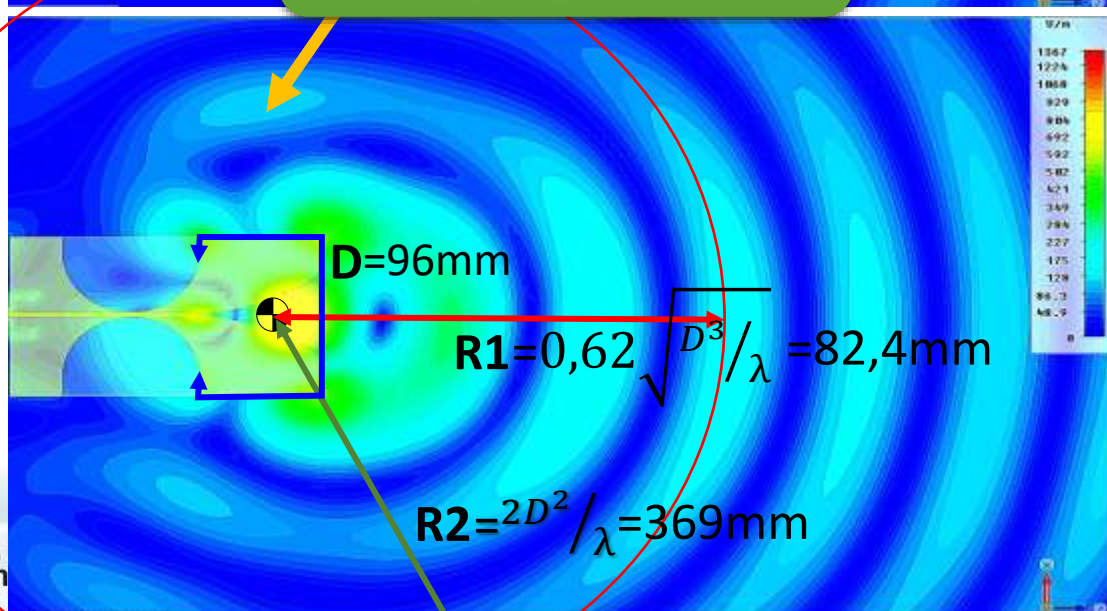


Diagrama de distribuição de campos elétricos no plano x-z, a 6 GHz da AVA-974.

2012-2015





Tomografia por Micro-ondas

Imagens através de Micro-ondas de campo próximo

www.LabMax.org

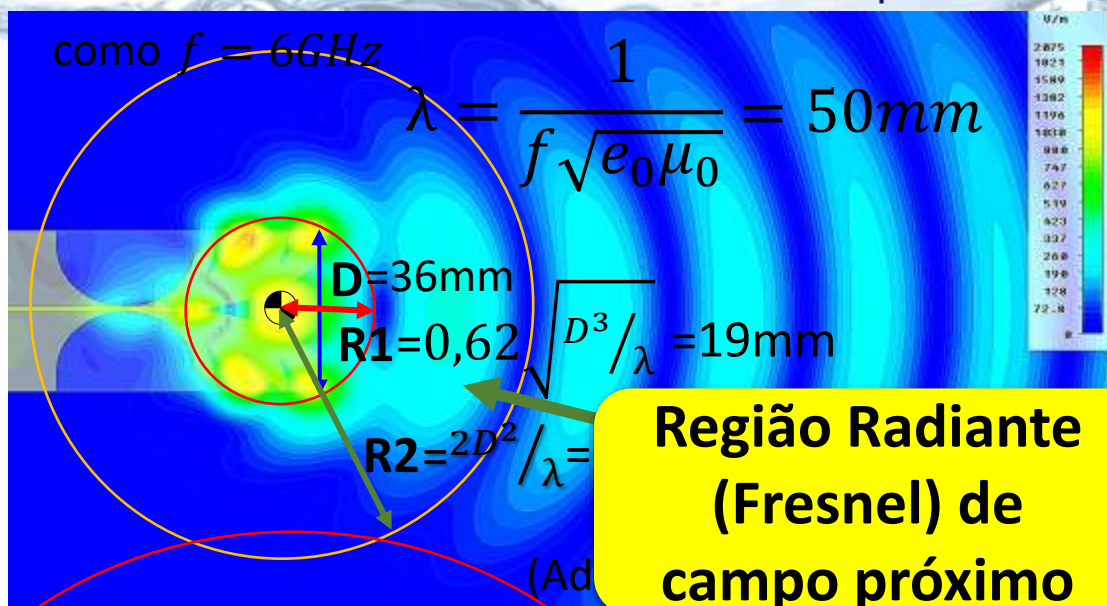


Diagrama de distribuição de campos elétricos no plano x-z, a 6 GHz da Palm Tree AVA-974.

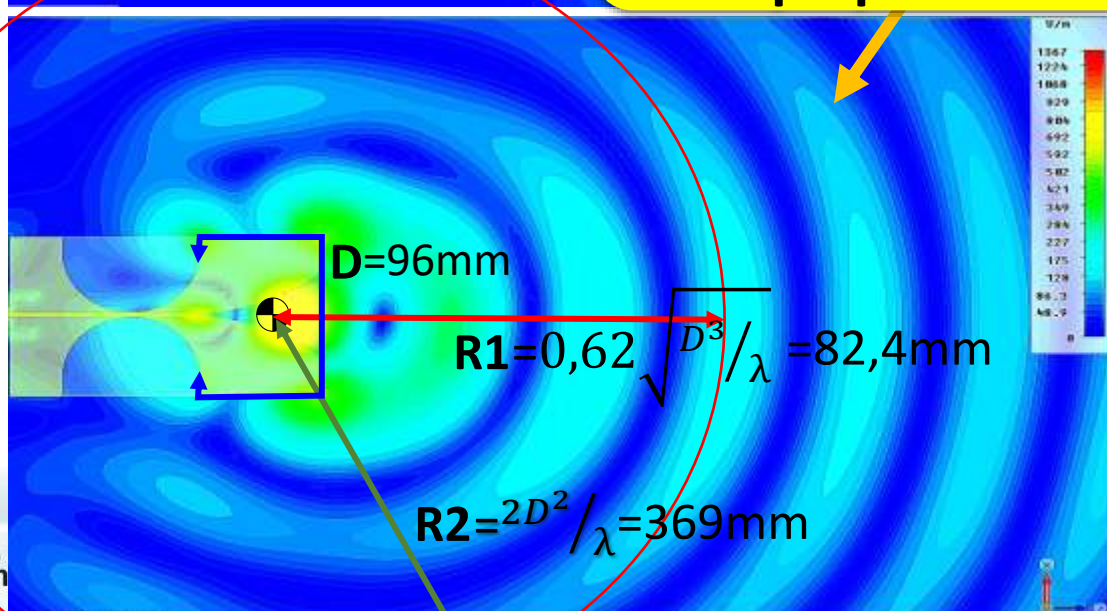


Diagrama de distribuição de campos elétricos no plano x-z, a 6 GHz da AVA-974.

2012-2015



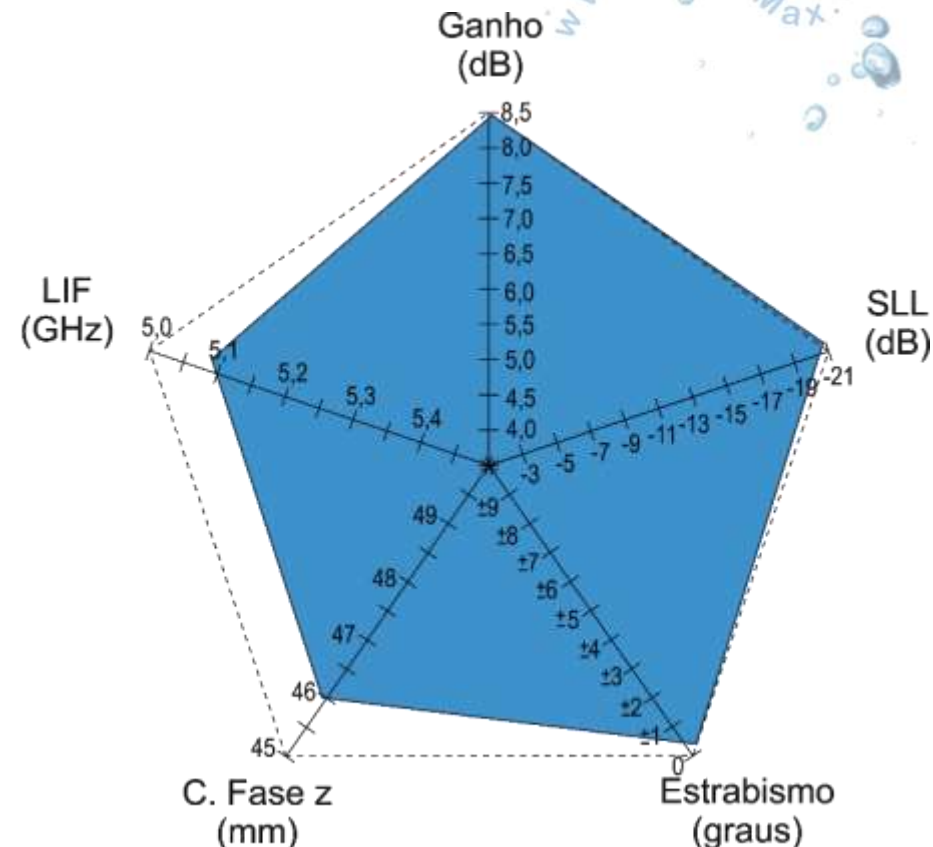
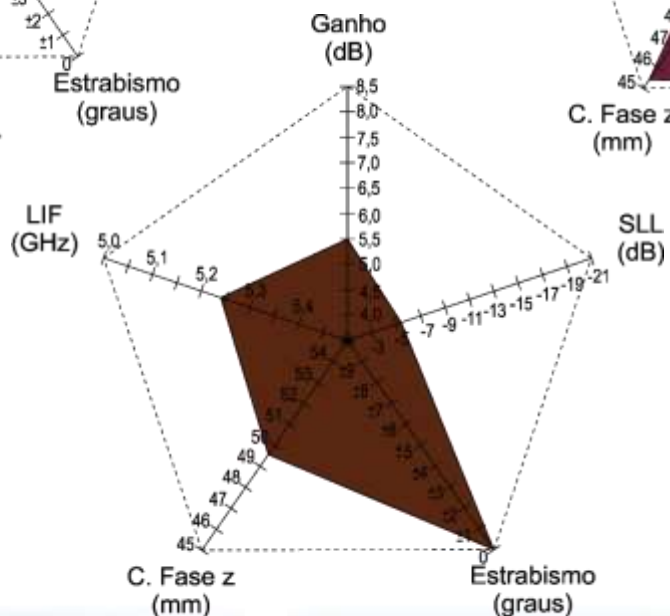
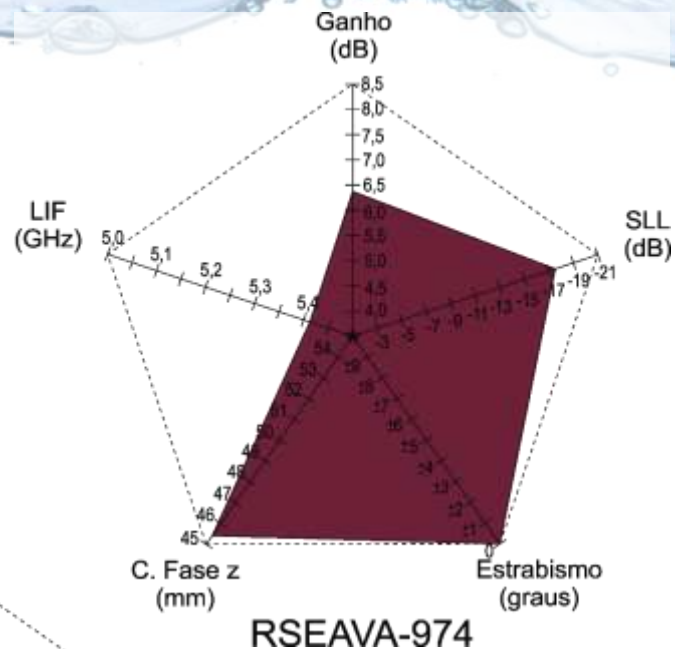
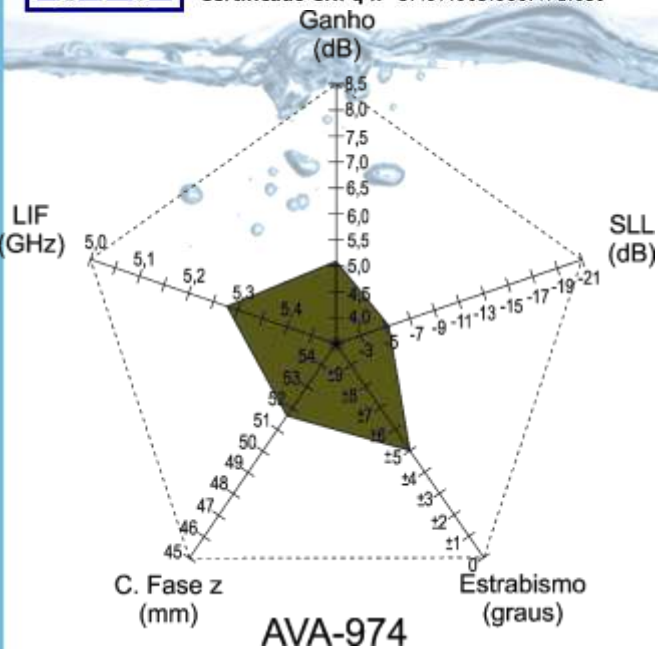


Fomento a Pesquisa PRP do
 IFSP via Edital nº. 823/2018



Tomografia por Micro-ondas

Imagens através de Micro-ondas de campo próximo



2012-2015



TSEAVA-974



Instituto Federal de São Paulo
Laboratório Maxwell
 Micro-ondas e Eletromagnetismo Aplicado
 Certificado CNPq nº 5.497.663.866.471.659



LittleMax
 e a luta contra o Câncer
 Cerebral Infantil

Fomento a Pesquisa PRP do
 IFSP via Edital n.º 823/2018



Academia Cearense
 de Matemática - ACM

Tomografia por Micro-ondas

Imagens através de Micro-ondas de campo próximo

Praia Grande - SP



MINISTÉRIO DA
EDUCAÇÃO

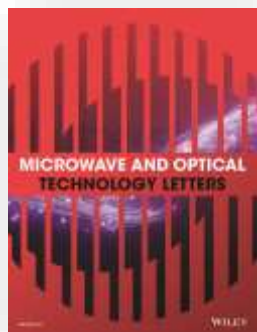


Dr. Alexandre Manicoba de Oliveira
amanicoba@ifsp.edu.br



Tomografia por Micro-ondas

Imagens através de Micro-ondas de campo próximo



2016-2017

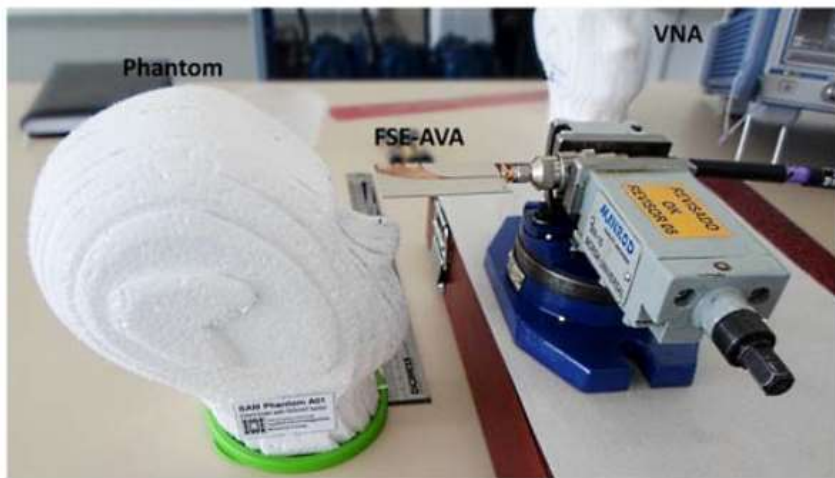


Figure 11 Real-world scenario of the SAM phantom imaged by the FSE-AVA.. [Color figure can be viewed at wileyonlinelibrary.com]



© 2016 Wiley Periodicals, Inc.
 DOI 10.1002/mop

A HIGH DIRECTIVE KOCH FRACTAL VIVALDI ANTENNA DESIGN FOR MEDICAL NEAR-FIELD MICROWAVE IMAGING APPLICATIONS

Alexandre M. de Oliveira,¹ João F. Justo,²
 Marcelo B. Perotoni,³ Sérgio T. Kofuji,² Alfredo G. Neto,⁴
 Regis C. Bueno,¹ and Henri Baudrand⁵

¹Maxwell Institute of Microwaves and Applied Electromagnetism, Federal Laboratory of São Paulo, CEP 08673-010, Suzano, SP, Brazil;
 Corresponding author: a.m.deoliveira@ieee.org
²Department of Electronic Systems Engineering, Polytechnic School of the University of São Paulo, CEP 05508-900, São Paulo, SP, Brazil
³ABC Federal University, CEP 09210-180, Santo André, SP, Brazil
⁴Group of Telecommunications and Applied Electromagnetism at Federal Institute of Paraíba
⁵National Institute Polytechnic of Toulouse, Toulouse, France

Received 19 July 2016

ABSTRACT: We present a new fractal slot edge antipodal Vivaldi antenna (AVA). When compared to a conventional AVA, it simultaneously extends the low-end bandwidth limitation, mitigates the side lobe level, and increases the main lobe gain. © 2016 Wiley Periodicals, Inc. Microwave Opt Technol Lett 59:337–346, 2017; View this article online at wileyonlinelibrary.com. DOI 10.1002/mop.30293



Tomografia por Micro-ondas

Imagens através de Micro-ondas de campo próximo

www.LabMax.org

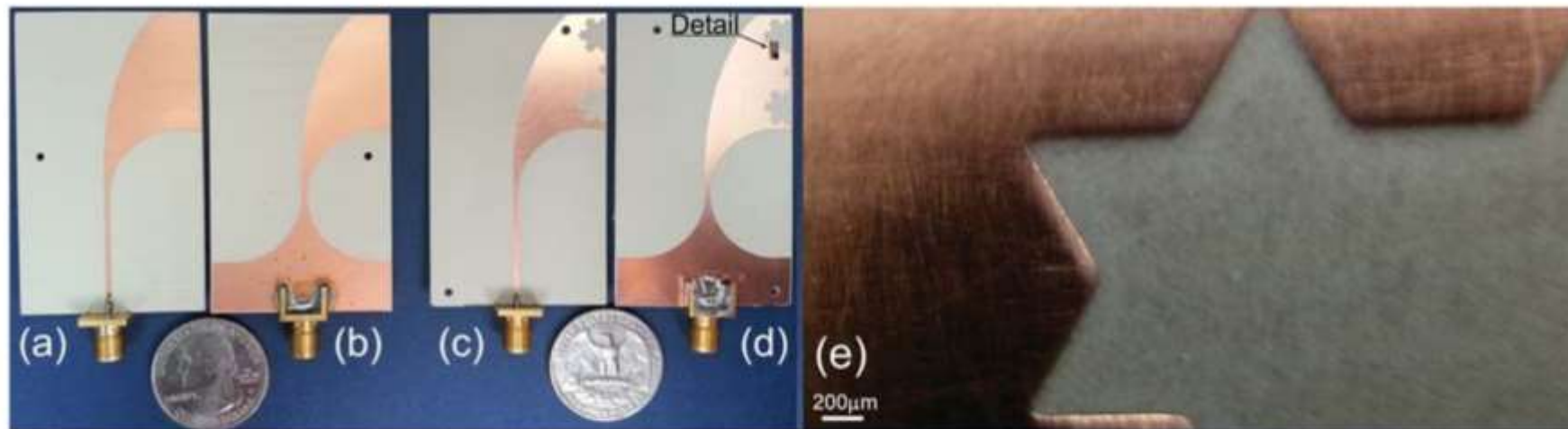


Figure 1 AVA (a, b) and FSE-AVA (c, d) photograph, top view on the left and bottom view on the right. (e) Detail of the third generation of the fractal. [Color figure can be viewed at wileyonlinelibrary.com]

2016-2017





Tomografia por Micro-ondas

Imagens através de Micro-ondas de campo próximo

www.LabMax.org

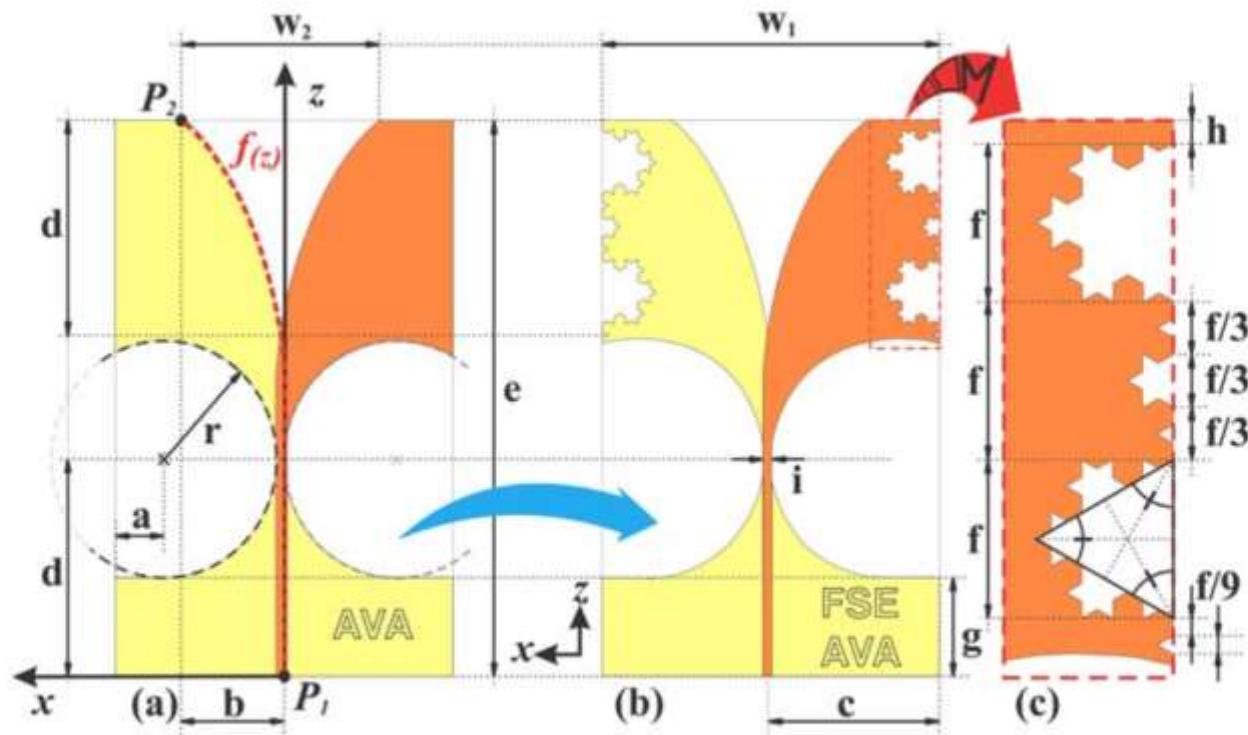


Figure 2 Design and parameters of antenna in xz -plane: (a) reference AVA, (b) proposed FSE-AVA, (c) details of the fractal design. [Color figure can be viewed at wileyonlinelibrary.com]

2016-2017





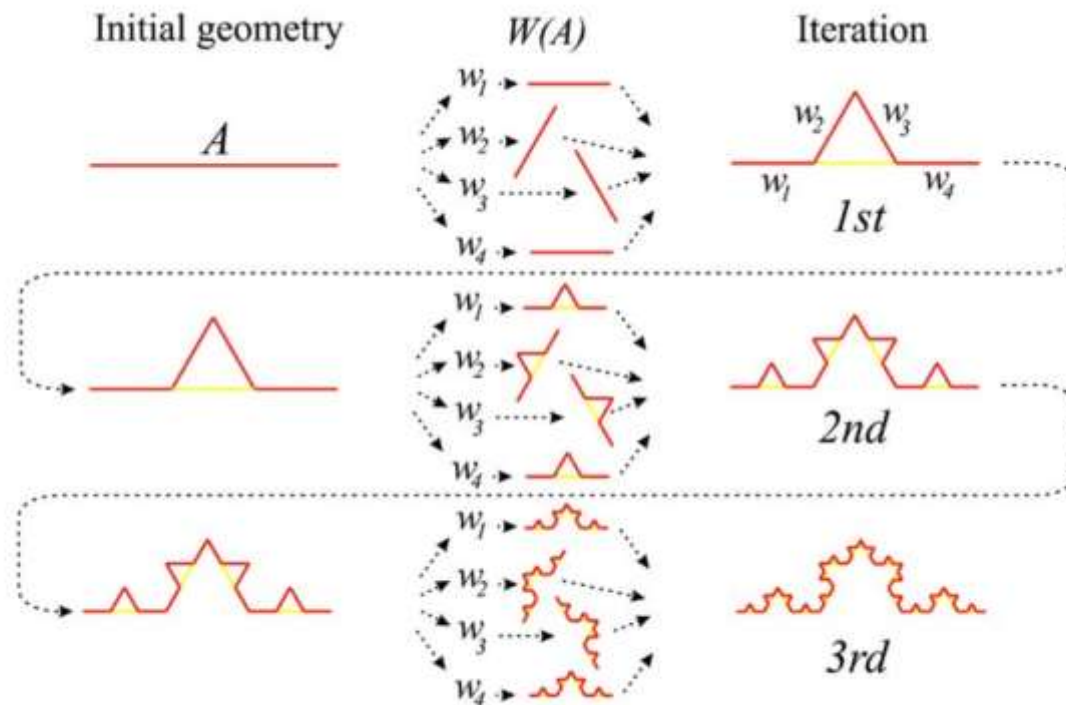
Fomento a Pesquisa PRP do
 IFSP via Edital n° 823/2018



Tomografia por Micro-ondas

Imagens através de Micro-ondas de campo próximo

www.LabMax.org



$$w(A) = \cup_{n=1}^4 w_n(A) \quad (1)$$

$$w_1 \begin{pmatrix} x \\ y \end{pmatrix} = \begin{pmatrix} 1/3 & 0 \\ 0 & 1/3 \end{pmatrix} \begin{pmatrix} x \\ y \end{pmatrix} \quad (2)$$

$$w_2 \begin{pmatrix} x \\ y \end{pmatrix} = \begin{pmatrix} \cos 60^\circ/3 & -\sin 60^\circ/3 \\ -\sin 60^\circ/3 & \cos 60^\circ/3 \end{pmatrix} \begin{pmatrix} x \\ y \end{pmatrix} + \begin{pmatrix} 1/3 \\ 0 \end{pmatrix} \quad (3)$$

$$w_3 \begin{pmatrix} x \\ y \end{pmatrix} = \begin{pmatrix} \cos 60^\circ/3 & -\sin 60^\circ/3 \\ -\sin 60^\circ/3 & \cos 60^\circ/3 \end{pmatrix} \begin{pmatrix} x \\ y \end{pmatrix} + \begin{pmatrix} 1/2 \\ \sin 60^\circ/2 \end{pmatrix} \quad (4)$$

$$w_4 \begin{pmatrix} x \\ y \end{pmatrix} = \begin{pmatrix} 1/3 & 0 \\ 0 & 1/3 \end{pmatrix} \begin{pmatrix} x \\ y \end{pmatrix} + \begin{pmatrix} 2/3 \\ 0 \end{pmatrix} \quad (5)$$

Figure 3 Three iterations of the Koch curve IFS from the initial geometry A. [Color figure can be viewed at wileyonlinel]

2016-2017





Tomografia por Micro-ondas

Imagens através de Micro-ondas de campo próximo

www.LabMax.org

2016-2017

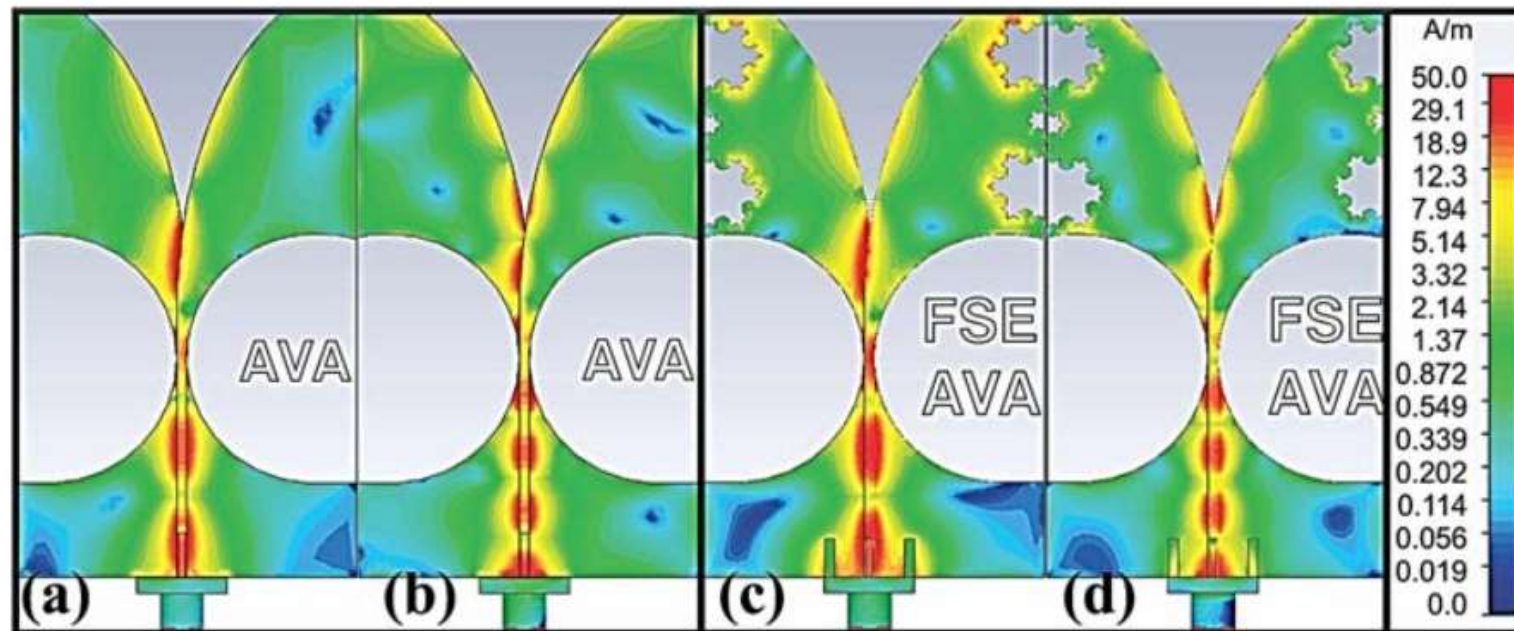


Figure 7 Surface current of (a) AVA at 7 GHz, (b) AVA at 11 GHz, (c) FSE-AVA at 7 GHz, and (d) FSE-AVA at 11 GHz. [Color figure can be viewed at wileyonlinelibrary.com]



Tomografia por Micro-ondas

Imagens através de Micro-ondas de campo próximo

www.LabMax.org

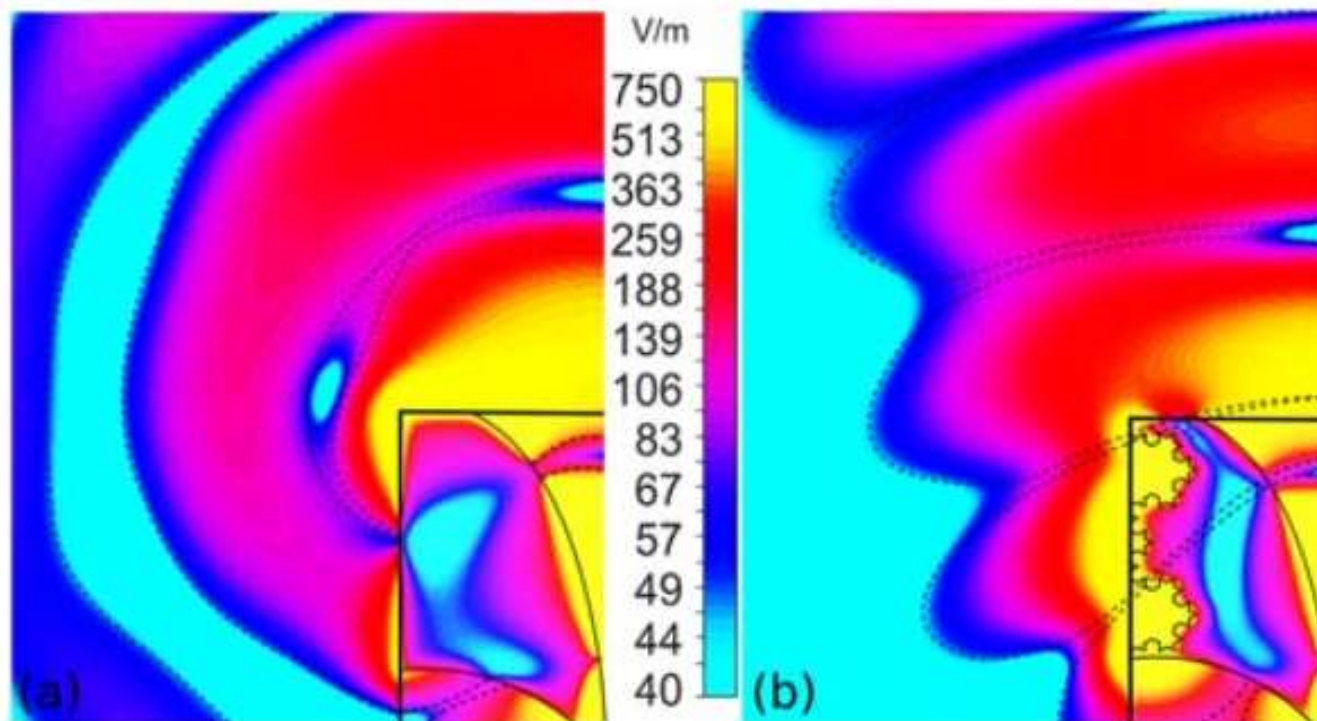


Figure 8 *E*-field in *xz*-plane at 7 GHz for (a) AVA and (b) FSE-AVA.
 [Color figure can be viewed at wileyonlinelibrary.com]

2016-2017





Tomografia por Micro-ondas

Imagens através de Micro-ondas de campo próximo

www.LabMax.org

2016-2017

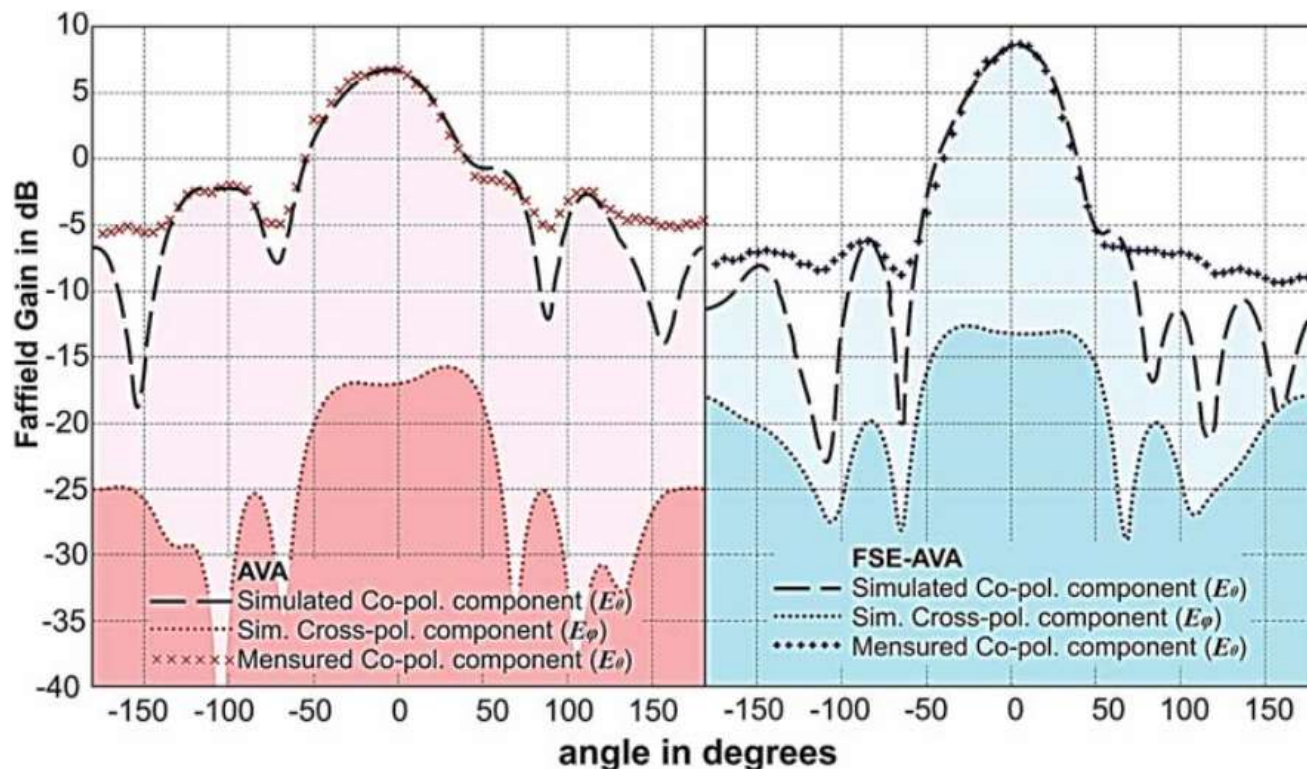


Figure 9 Measured and simulated gain pattern at 7 GHz of the AVA (left) and FSE-AVA (right). [Color figure can be viewed at wileyonlinelibrary.com]



Tomografia por Micro-ondas

Imagens através de Micro-ondas de campo próximo

www.LabMax.org

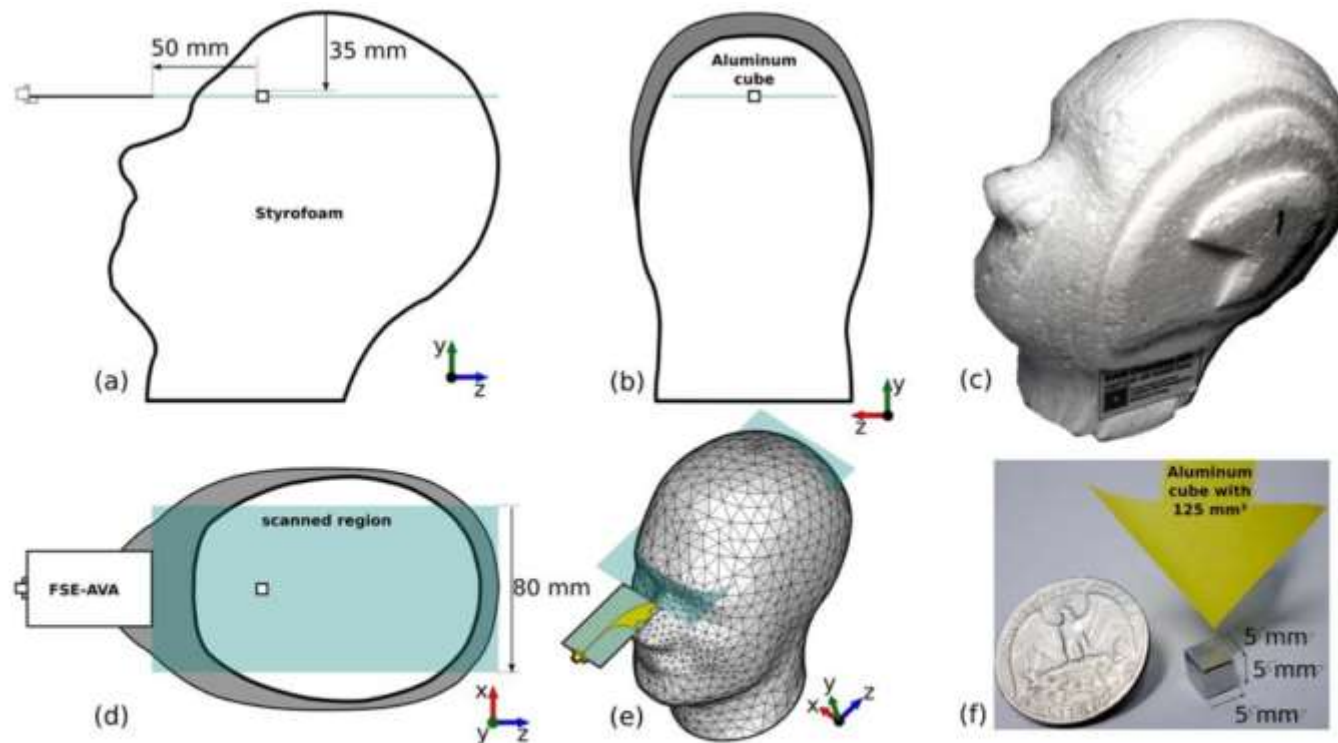


Figure 12 Testing environment consists of a non-realistic infant Phantom with the addition of an aluminum cube (target) with volume of 125 mm^3 . Detail of the target location in side view with a longitudinal section (a), in cross-sectional front view (b), Phantom photograph produced, cube detail in the top view in section (d), 3D illustration of the position FSE- AVA in front of the Phantom with the detail of the scanned area (e), and finally, the cube used as a target in detail (f). [Color figure can be viewed at wileyonlinelibrary.com]

2016-2017





Tomografia por Micro-ondas

Imagens através de Micro-ondas de campo próximo

www.LabMax.org

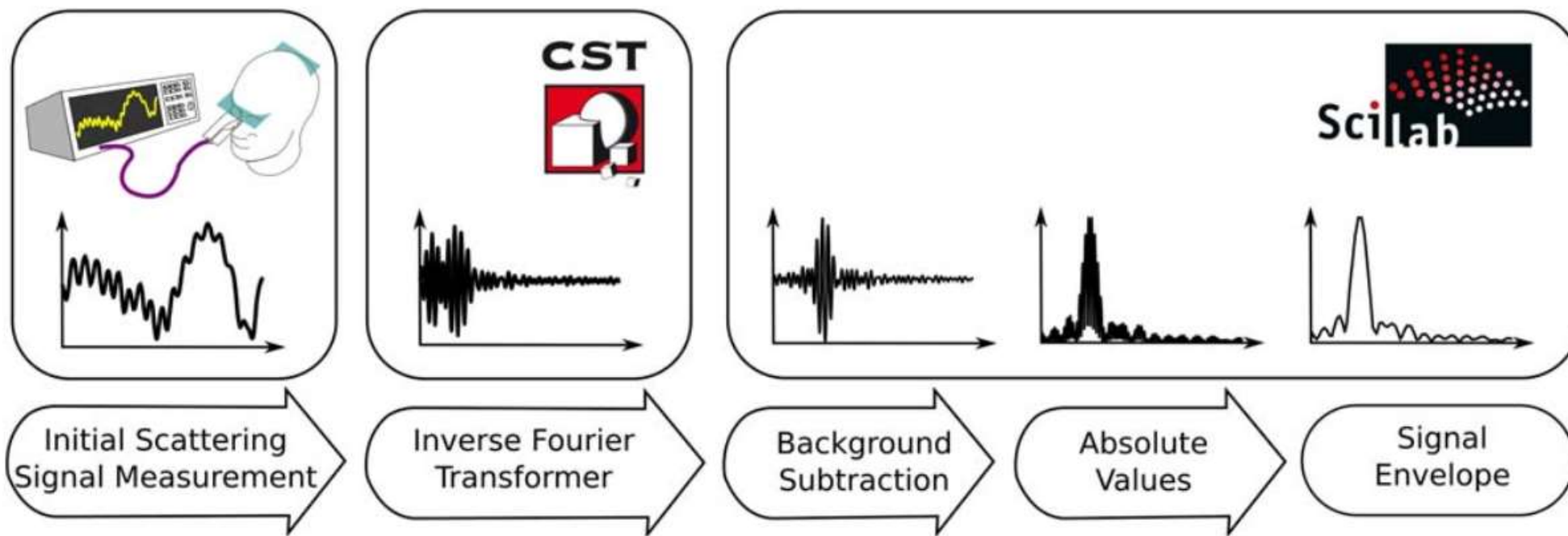


Figure 15 Data processing methodology for FSE-AVA near-field microwave imaging conceptual proof. [Color figure can be viewed at wileyonlinelibrary.com]

2016-2017





Tomografia por Micro-ondas

Imagens através de Micro-ondas de campo próximo

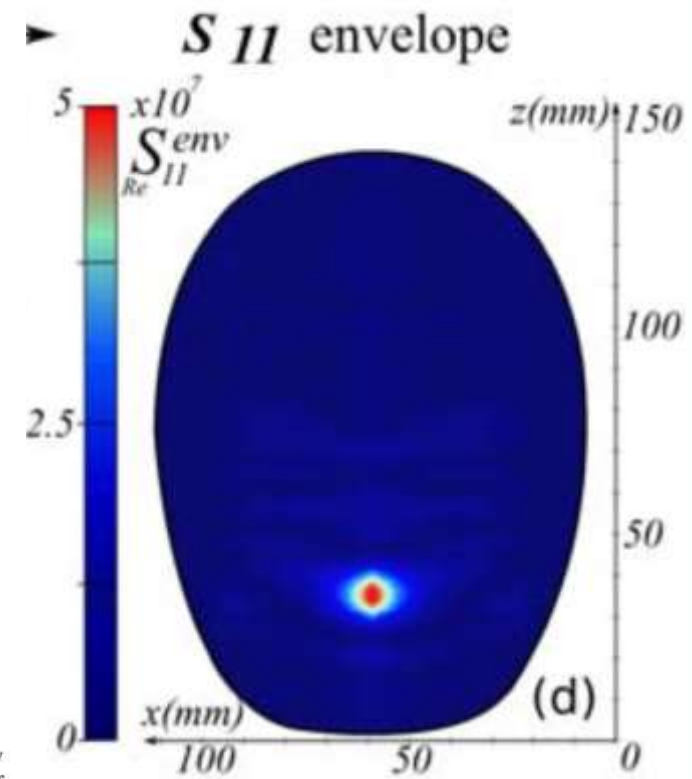
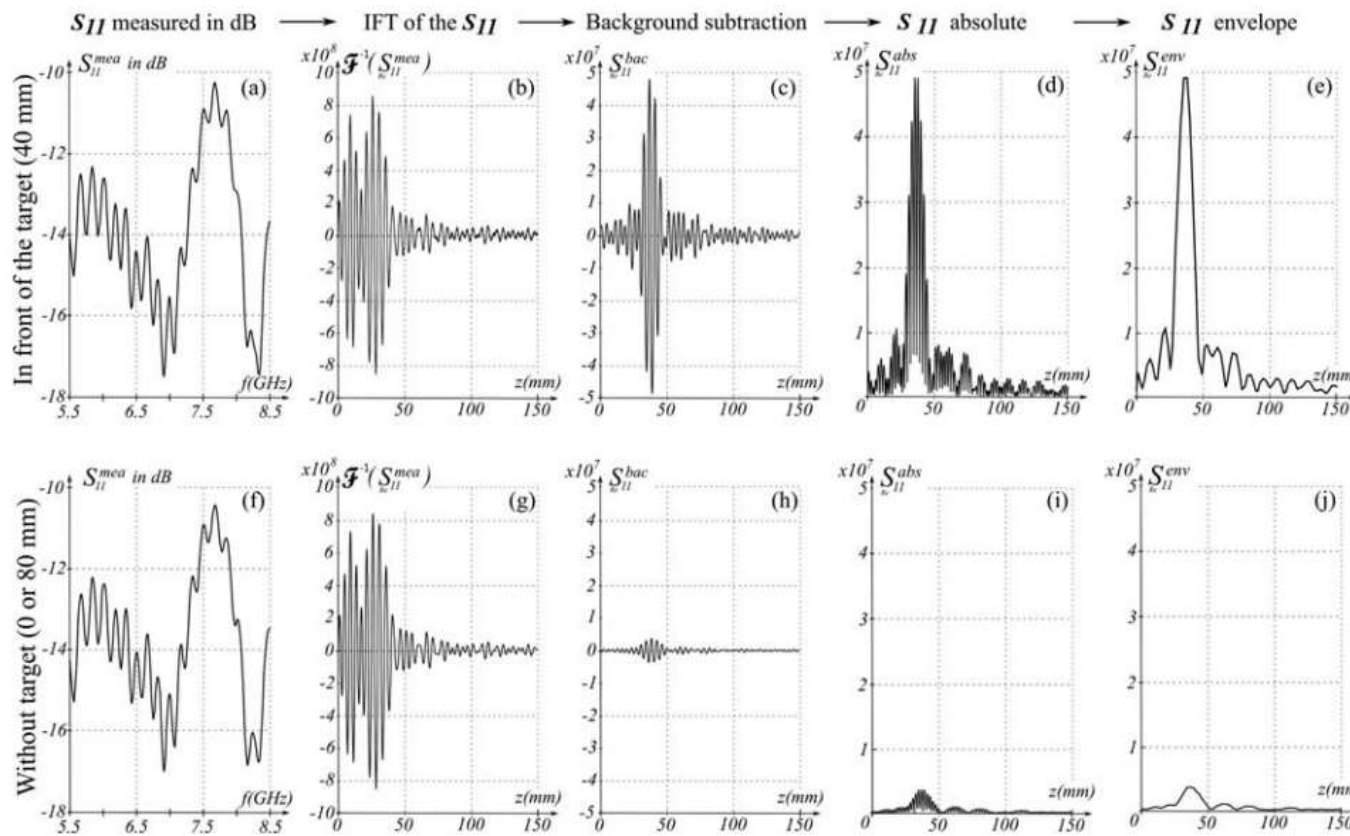


Figure 13 S_{11} -parameter with the FES-AVA in two positions: In front of the target, in the center of the scan area (40 mm), in dB, in the frequency domain (a) in time domain, with the application of IFT (b), with removal of background (c), absolute values (d) and the envelope (e); At the extreme of the scan area (position 0 or 80 mm) in dB, in the frequency domain (f), in the time domain, with the application of IFT (g), with the removal of the background (h), absolute values (i) and finally the envelope (j)

2016-2017





Fomento a Pesquisa PRP do
 IFSP via Edital n.º 823/2018



Tomografia por Micro-ondas

Imagens através de Micro-ondas de campo próximo

www.LabMax.org

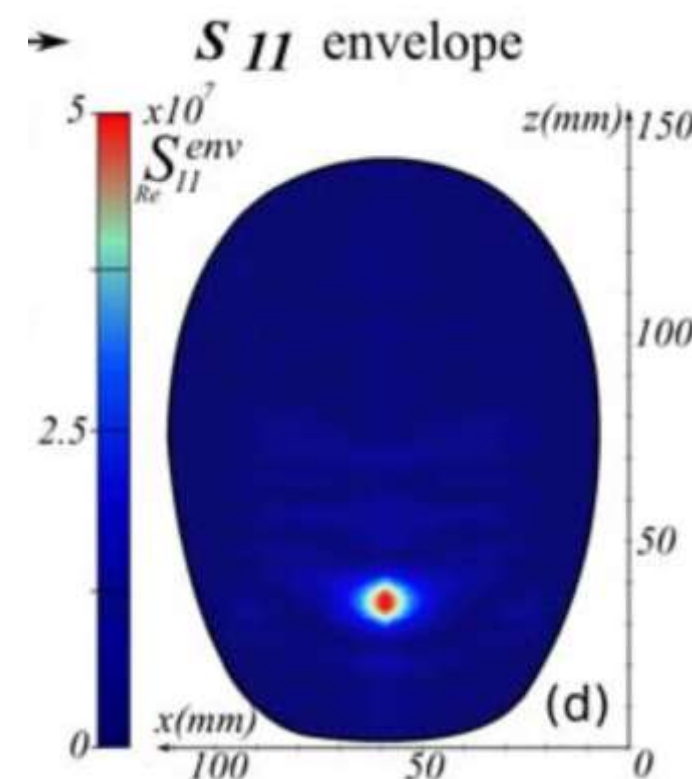
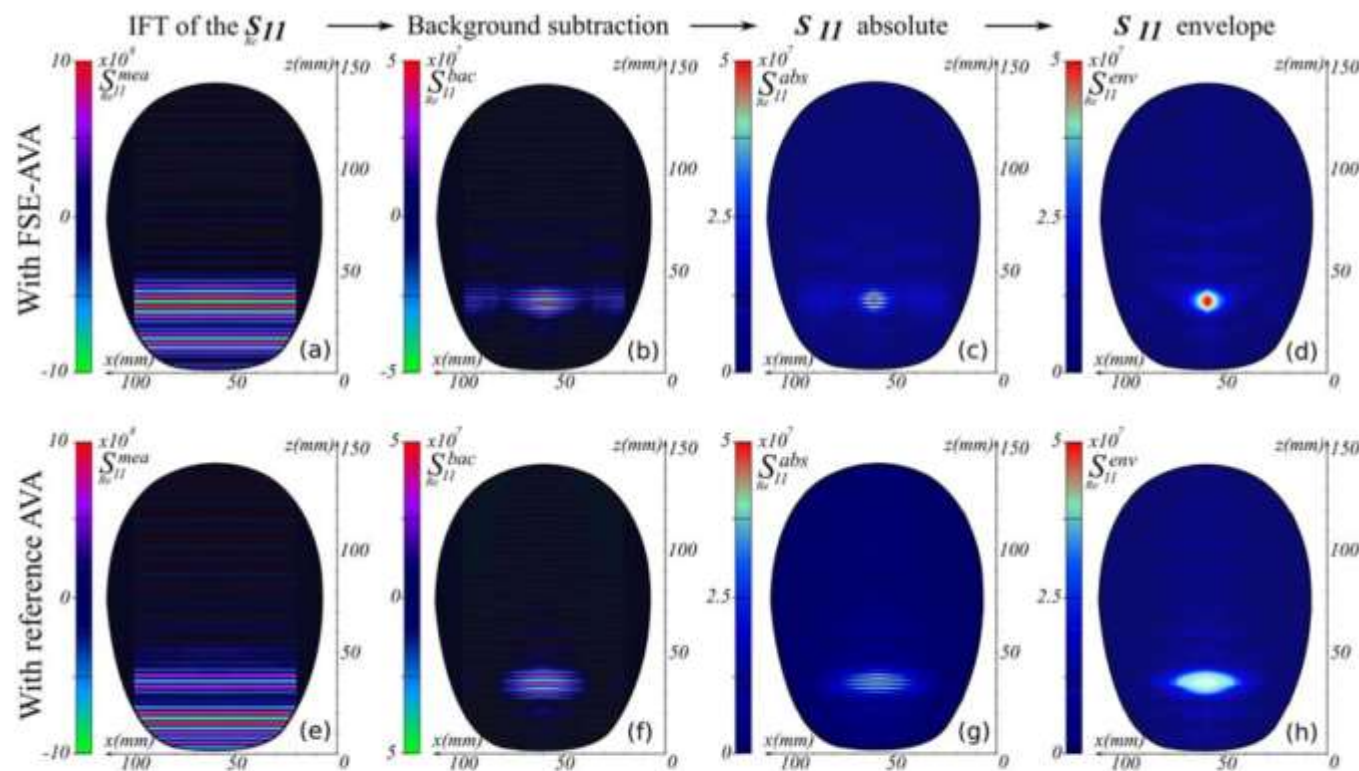


Figure 14 Two-dimensional head tumor scan maps with FSE-AVA in (a, b, c, and d), and with reference AVA in (e, f, g, and h). In (a, and e), the measured S_{11} map appears. In (b, and f), the map without background. In (c, and g), the map in absolute values. And finally in (d, and h), the final near-field microwave image obtained by applying the envelope of the previous map. [Color figure can be viewed at wileyonlinelibrary.com]

2016-2017





Instituto Federal de São Paulo
Laboratório Maxwell
 Micro-ondas e Eletromagnetismo Aplicado
 Certificado CNPq n° 5.497.663.866.471.659



LittleMax
 e a luta contra o Câncer
 Cerebral Infantil

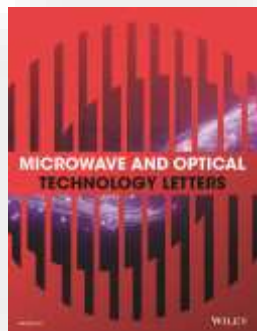
Fomento a Pesquisa PRP do
 IFSP via Edital n° 823/2018



Academia Cearense
 de Matemática - ACM

Tomografia por Micro-ondas

Imagens através de Micro-ondas de ... próximo



2018-2019



Dr. Nurhayati., MT



Received: 14 May 2019
 DOI: 10.1002/mop.32127

RESEARCH ARTICLE

Palm tree coplanar Vivaldi antenna for near field radar application

N. Nurhayati¹ | Alexandre M. De Oliveira² | João F. Justo³ | Eko Setijadi⁴ | Bagus E. Sukoco⁵ | E. Endryansyah¹

¹Department of Electrical Engineering, Universitas Negeri Surabaya, Surabaya, Indonesia

²Maxwell Laboratory of Microwave and Applied Electromag, Federal Institute of São Paulo, Cubatão, Brazil

³Department of Electronic Systems Engineering, Polytechnic School of the University of São Paulo, Brazil

⁴Department of Electrical Engineering, Institut Teknologi Sepuluh Nopember, Surabaya, Indonesia

⁵Pusat Penelitian Elektronika dan Telekomunikasi (PPET), Lembaga Ilmu Pengetahuan Indonesia (LIPI), Bandung, Indonesia

Correspondence

N. Nurhayati, Department of Electrical Engineering, Universitas Negeri Surabaya, Surabaya, Indonesia.
 Email: nurhayati@unesa.ac.id

derives the best side lobe level, which confirmed the possibility of applying the Palm Tree technique to coplanar Vivaldi antennas, in addition to the antipodal ones, as originally proposed.

KEYWORDS

antipodal, coplanar, exponential slot, radiation pattern, Vivaldi

1 | INTRODUCTION

Vivaldi antenna is a simple and robust planar device, which has been the focus of recent intensive research, mostly due to its superior unique properties, it is compact, easy to manufacture, with small dimensions and high gain, and could be integrated directly in a circuit board.¹ As a result, it is suitable for many ultra-wideband (UWB) microwave applications. There are many applications for L and S bands, such as cell phone and wireless communication,² ground penetrating radar,³ software defined and cognitive radios,⁴ medical imaging and on-body telemetry,^{5,6} astronomy,⁷ satellite communication, surveillance and amateur radio. All such application needs reliable system mainly for antenna optimization as front end telecommunication device.

Despite such features, the Vivaldi antenna still carries many shortcomings. The original antenna design has limitations, particularly on directivity and gain, such that a design optimization procedure is generally required for a specific application. In the last few years, many strategies have been developed to improve those properties, for example by adding triangular slots,⁸ using double antipodal structures,⁹ and metamaterials.¹⁰ However, all those solutions compromise the main corner of the antenna, increasing the final antenna dimensions. Therefore, it is

Abstract

This paper presents an ultra-wideband device that has a radiation pattern. This paper presents a coplanar, regular and antipodal structure. Therefore, it is



MINISTÉRIO DA
 EDUCAÇÃO





Instituto Federal de São Paulo
Laboratório Maxwell
 Micro-ondas e Eletromagnetismo Aplicado
 Certificado CNPq nº 5.497.663.866.471.659



LittleMax
 e a luta contra o Câncer
 Cerebral Infantil

Fomento a Pesquisa PRP do
 IFSP via Edital n.º 823/2018



Academia Cearense
 de Matemática - ACM

Tomografia por Micro-ondas

Imagens através de Micro-ondas de campo próximo

LabMat.org



Dr. Nurhayati, MT

2018-2019



Dr. Alexandre Maniçoba de Oliveira
amanicoba@ifsp.edu.br



Tomografia por Micro-ondas

Imagens através de Micro-ondas de campo próximo

www.LabMax.org



Dr. Nurhayati, MT

2018-2019

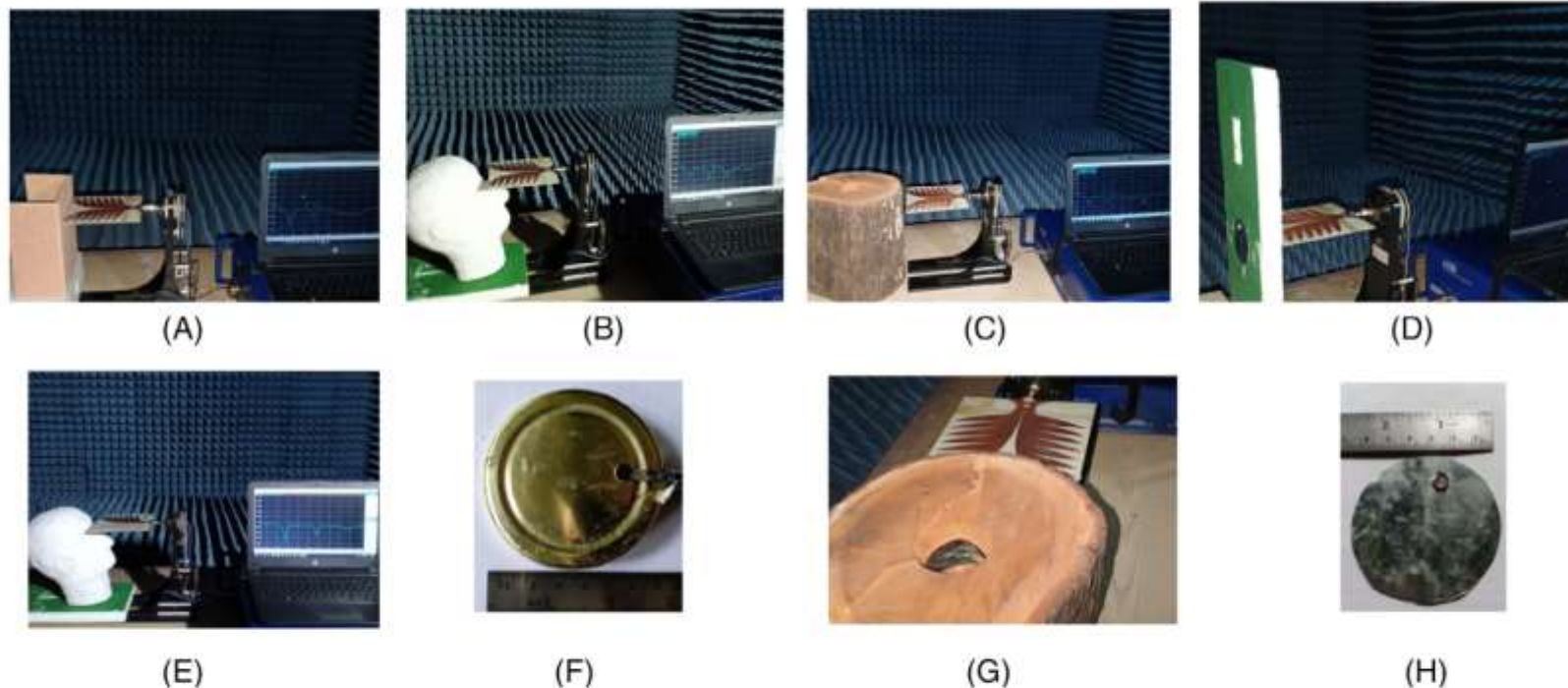


FIGURE 12 Fabricated antennas: A, R-AVA front view; B, R-CVA front view; C, R-CVA back view; D, ESE-AVA front view; E, ESE-CVA front view; and F, ESE-CVA back view. ESE-AVA, exponential slot edge antipodal Vivaldi antenna; ESE-CVA, exponential slot edge coplanar Vivaldi antenna; R-AVA, regular antipodal Vivaldi antenna; R-CVA, regular coplanar Vivaldi antenna [Color figure can be viewed at wileyonlinelibrary.com]



Tomografia por Micro-ondas

Imagens através de Micro-ondas de campo próximo



Dr. Nurhayati, MT

2018-2019

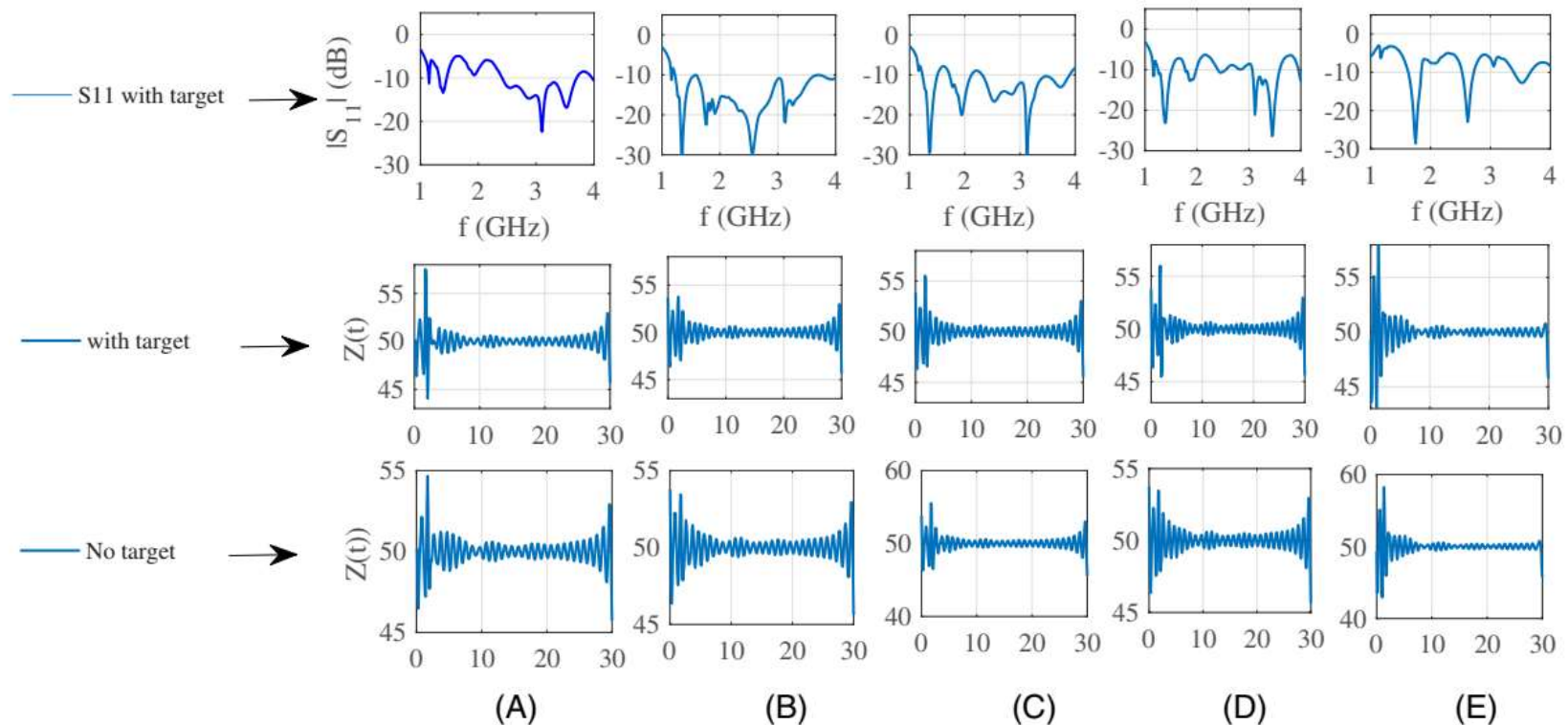


FIGURE 13 Measurement result of S11 with target in the first row, TDR signal for object with target in the second row, TDR signal for object without target in the third row, Substraction object with target and without target in fourth row and the magnitude of the subtraction in the fifth row for object:: (A) CVA with thin board, (B) CVA with head phantom from styrofoam, (C) CVA with thick wood, (D) CVA with thin styrofoam, and (E). AVA with head phantom from styrofoam. AVA, antipodal Vivaldi antenna; CVA, coplanar Vivaldi antenna; TDR, time domain reflectometry [Color figure can be viewed at wileyonlinelibrary.com]



Tomografia por Micro-ondas

Imagens através de Micro-ondas de campo próximo



Dr. Nurhayati, MT

2018-2019

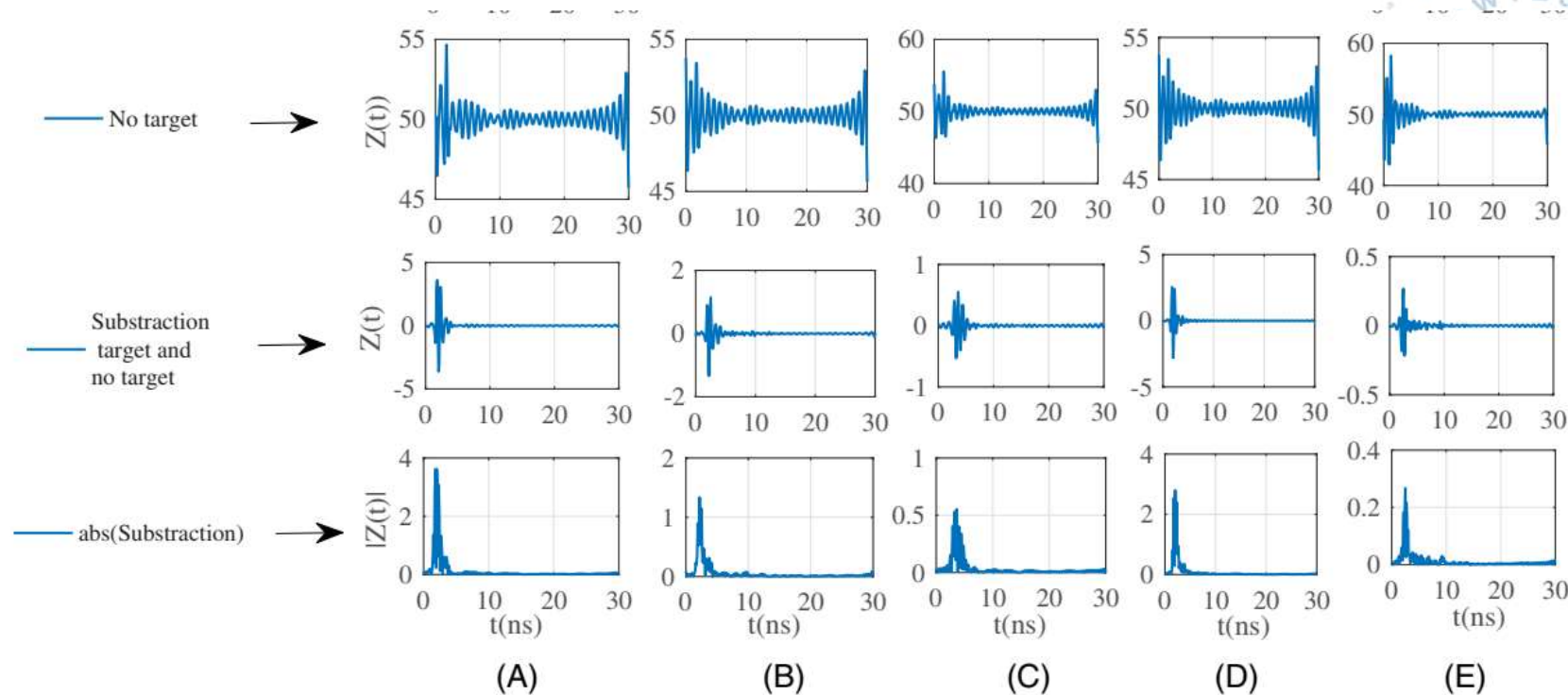


FIGURE 13 Measurement result of S11 with target in the first row, TDR signal for object with target in the second row, TDR signal for object without target in the third row, Subtraction object with target and without target in fourth row and the magnitude of the subtraction in the fifth row for object:: (A) CVA with thin board, (B) CVA with head phantom from styrofoam, (C) CVA with thick wood, (D) CVA with thin styrofoam, and (E). AVA, antipodal Vivaldi antenna; CVA, coplanar Vivaldi antenna; TDR, time domain reflectometry [Color figure can be viewed at wileyonlinelibrary.com]



Instituto Federal de São Paulo
Laboratório Maxwell
 Micro-ondas e Eletromagnetismo Aplicado
 Certificado CNPq nº 5.497.663.866.471.659



LittleMax
 e a luta contra o Câncer
 Cerebral Infantil

Fomento a Pesquisa PRP do
 IFSP via Edital n.º 823/2018



Academia Cearense
 de Matemática - ACM

Tomografia por Micro-ondas

Imagens através de Micro-ondas de campo próximo

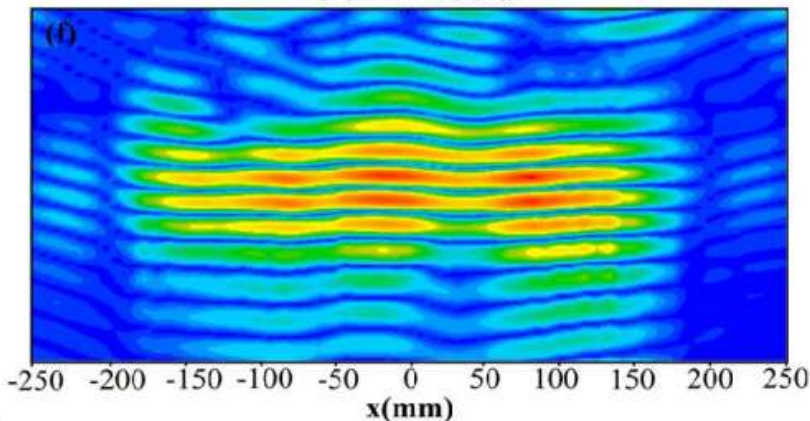


IEEE 2020 THE THIRD INTERNATIONAL
 CONFERENCE ON VOCATIONAL EDUCATION
 AND ELECTRICAL ENGINEERING (ICVEE)



Raimundo Eider

$$a[n] = \text{ABS}(s[n])$$



A Vivaldi Antenna Palm Tree Class with Koch Square Fractal Slot Edge for Near-Field Microwave Biomedical Imaging Applications

1st Raimundo Eider Figueredo
 Maxwell Laboratory of
 Microwaves and Applied
 Electromagnetism, Federal
 Institute of São Paulo
 Cubatão, Brazil
 raimundo@labmax.org

2nd Alexandre M. de Oliveira
 Maxwell Laboratory of
 Microwaves and Applied
 Electromagnetism, Federal
 Institute of São Paulo
 Cubatão, Brazil
 amanicoba@labmax.org

5th Ingrid C. Nogueira
 Christus University Center
 Fortaleza, Brazil
 ingridenfisio@gmail.com

6th João F. Justo
 Department of Electronic
 Systems Engineering at the
 Polytechnic School of the
 University of São Paulo,
 São Paulo, Brasil
 jjusto@labmax.org

3rd Nurhayati Nurhayati
 Department of Electrical
 Engineering, Universitas Negeri
 Surabaya
 Surabaya, Indonesia
 nurhayati@unesa.ac.id

7th Marcelo B. Perotoni
 ABC Federal University,
 Santo André, Brazil
 marcelo.perotoni@labmax.org

4th Antonio Mendes de O. Neto
 Maxwell Laboratory of
 Microwaves and Applied
 Electromagnetism, Federal
 Institute of São Paulo
 Suzano, Brazil
 antonio@labmax.org

8th Arnaldo de Carvalho Jr.
 Maxwell Laboratory of
 Microwaves and Applied
 Electromagnetism, Federal
 Institute of São Paulo
 Cubatão, Brazil
 adecarvalhojr@labmax.org

Abstract— This article presents the modeling of an antipodal Vivaldi antenna (AVA), Palm Tree Class, with radiating fractal slot edge (FSE), in the form of a Koch Square Fractal (SK), labeled as SK-FSE-AVA. The surface currents of the proposed antenna are analyzed, as well as the return loss, directivity, side lobe level (SLL), and Main Lobe (ML) gain. Improvement on directivity is observed when compared to an AVA, with 8.41 dB of gain in the main lobe at 4 GHz, SLL of -11.70 dB, and the squint of 0.10°. SK-FSE-AVA has 9.23 dB of gain in the main lobe at 4 GHz, SLL of -13.50 dB, and the squint of 0.2°. This antenna could be used in ultra-wideband (UWB) systems for applications on Near-Field Microwave Imaging (NMI). To show the feasibility of this application, a 3D numerical simulation of a model containing lung tissue with a malignant tumor is presented, using the proposed antenna and the respective imaging results.

Keywords—Ultra Wide-Band (UWB), Vivaldi Antennas, fractal slot edge (FSE).

1. INTRODUCTION

Any biological tissue has a dielectric constant (ϵ), be it tissue or a malignant foreign body [1], such that, when electromagnetic radiation, such as an antenna, cause different reflections to that, when captured and processed, it generates images that

Several construction techniques have been proposed on the AVA, improving Fairfield characteristics (gain, SLL) [2], [7], [10]. These improvements come at the expense of geometrical modifications, incurring larger sizes, metamaterial parasitic director [1], [8], with dielectric lenses [10]. Other lenses [6], [8], and polylactic (PLA) substrate and regular slot techniques, such as tapered slot edge (TSE) and regular slot edge (RSE) of cavity resonators [2], [5], [7], preserve the original dimensions but presents smaller efficiencies due to the confined (non-radiating) fields trapped in the cavities [2], [7], [11]. The ones with radiant exponential [7], [10], [12] and fractal (FSE) [2] slot edge currents by directing them to the main radiator (Palm Tree Class), which reduces SLL, increasing gain and ML, simultaneously improving directivity and squint [2], [7], [12].

We proposed here a new antenna design, based on the work of [2] and [11], however, using Koch's square fractal to improve gain, directivity, and squint, in addition to decreasing SLL and increasing ML. The goal is to provide more stable antenna radiation, reducing external interference by improving its ability to track images [1], [2].

This article is oriented as follows: Section II presents the results of the respective fractal, while Section III shows the results of the antenna. In Section IV, the results of the processing are presented.



MINISTÉRIO DA
 EDUCAÇÃO





Tomografia por Micro-ondas

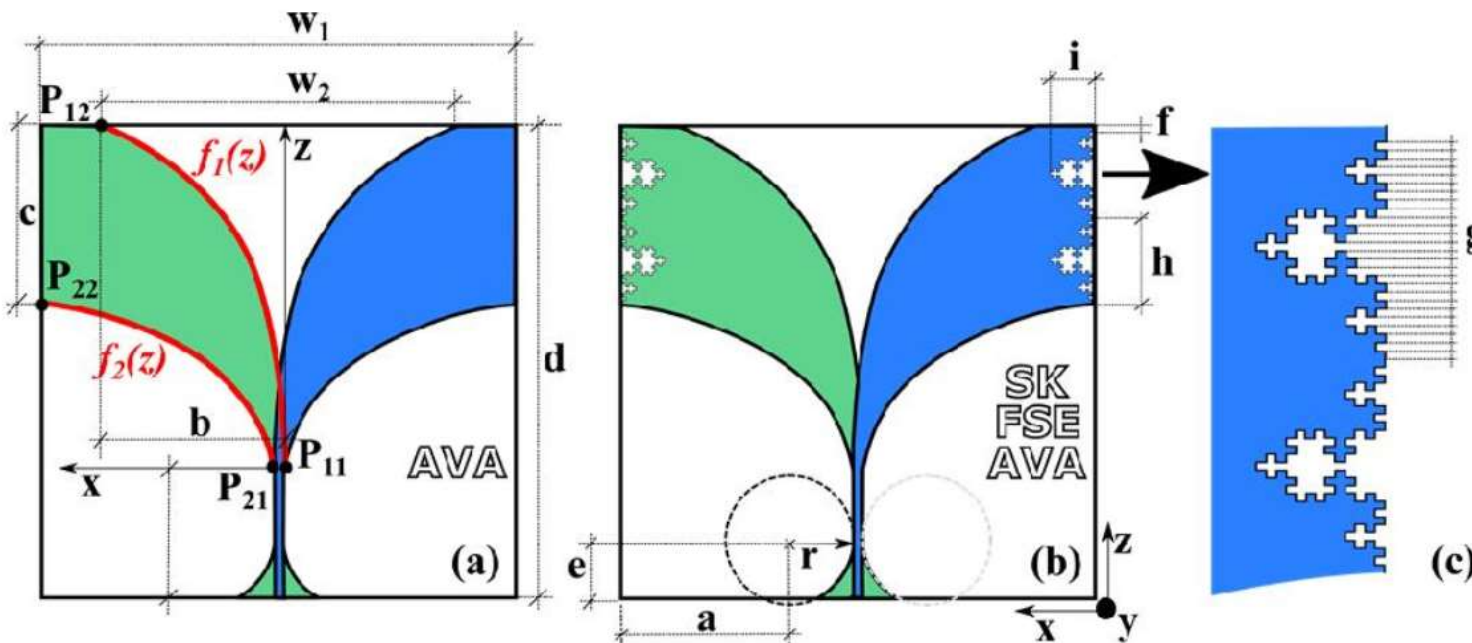
Imagens através de Micro-ondas de campo próximo

www.LabMax.org



Raimundo Eider

2019-2020



$$f(z) = c_1 e^{Rz} + c_2 \quad (1)$$

$$c_1 = \frac{x_2 - x_1}{e^{Rz_2} - e^{Rz_1}} \quad (2)$$

$$c_2 = \frac{x_2 e^{Rz_2} - x_1 e^{Rz_1}}{e^{Rz_2} - e^{Rz_1}} \quad (3)$$

$$W(A) = \bigcup_{n=1}^N w_n(A) \quad (4)$$

Fig. 1. Dimensions of AVA (a), SK-FSA-AVA (b), and fractals of SK-FSE-AVA (c).



Tomografia por Micro-ondas

Imagens através de Micro-ondas de campo próximo

www.LabMax.org



Raimundo Eider

2019-2020

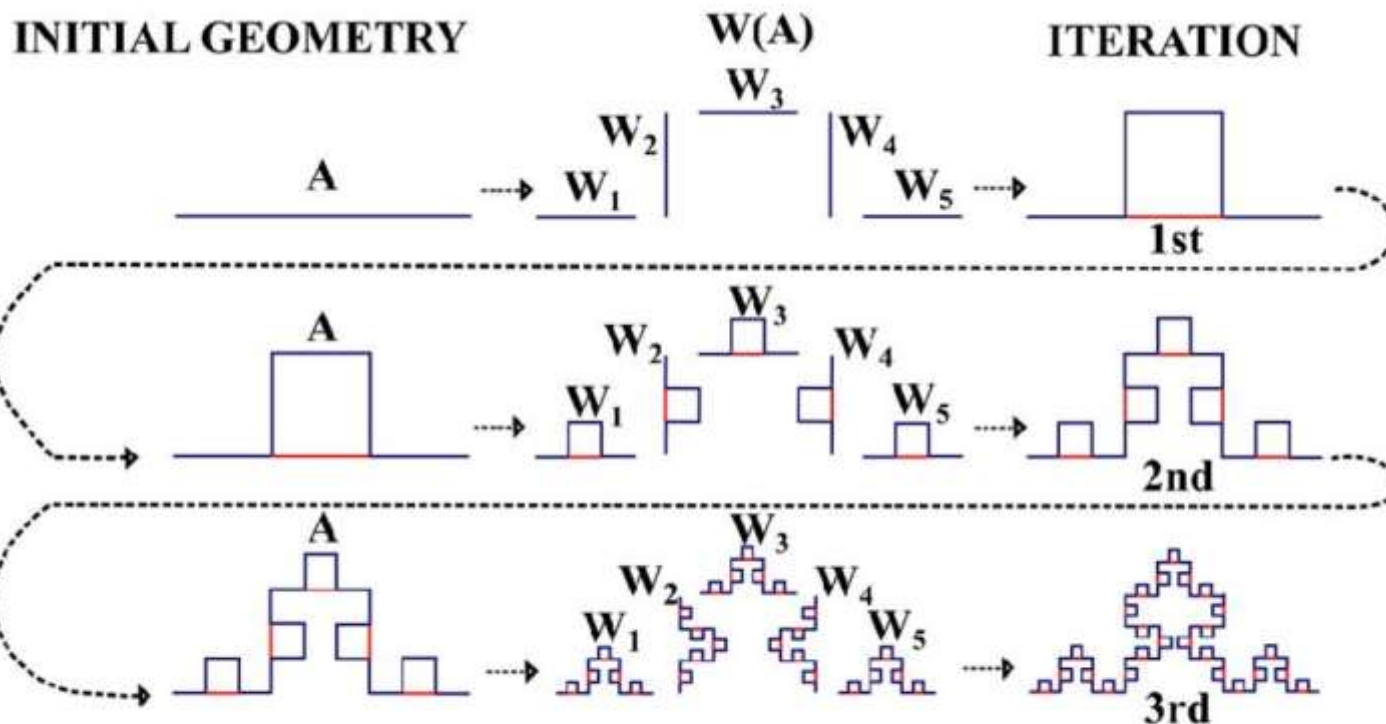


Fig. 2. Development of Koch's Foursquare Fractal using IFS.



Tomografia por Micro-ondas

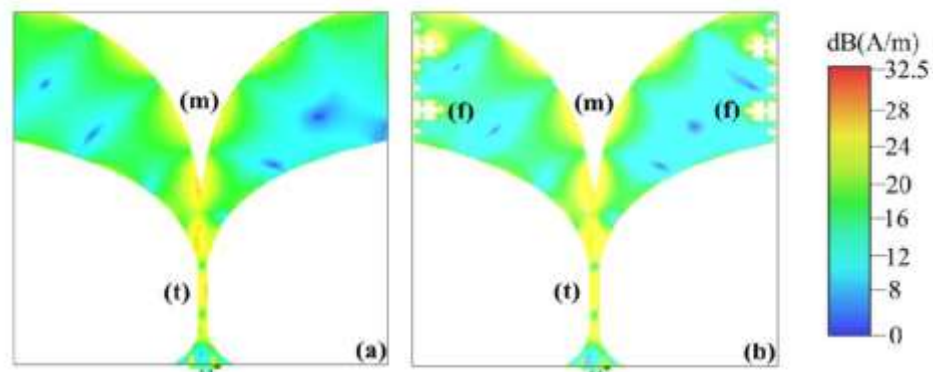
Imagens através de Micro-ondas de campo próximo

www.LabMax.org



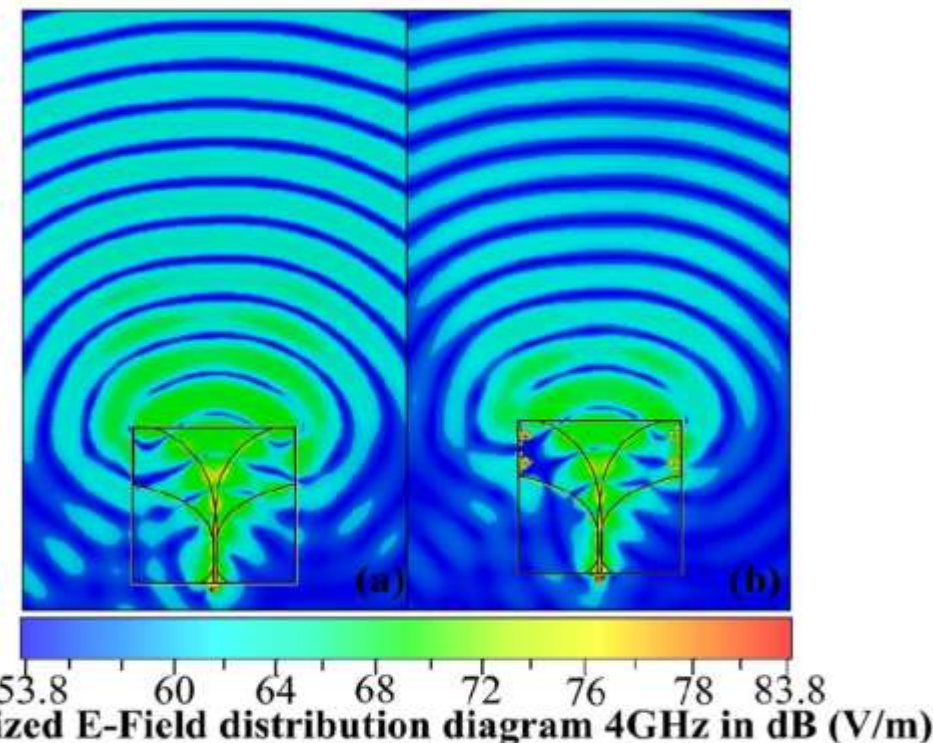
Raimundo Eider

2019-2020



Surface current of AVA (a) and SK-FSE-AVA (b) at 4GHz in dB (A/m)

Fig. 7. Surface current of AVA (a) and SK-FSE-AVA (b) at 4GHz in dB (A/m)



E-Field of AVA (a) and SK-FSE-AVA (b) at 4GHz in dB (V/m)

Fig. 8. E-Field of AVA (a) and SK-FSE-AVA (b) at 4GHz in dB (V/m)



Tomografia por Micro-ondas

Imagens através de Micro-ondas de campo próximo



Raimundo Eider

2019-2020

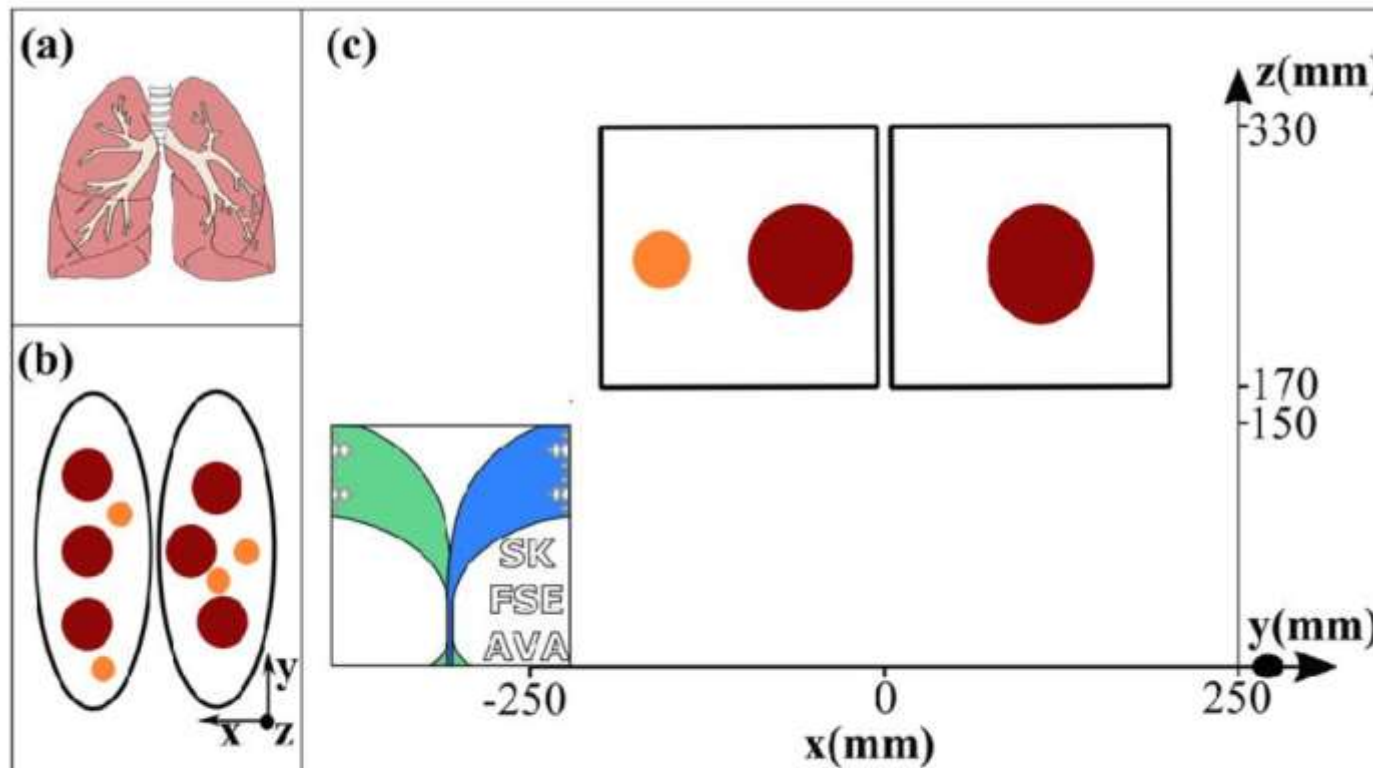


Fig. 9. Lung (a), representation of the lung with tumors for simulation purposes (b), and SK-FSE-AVA running in the x-axis (c).

www.LabMax.org



Tomografia por Micro-ondas

Imagens através de Micro-ondas de campo próximo

www.LabMax.org



Raimundo Eider

2019-2020

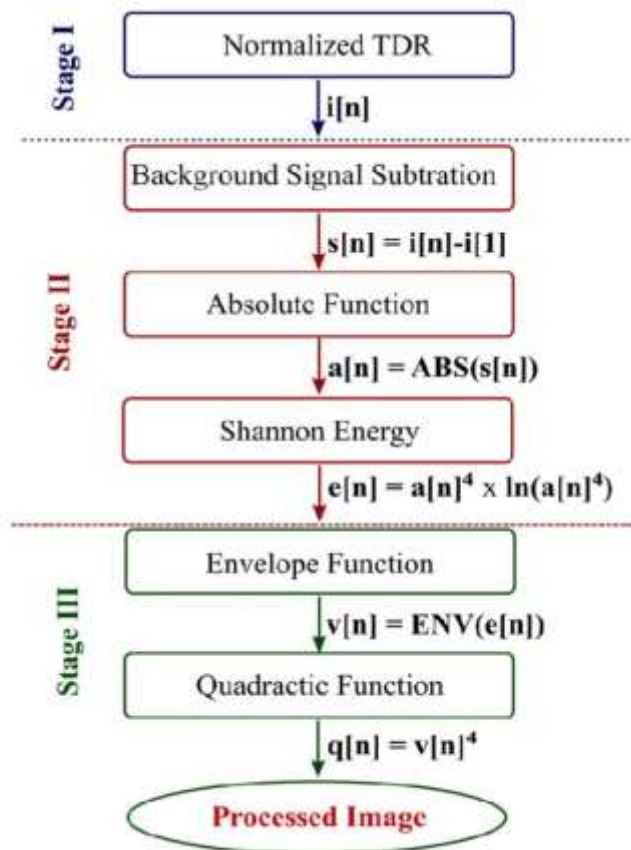


Fig. 10. Flowchart of image processing.



Tomografia por Micro-ondas

Imagens através de Micro-ondas de campo próximo



Raimundo Eider

2019-2020

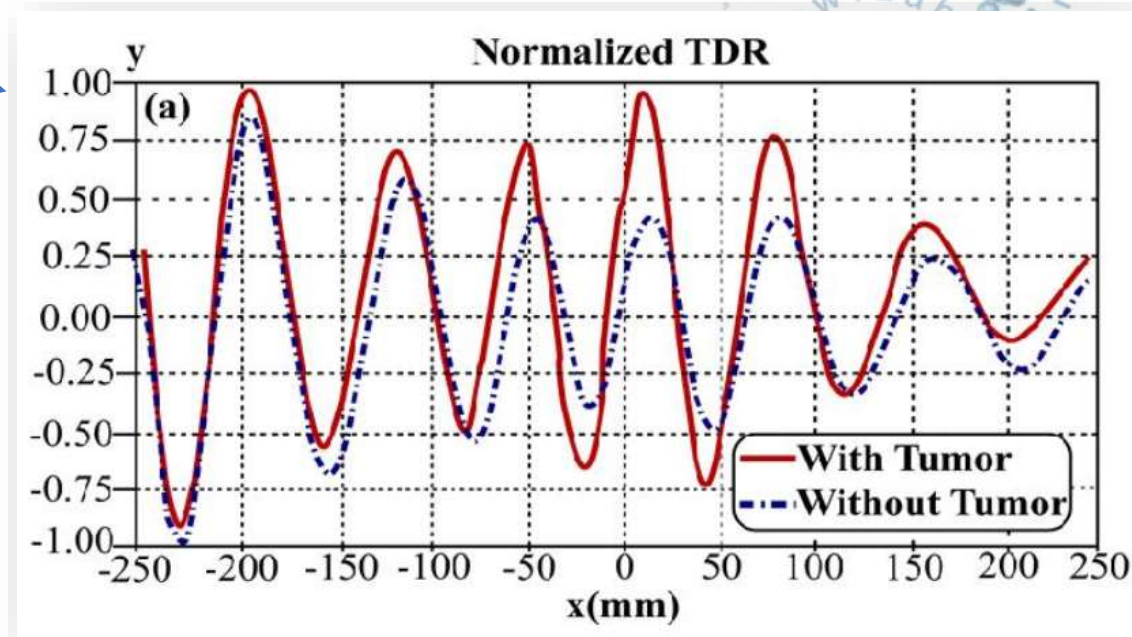
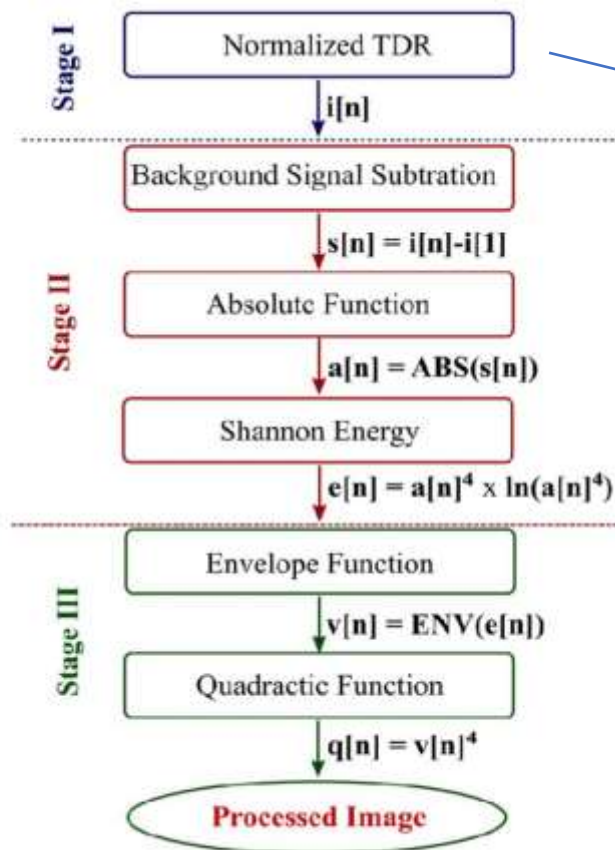


Fig. 10. Flowchart of image processing.



Tomografia por Micro-ondas

Imagens através de Micro-ondas de campo próximo



Raimundo Eider

2019-2020

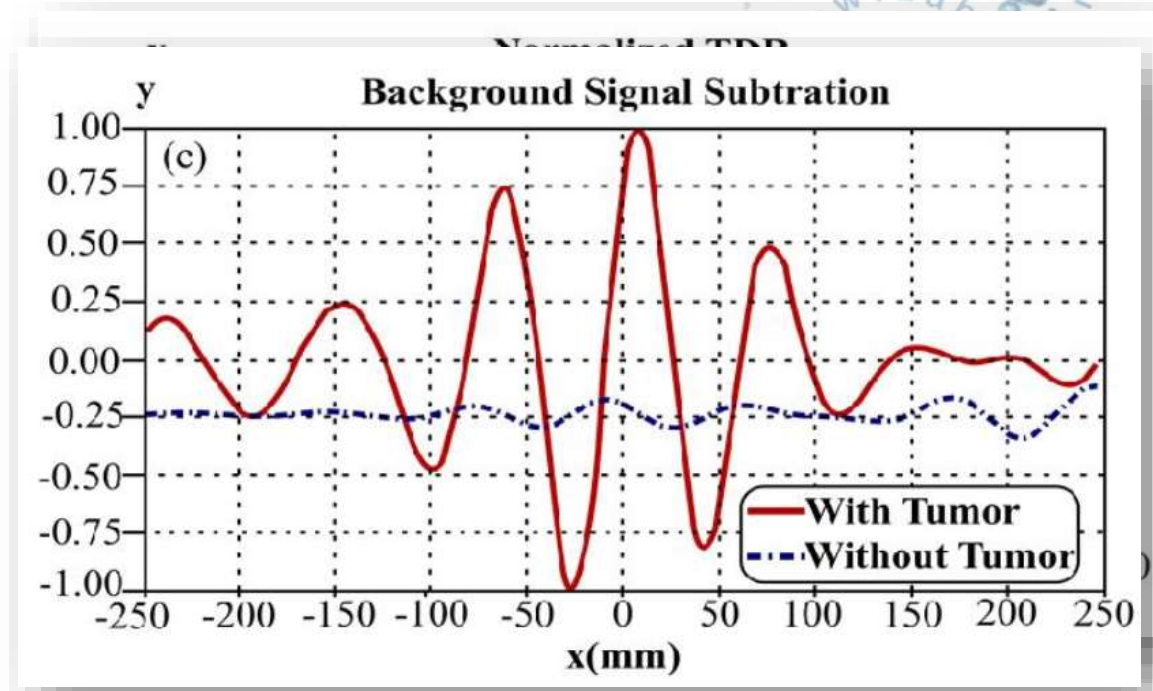
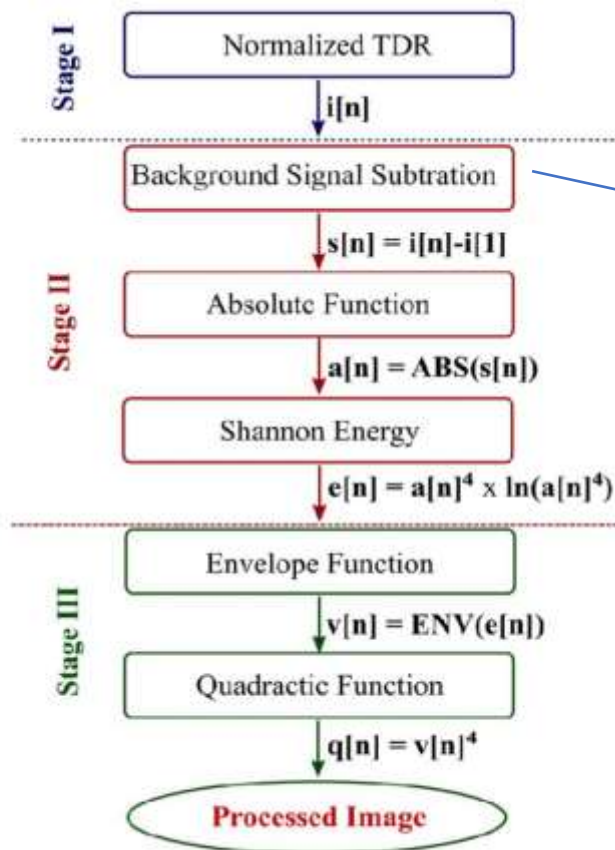


Fig. 10. Flowchart of image processing.



Tomografia por Micro-ondas

Imagens através de Micro-ondas de campo próximo



Raimundo Eider

2019-2020

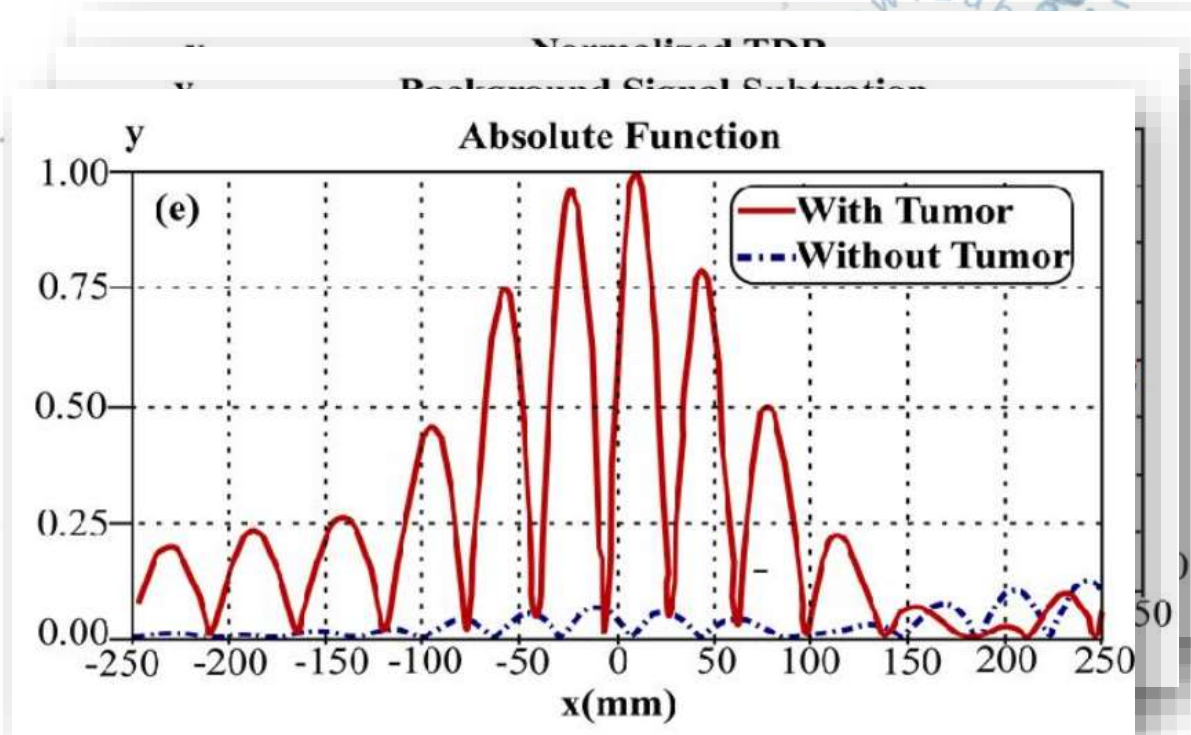
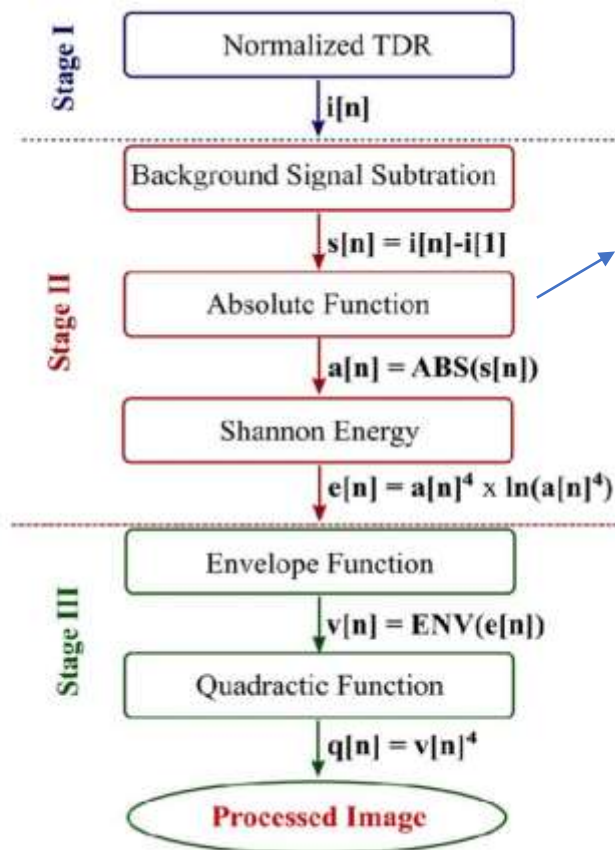


Fig. 10. Flowchart of image processing.



Tomografia por Micro-ondas

Imagens através de Micro-ondas de campo próximo



Raimundo Eider

2019-2020

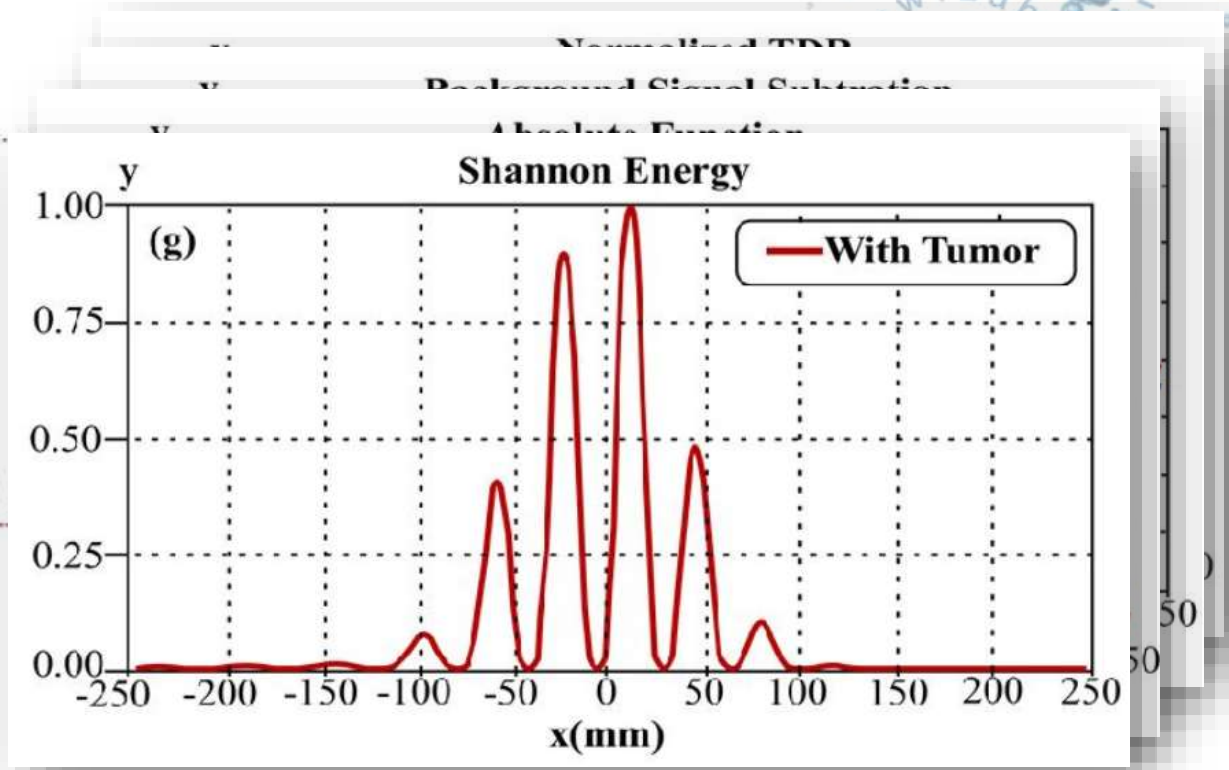
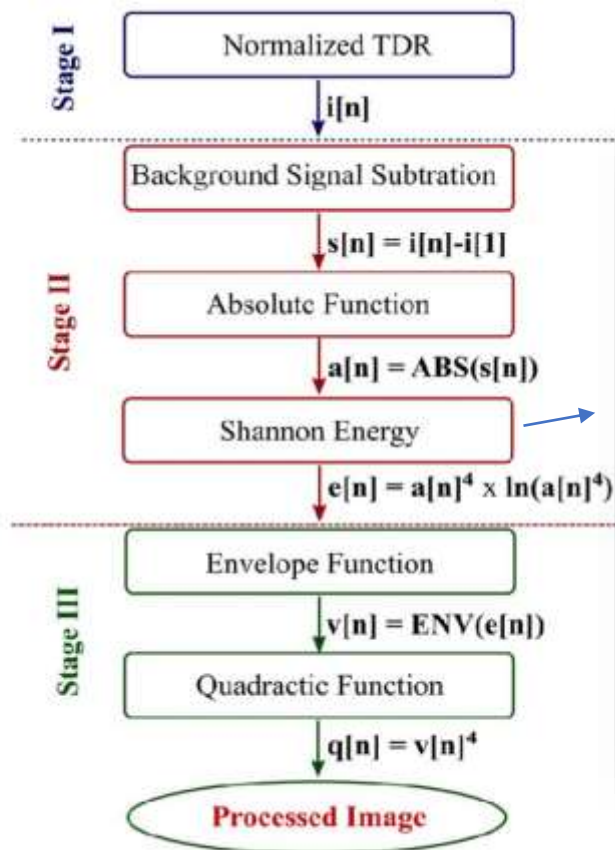


Fig. 10. Flowchart of image processing.



Tomografia por Micro-ondas

Imagens através de Micro-ondas de campo próximo



Raimundo Eider

2019-2020

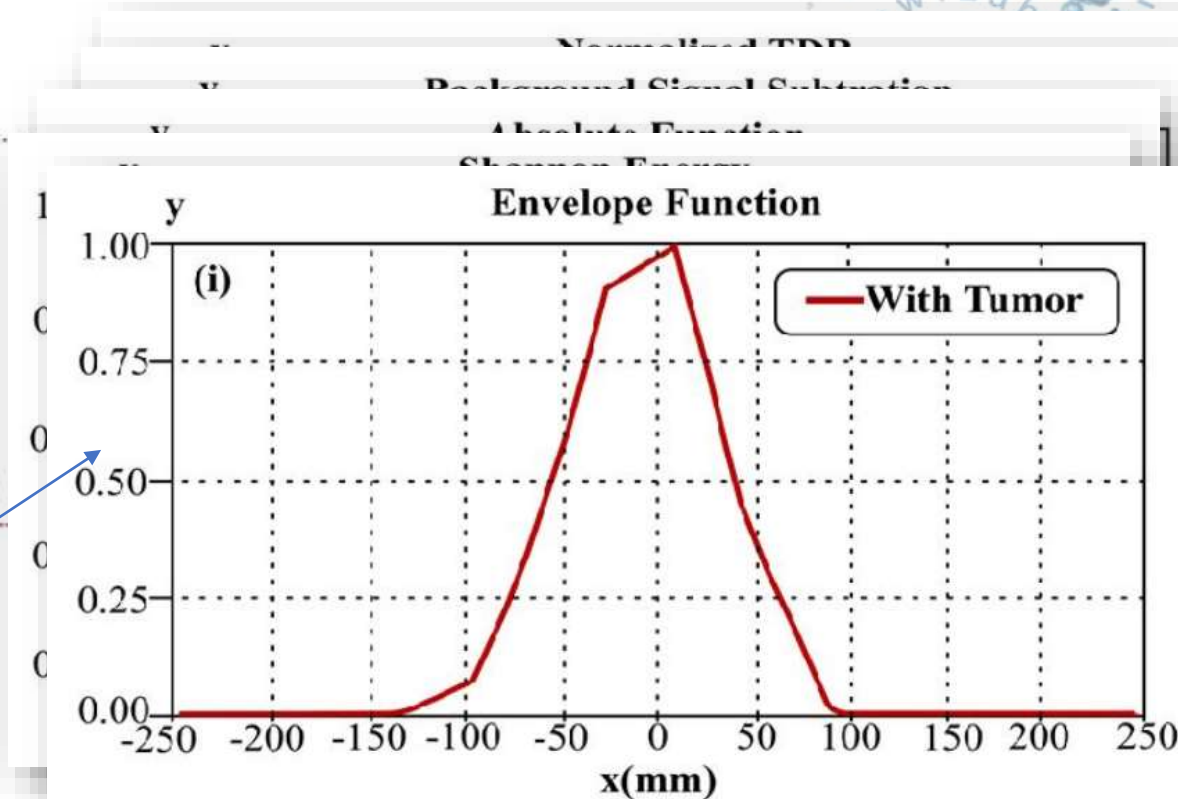
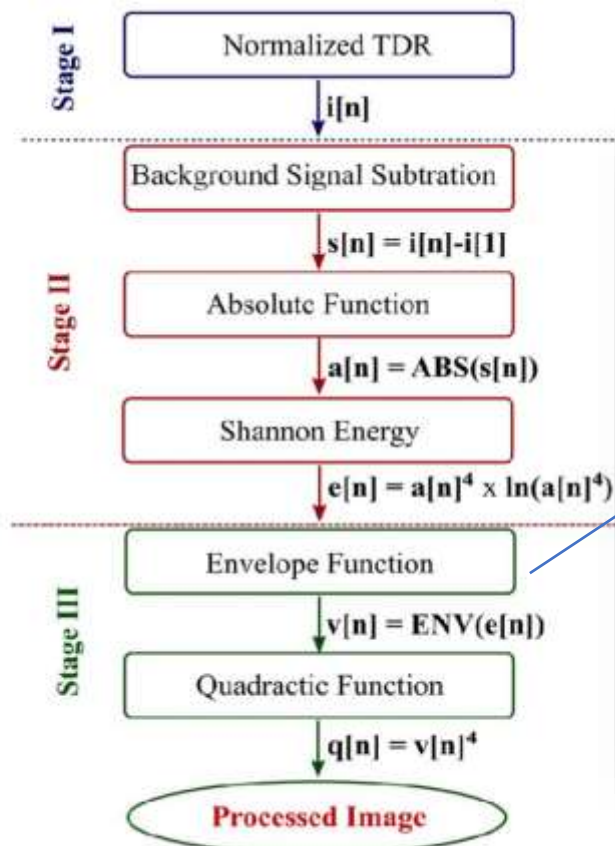


Fig. 10. Flowchart of image processing.



Tomografia por Micro-ondas

Imagens através de Micro-ondas de campo próximo



Raimundo Eider

2019-2020

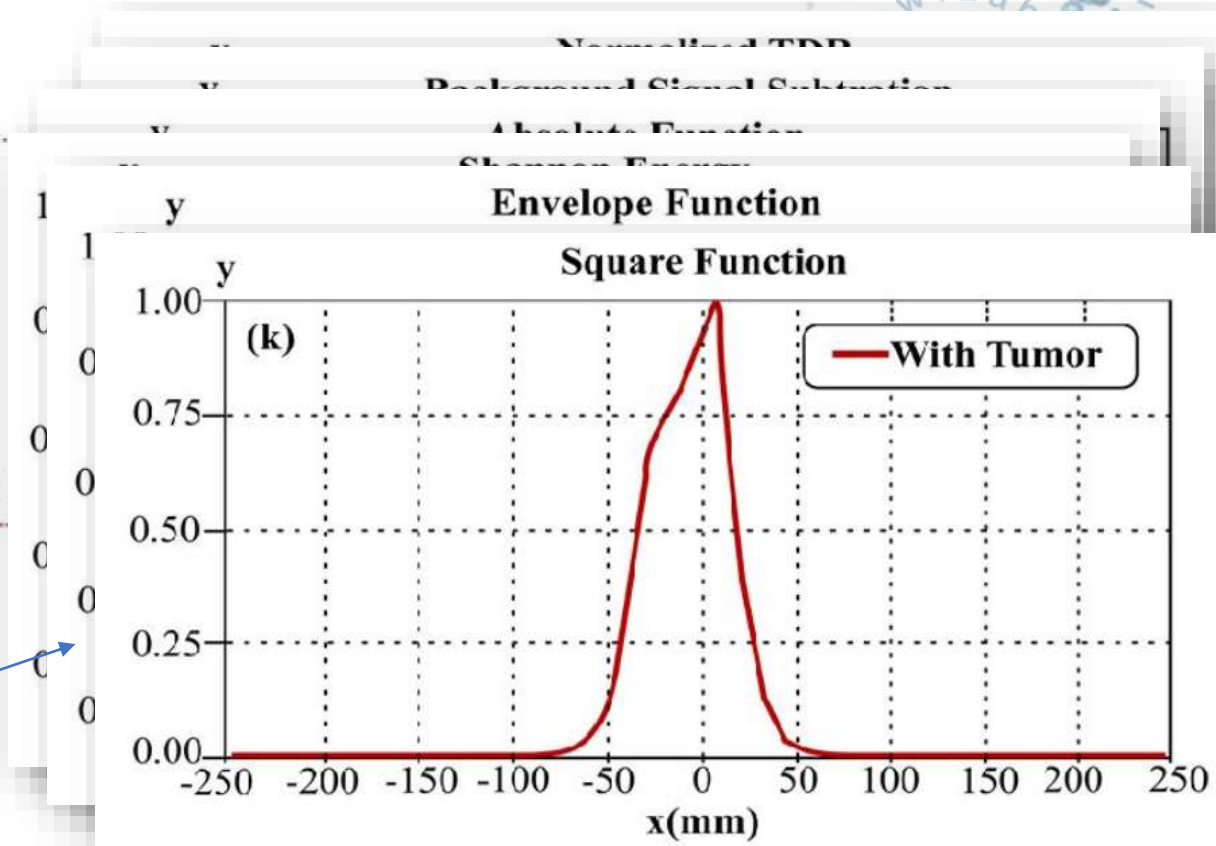
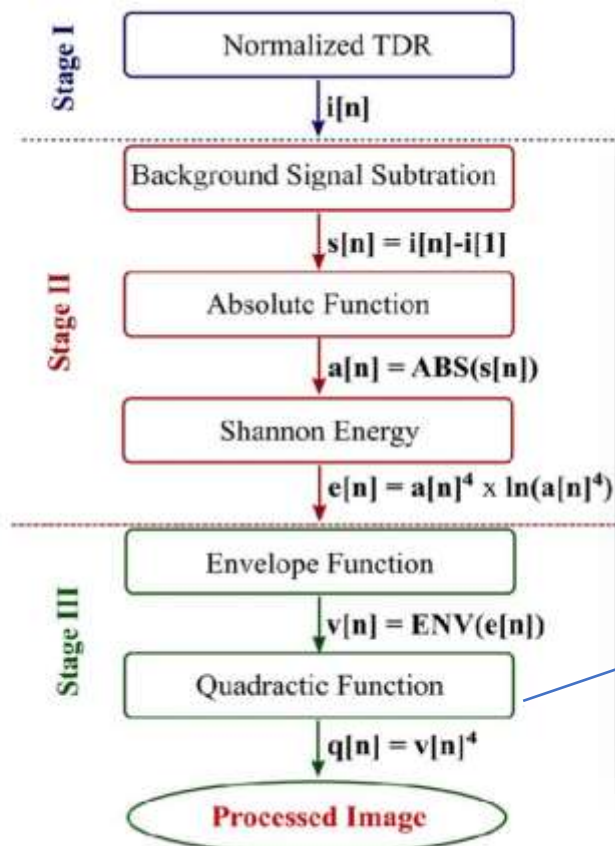


Fig. 10. Flowchart of image processing.



Fomento a Pesquisa PRP do
 IFSP via Edital n.º 823/2018



Tomografia por Micro-ondas

Imagens através de Micro-ondas de campo próximo

www.LabMax.org



Raimundo Eider

2019-2020

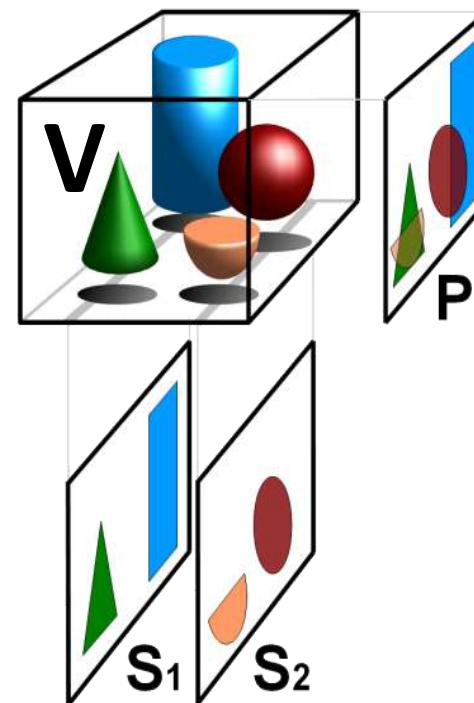
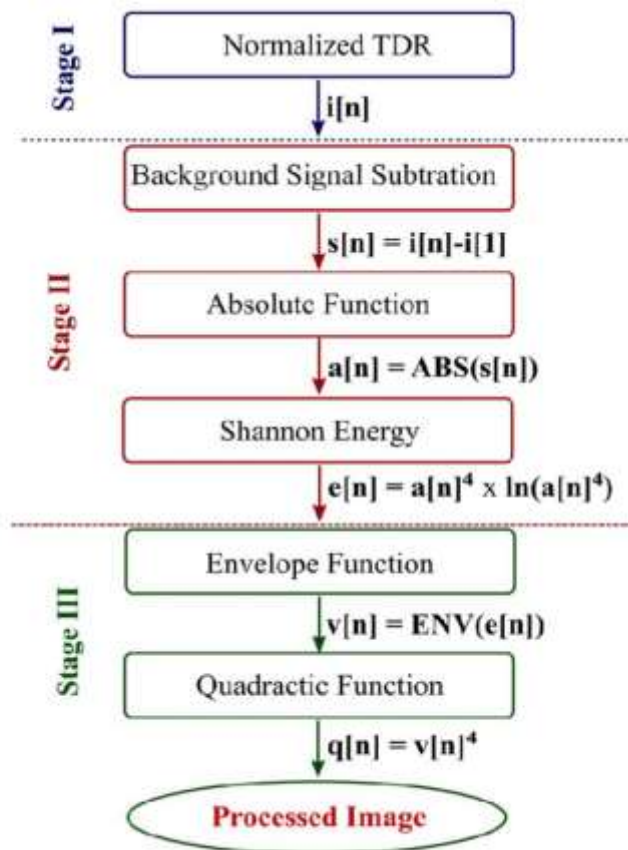


Fig. 10. Flowchart of image processing.



Tomografia por Micro-ondas

Imagens através de Micro-ondas de campo próximo



Raimundo Eider

2019-2020

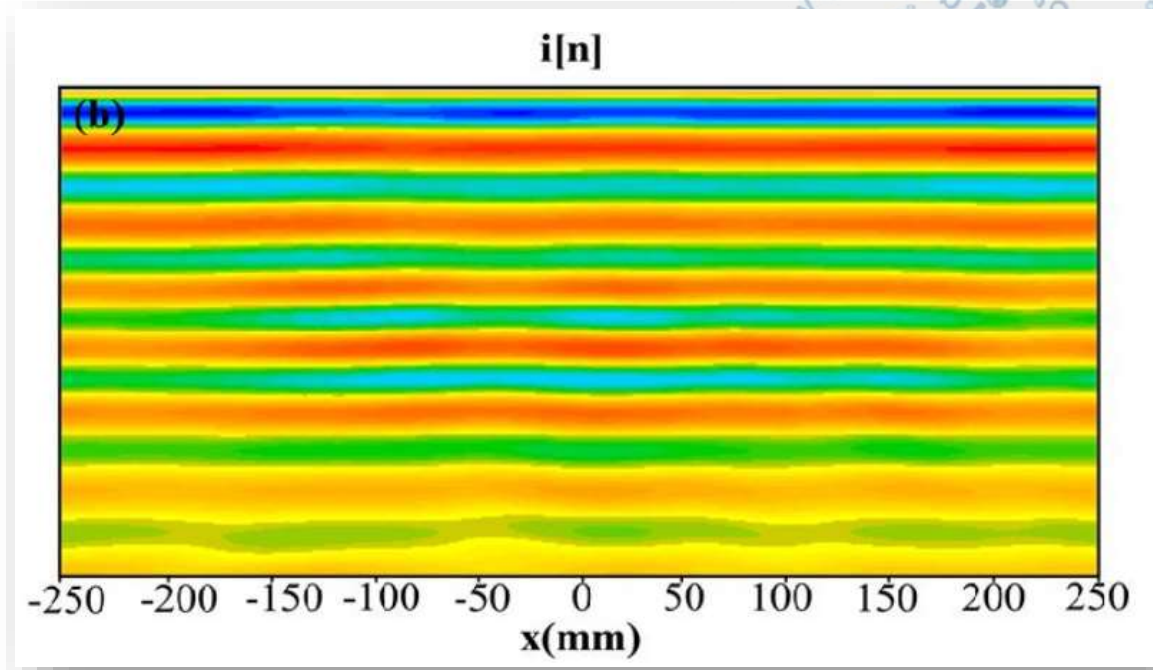
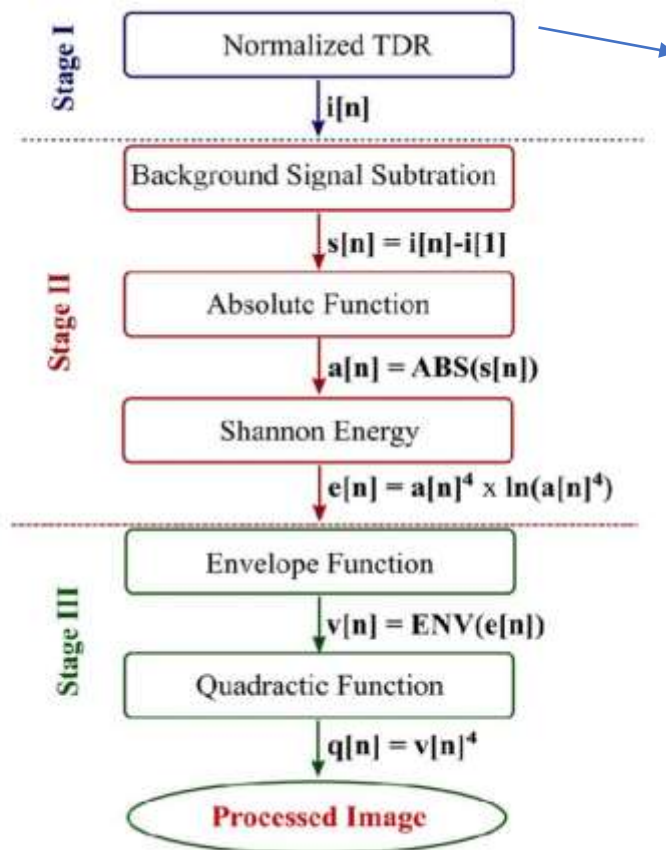


Fig. 10. Flowchart of image processing.



Tomografia por Micro-ondas

Imagens através de Micro-ondas de campo próximo



Raimundo Eider

2019-2020

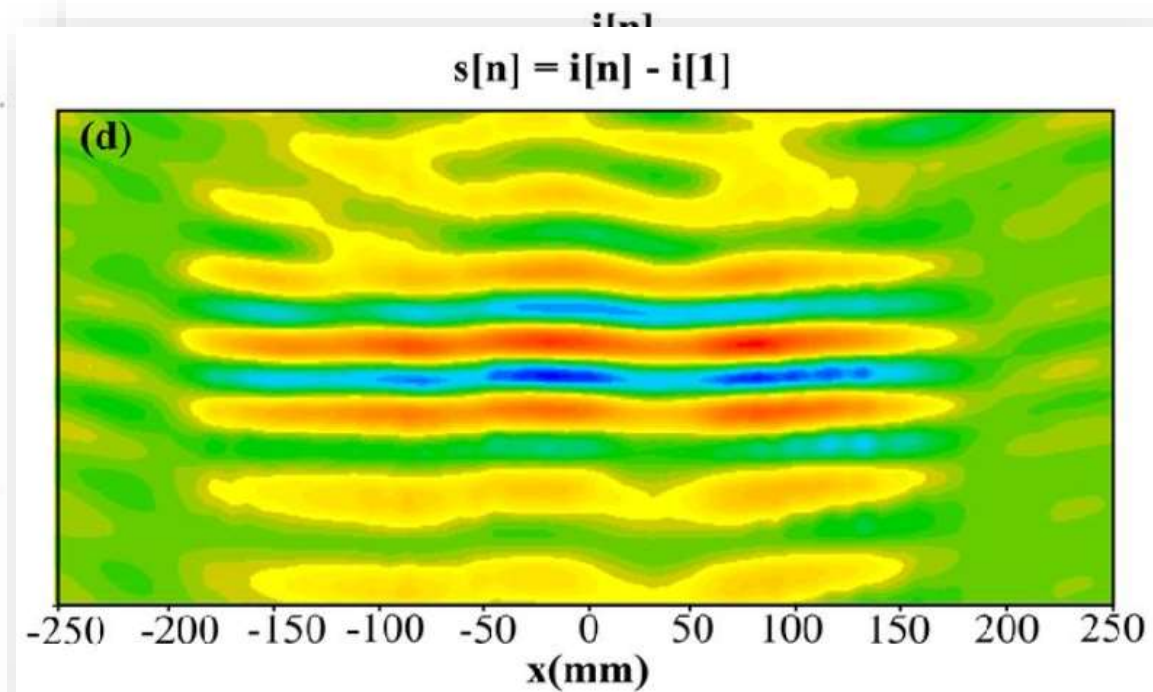
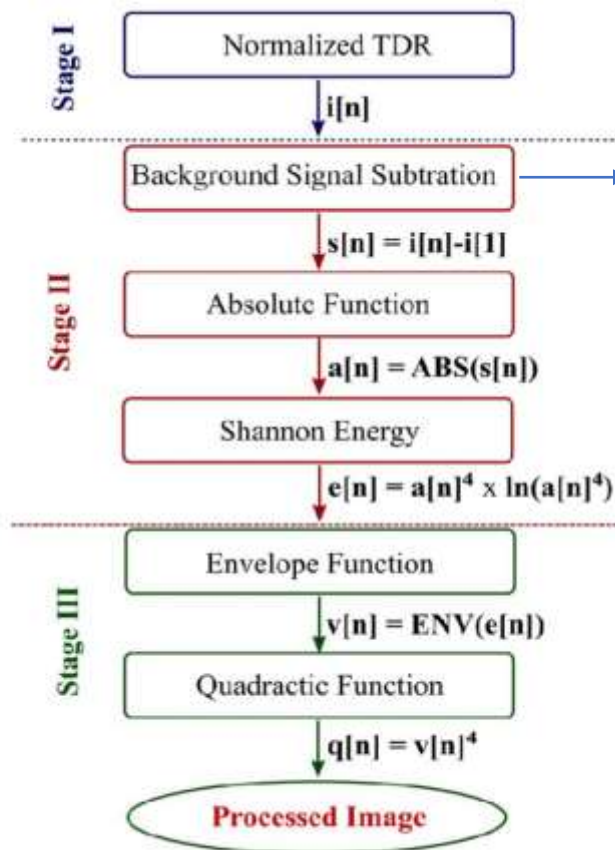


Fig. 10. Flowchart of image processing.



Tomografia por Micro-ondas

Imagens através de Micro-ondas de campo próximo



Raimundo Eider

2019-2020

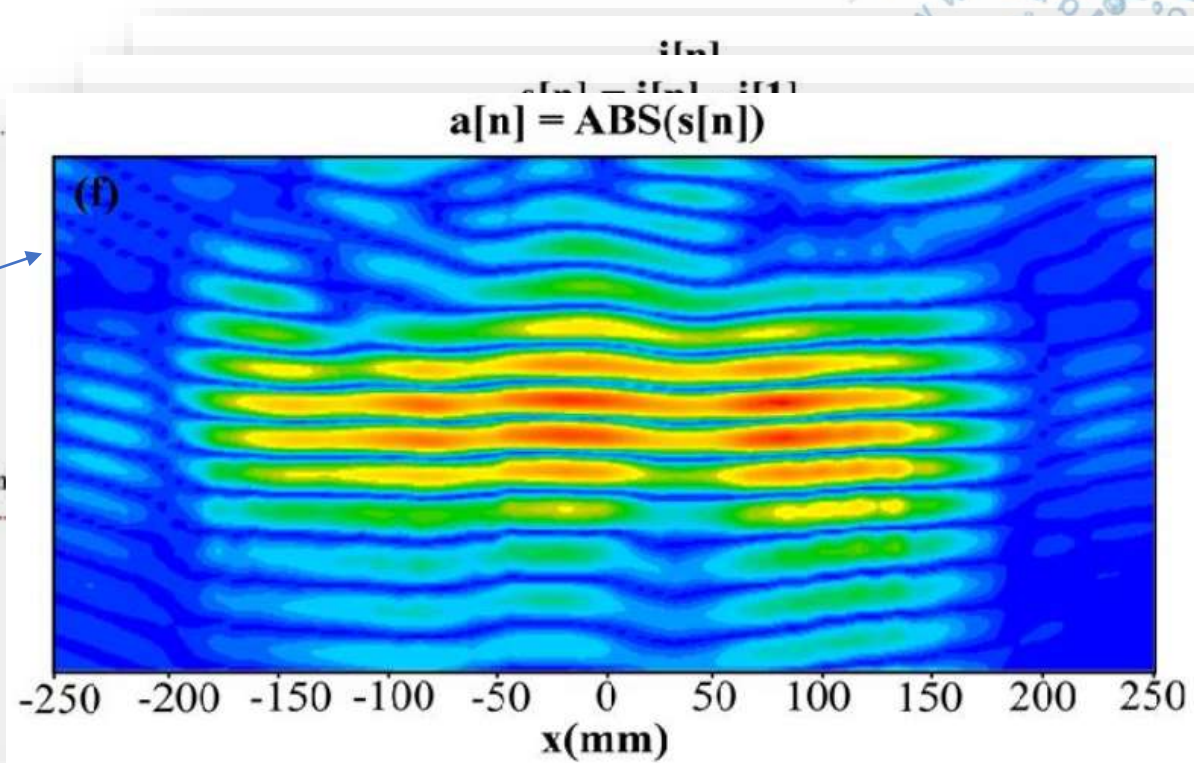
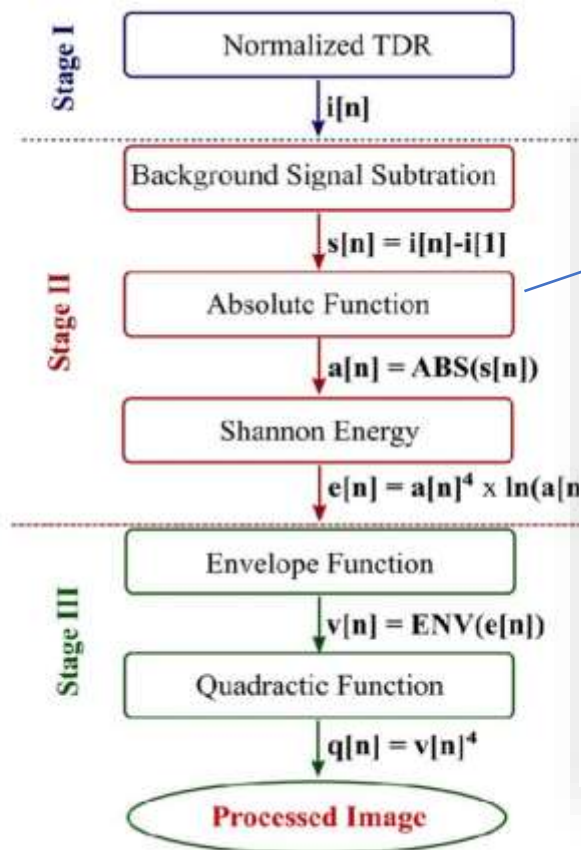


Fig. 10. Flowchart of image processing.



Tomografia por Micro-ondas

Imagens através de Micro-ondas de campo próximo



Raimundo Eider

2019-2020

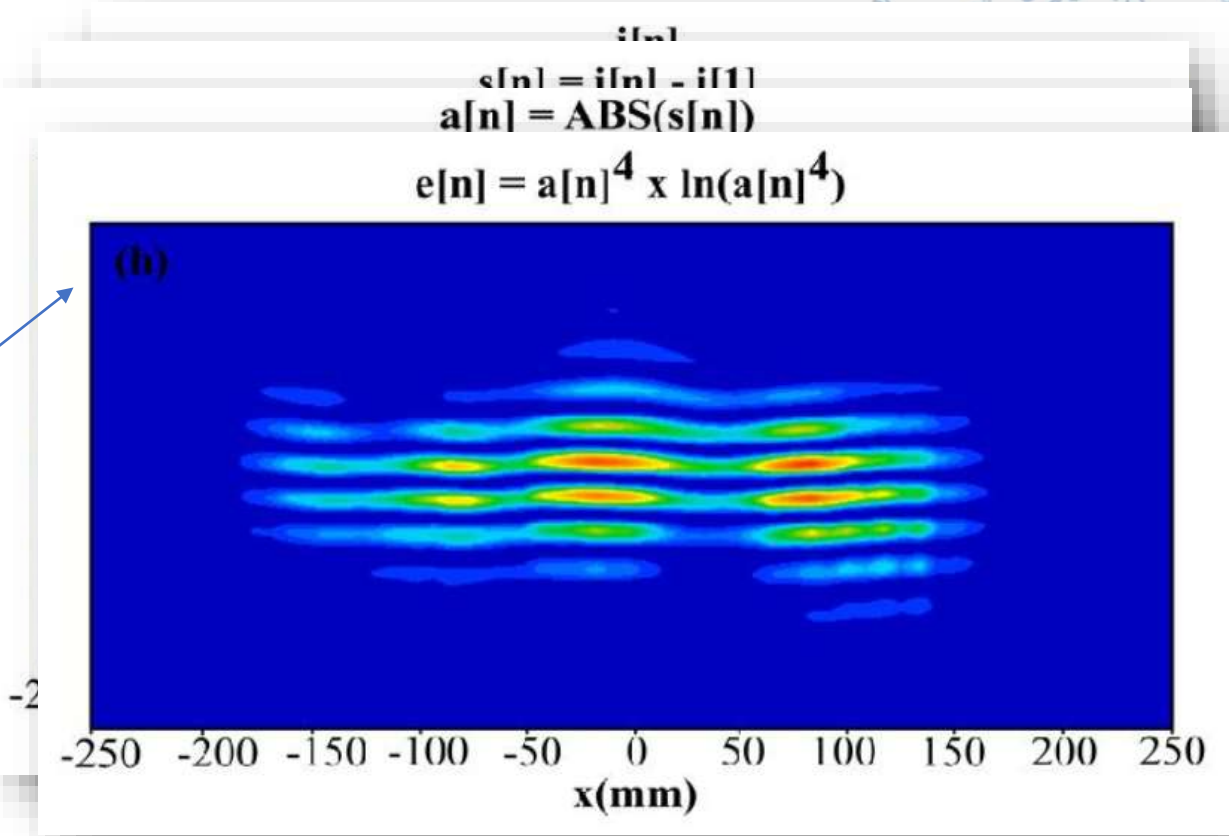
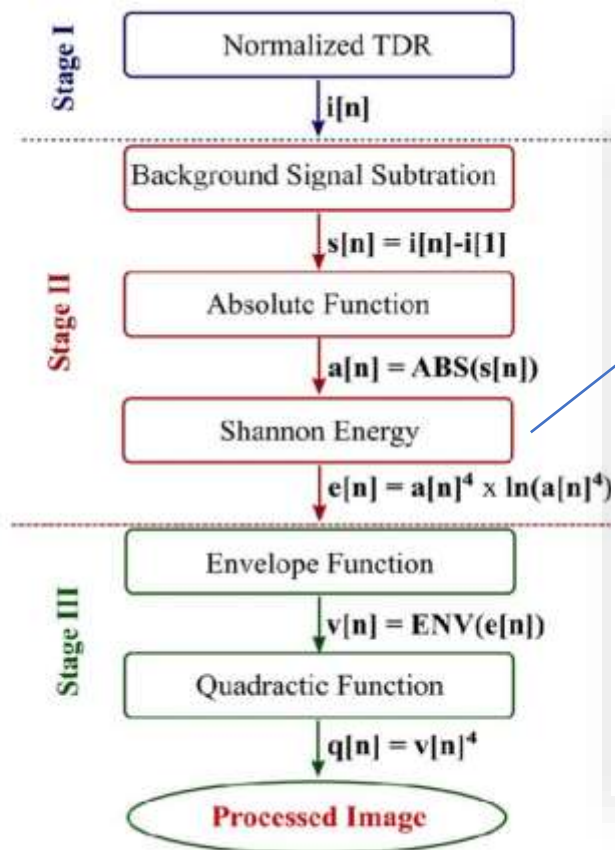


Fig. 10. Flowchart of image processing.



Tomografia por Micro-ondas

Imagens através de Micro-ondas de campo próximo



Raimundo Eider

2019-2020

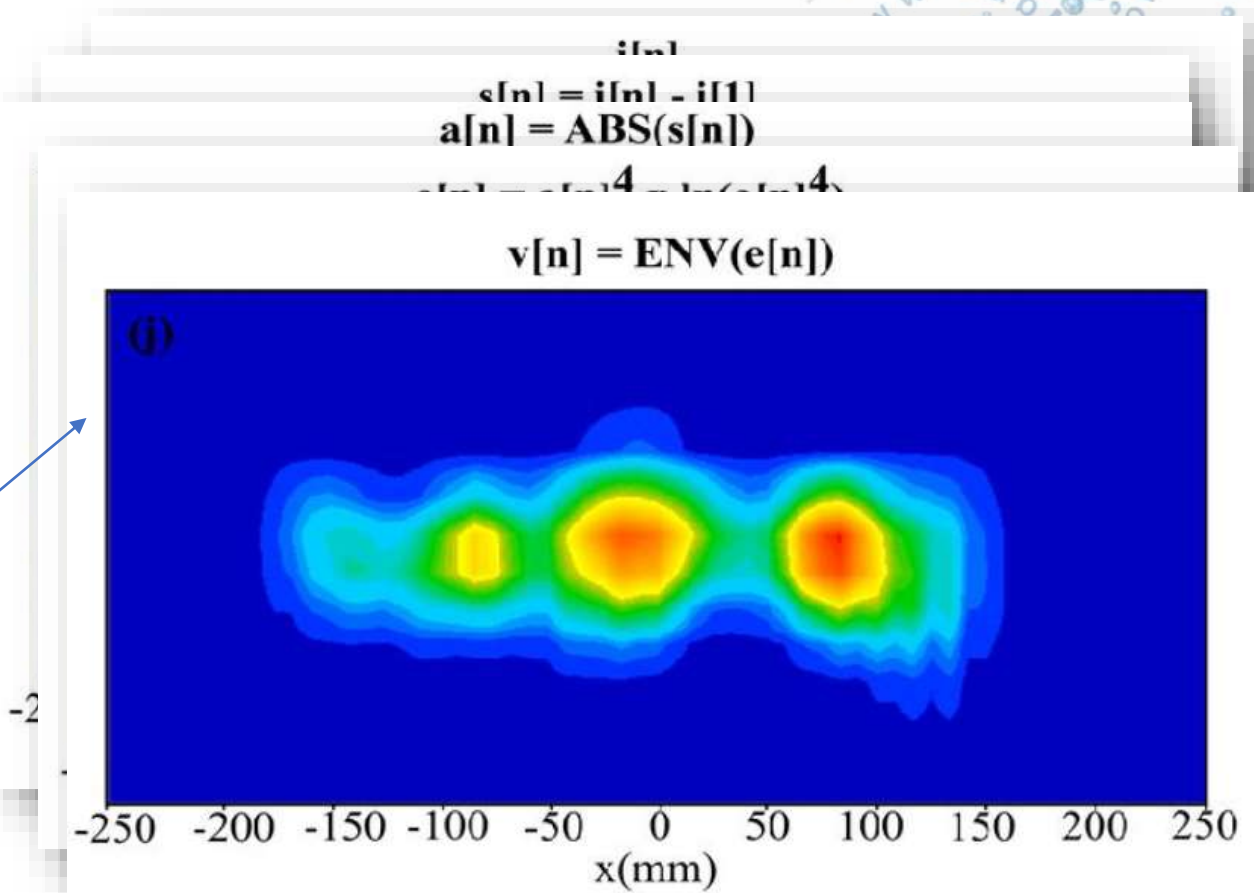
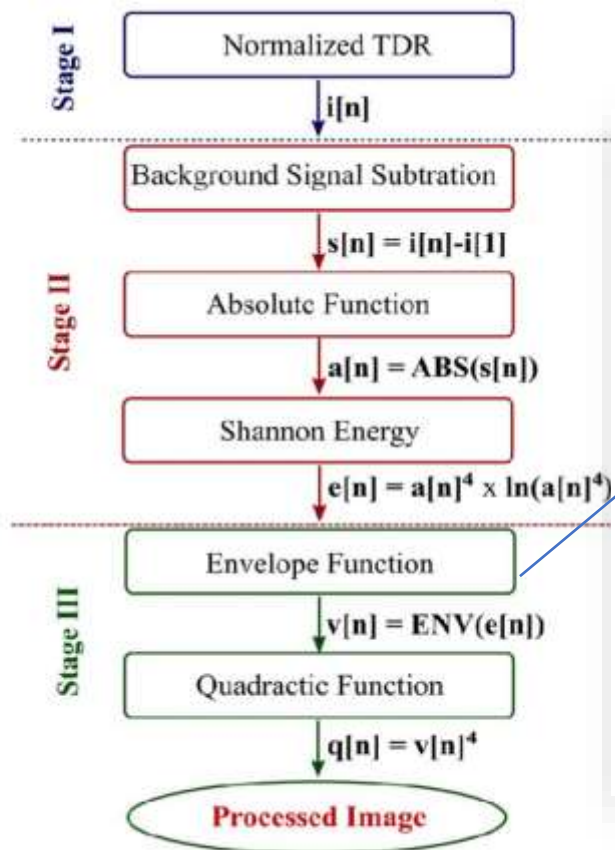


Fig. 10. Flowchart of image processing.



Fomento a Pesquisa PRP do
 IFSP via Edital n.º 823/2018



Tomografia por Micro-ondas

Imagens através de Micro-ondas de campo próximo



Raimundo Eider

2019-2020

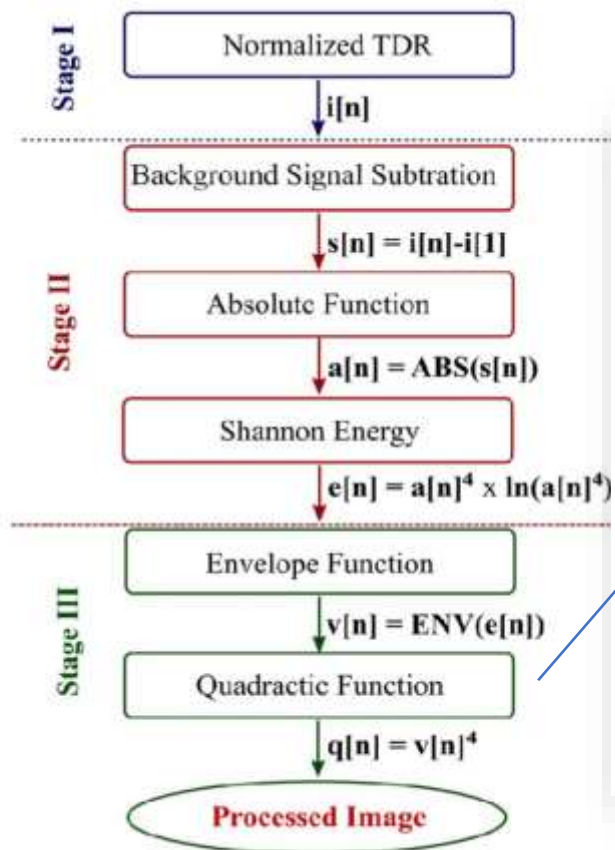
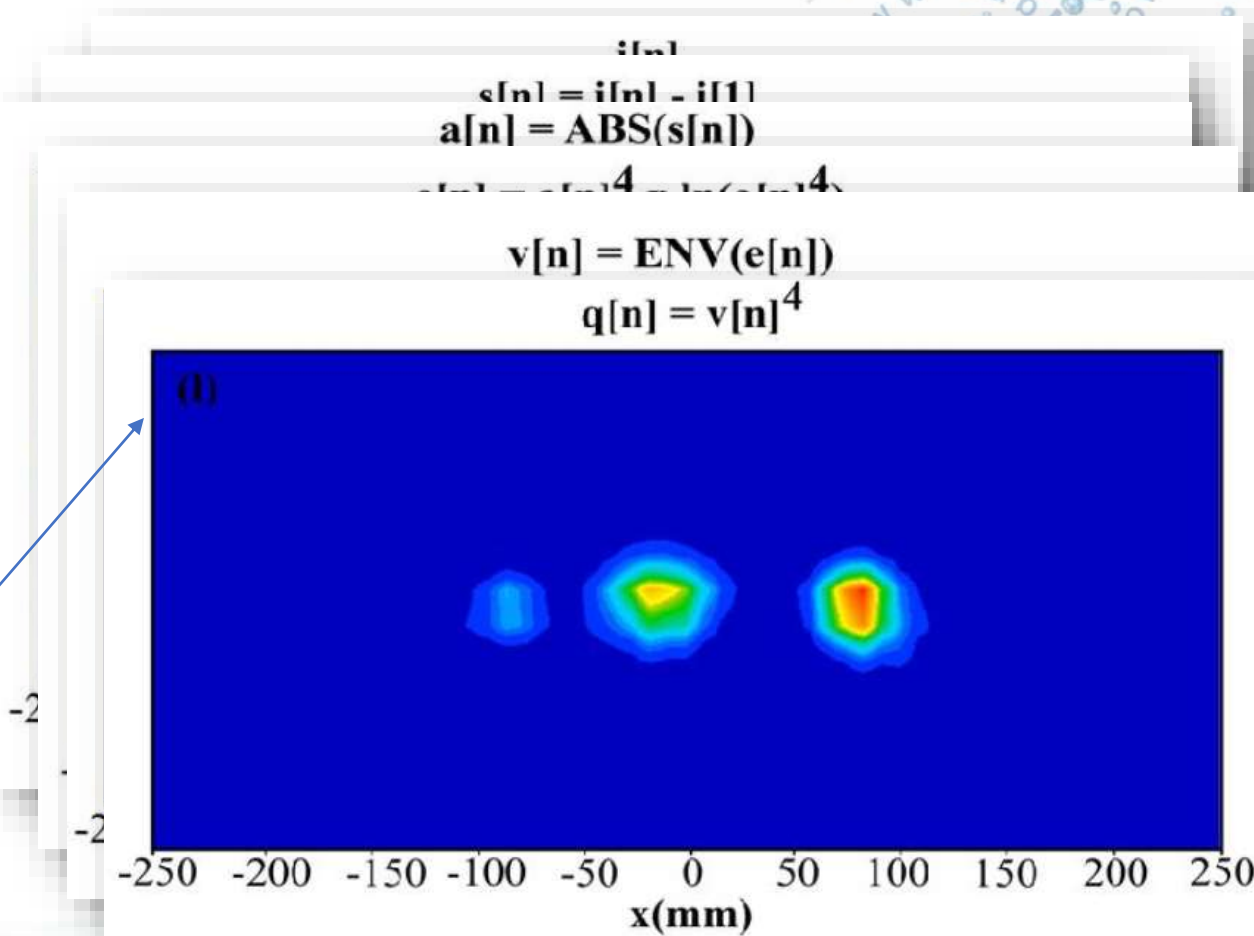


Fig. 10. Flowchart of image processing.





Fomento a Pesquisa PRP do IFSP via Edital n.º 823/2018



Raimundo Eider

2019-2020

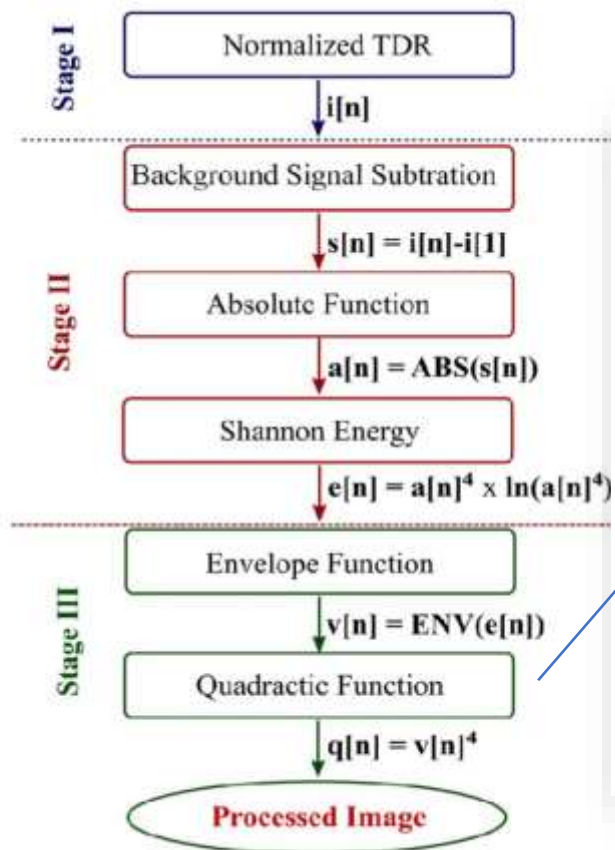
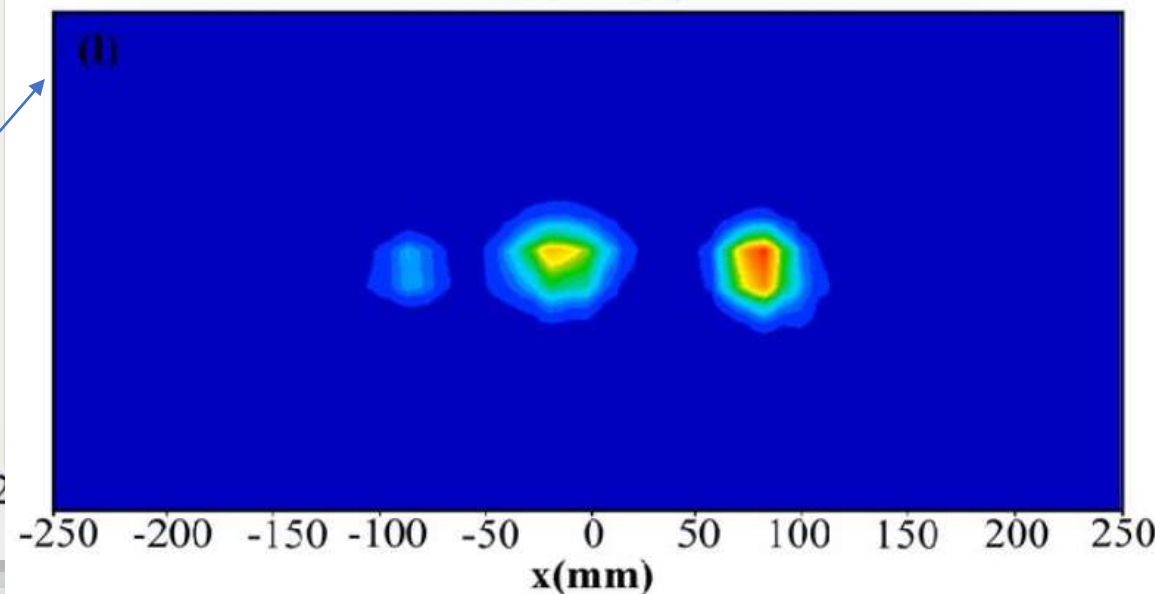
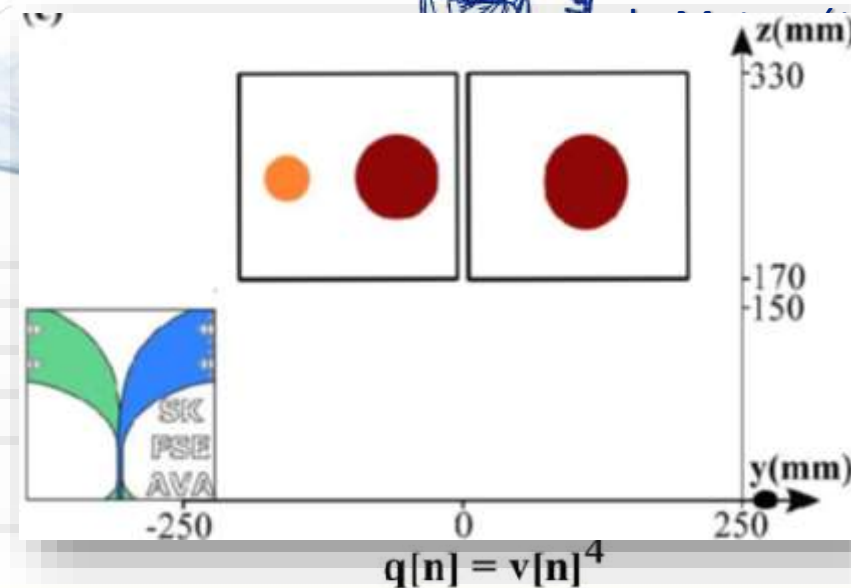


Fig. 10. Flowchart of image processing.





2019-2020



Raimundo Eider

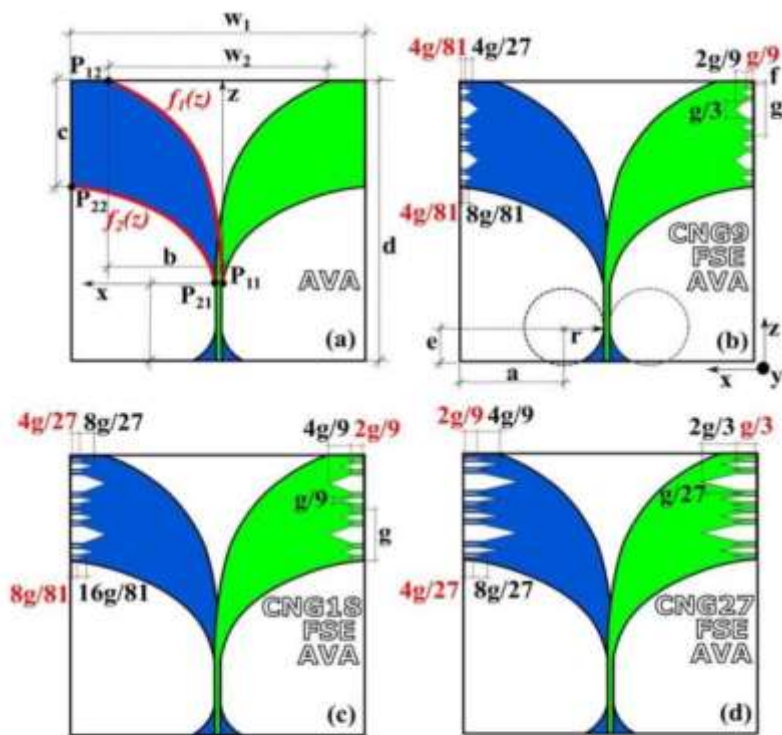


Fig. 1. Parameter and Dimensions: (a) AVA, (b) CNG9-FSE-AVA, (c) CNG18-FSE-AVA, (d) CNG27-FSE-AVA.

Indonesian Journal of Electrical and Electronics Engineering, Volume 03 Nomor 01 Tahun 2020, 25-31

VIVALDI ANTIPODAL ANTENNA WITH HIGH GAIN AND REDUCED SIDE LOBE LEVEL USING SLOT EDGE WITH NEW NEOGOTHIC FRACTAL IMAGES FOR TUMOR DETECTION

Raimundo Eider Figueredo¹, Alexandre M. de Oliveira², Antonio M. de O. Neto³, Alexandre J. R. Serres⁴, Auzuir R. De Alexandria⁵, João F. Justo⁶, Marcelo B. Perotoni⁷, Nurhayati⁸, and Ingrid C. Nogueira⁹

^{1,2,3,4,5,6,7,8,9}Maxwell Laboratory of Microwave and Applied Electromagnetism at the Federal Institute of São Paulo, Brazil
⁴Department of Electrical Engineering and Applied Electromagnetism at the Federal Institute of São Paulo, Brazil
⁵Federal Institute of Ceará, Brazil
⁶Electronic Systems Engineering Department, Polytechnic School of the University of São Paulo, Brazil
⁷Federal University of ABC, Brazil
⁸Department of Electrical Engineering, Universitas Negeri Surabaya in Indonesia
⁹Christus University Center, Brazil

Abstract – This article addresses the study of the Vivaldi Antipodal Antenna (AVA) seeking to improve the gain, decrease the Side Lobe Level (SLL) and the squint, to make the antenna more directive and obtain a more stable radiation pattern. Its intended application lies in the generation of biological microwave imaging to detect brain tumors. With this objective, the Fractal Slot Edge (FSE) technique was applied with a new fractal developed and based on the Cantor set. The application of this fractal, called Cantor Neogothic Fractal (CNG), formed different-sized cavities resulting, in this work, in three antennas that were analyzed through numerical computational simulation together with AVA. The antennas, called CNG9-FSE-AVA, CNG18-FSE-AVA, and CNG27-FSE-AVA, have areas equal to 354.66 mm², 709.33 mm² and 1064 mm², respectively. All antennas achieved the goal, however, CNG27-FSE-AVA presented the best results at 2 GHz, with a gain of 7.84 dBi, SLL -19.80 dB, and squint of -0.10 degree. Additionally, it was proved that the antenna is suitable to generate a near field microwave imaging of tumors in a brain model.

Keywords: Ultrawide band (UWB) system, fractals antennas, slot edge in Antennas Vivaldi.



Tomografia por Micro-ondas
 Imagens através de Micro-ondas de campo próximo

www.LabMax.org



Raimundo Eider

2019-2020

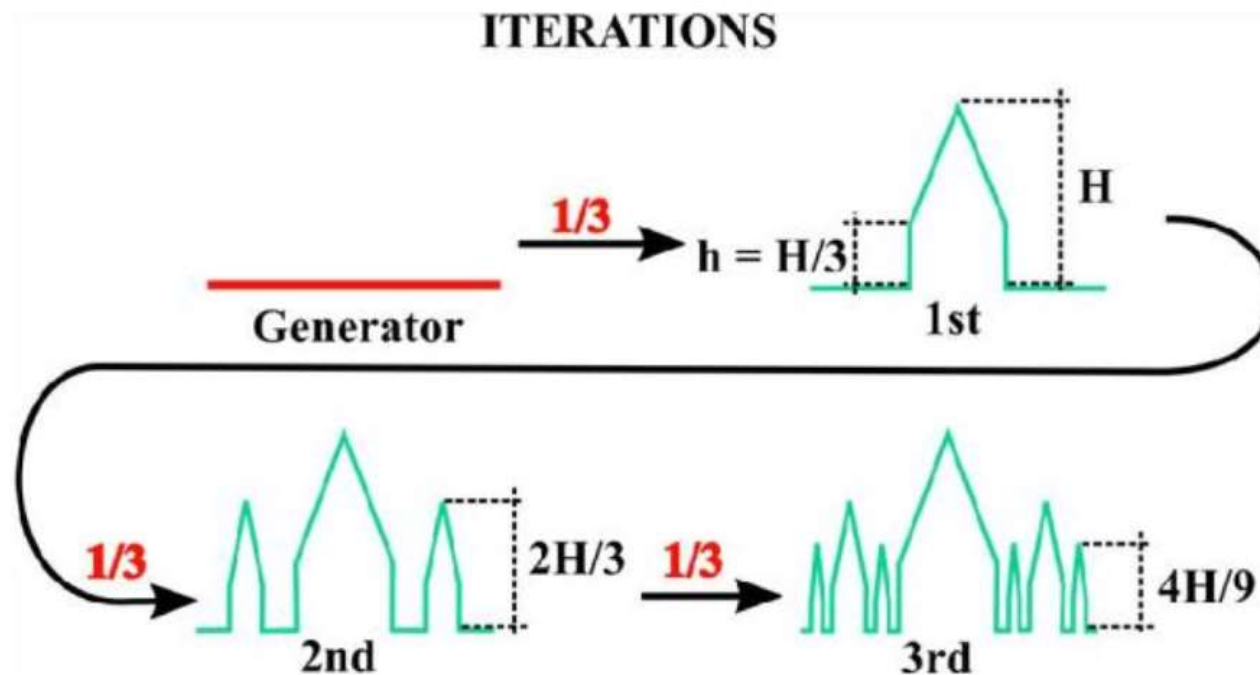


Fig. 2. Iterations new Neo-Gothic Fractal by Cantor.



Tomografia por Micro-ondas

Imagens através de Micro-ondas de campo próximo

www.LabMax.org



Raimundo Eider

2019-2020

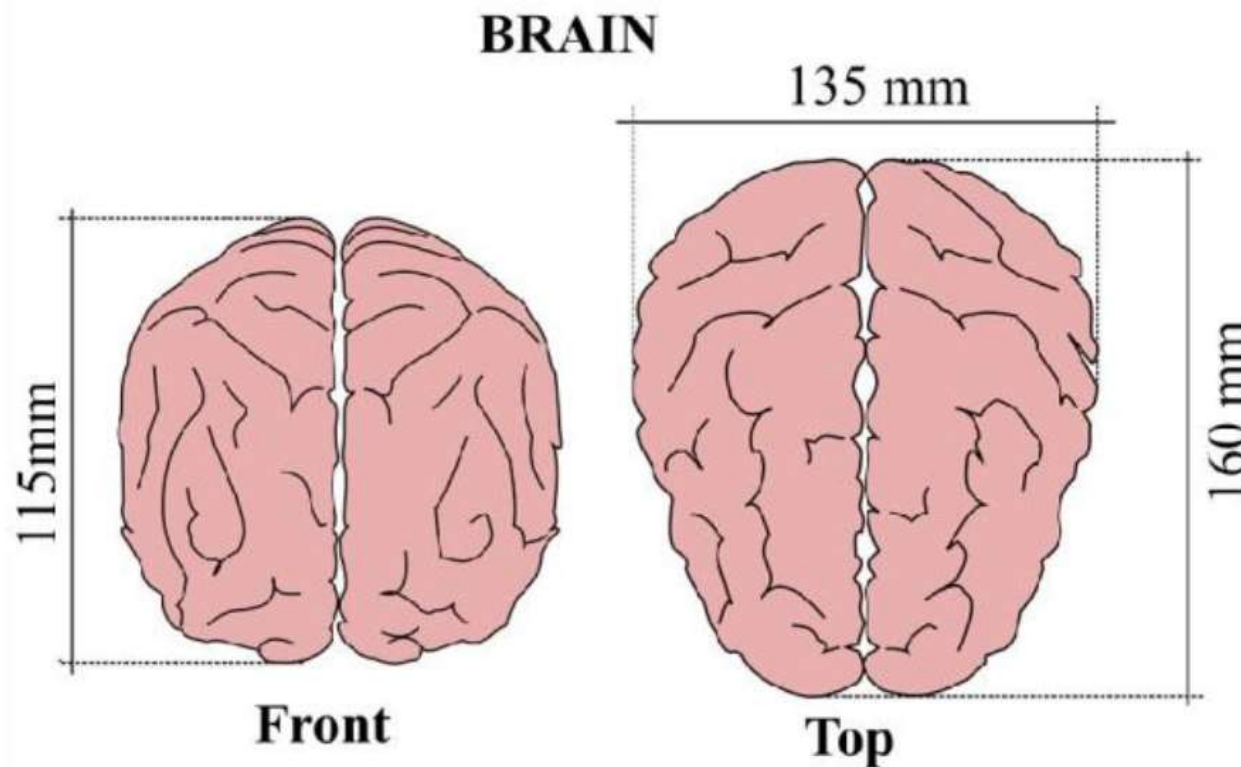


Fig. 7. Dimensions model brain.

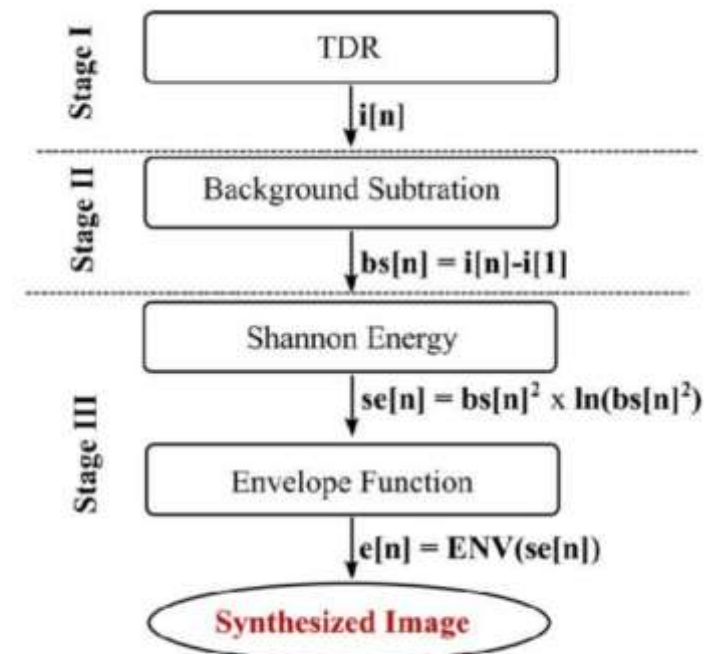


Fig. 8. Image Synthesized Stages.



Tomografia por Micro-ondas

Imagens através de Micro-ondas de campo próximo

www.LabMax.org

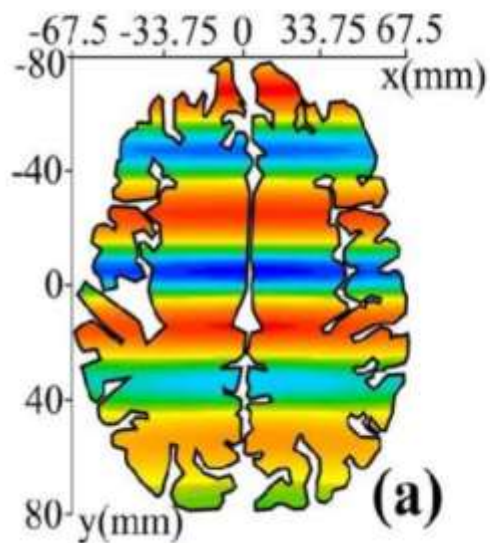


Raimundo Eider

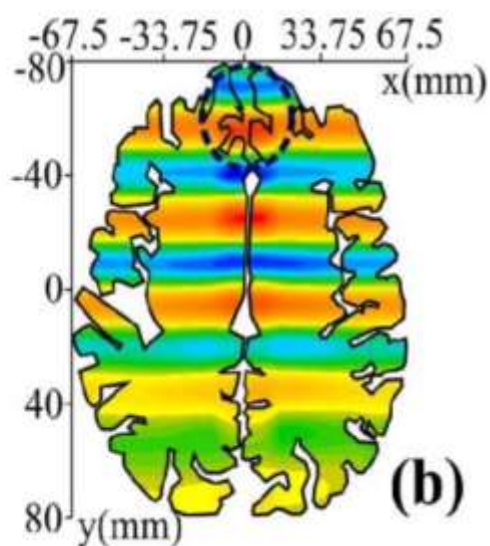
2019-2020



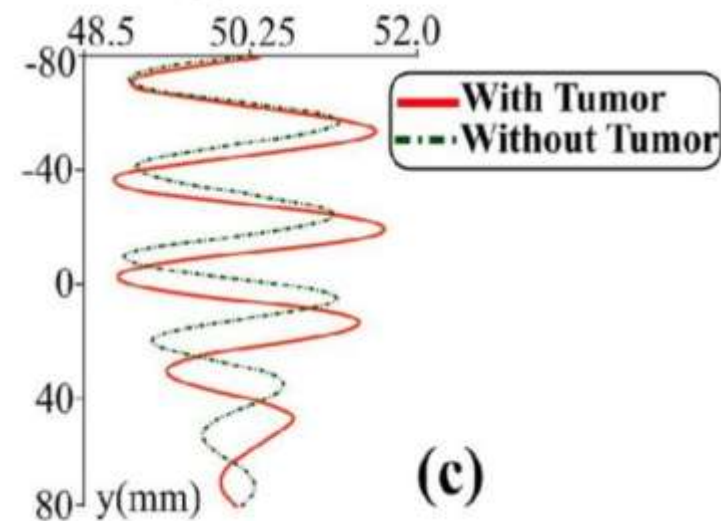
Without Tumor



With Tumor



Signal
 Image TDR





Tomografia por Micro-ondas

Imagens através de Micro-ondas de campo próximo

www.LabMax.org

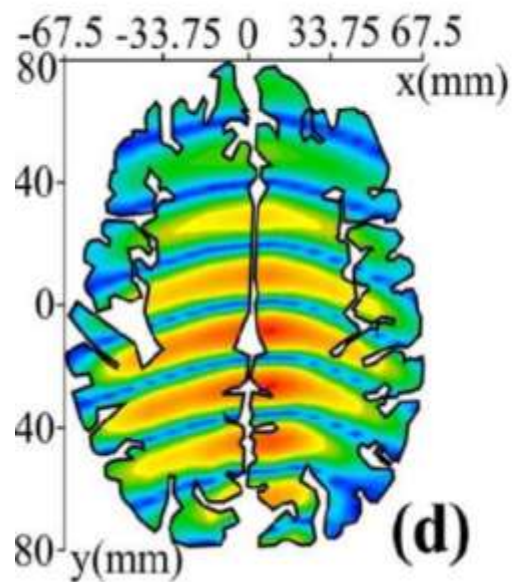


Raimundo Eider

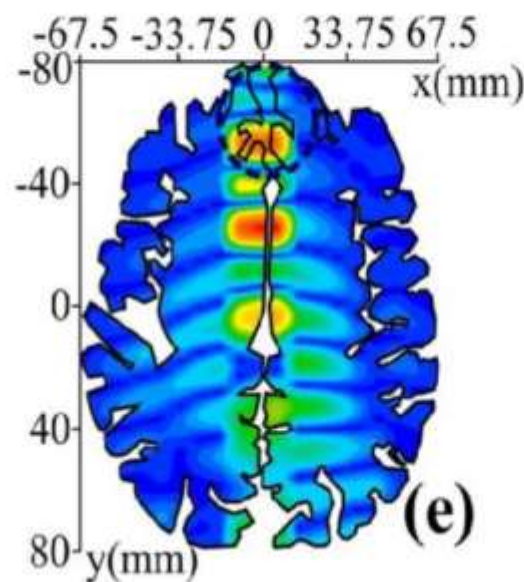
2019-2020



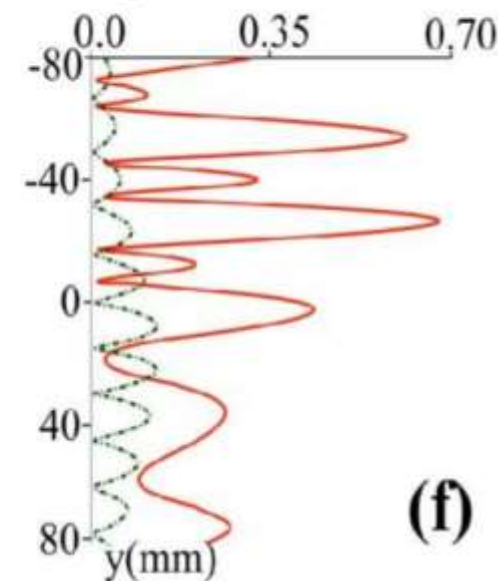
Without Tumor



With Tumor



Signal
 Background Subtration





Fomento a Pesquisa PRP do IFSP via Edital n° 823/2018



Tomografia por Micro-ondas

Imagens através de Micro-ondas de campo próximo

www.LabMax.org

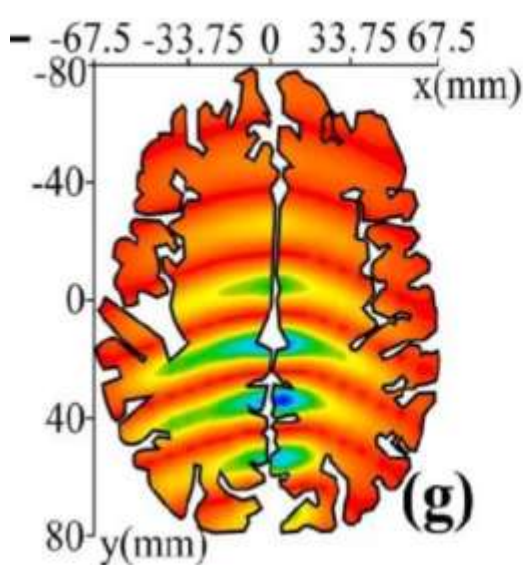


Raimundo Eider

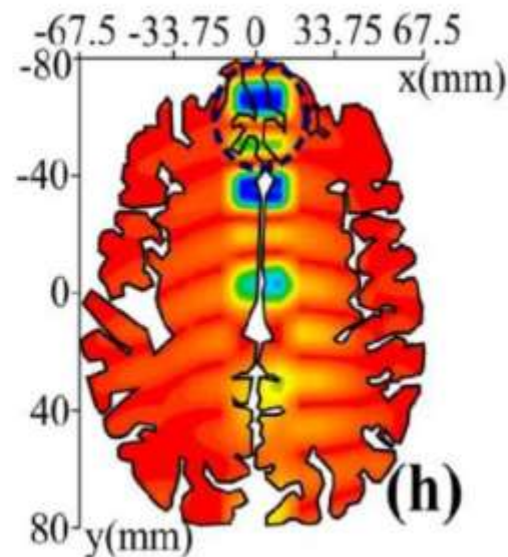
2019-2020



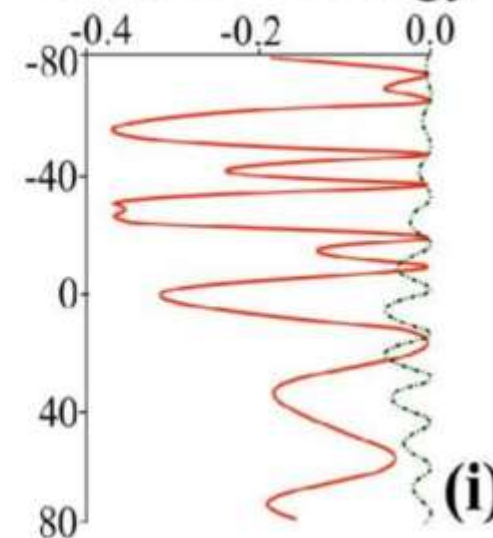
Without Tumor



With Tumor



Signal
 Shannon Energy





Tomografia por Micro-ondas

Imagens através de Micro-ondas de campo próximo

www.LabMax.org

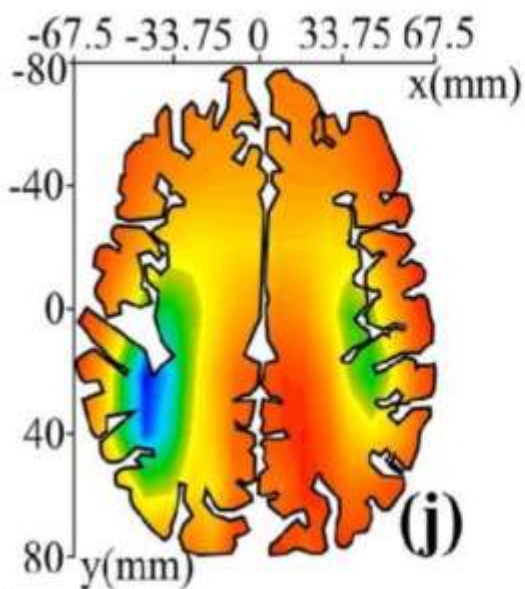


Raimundo Eider

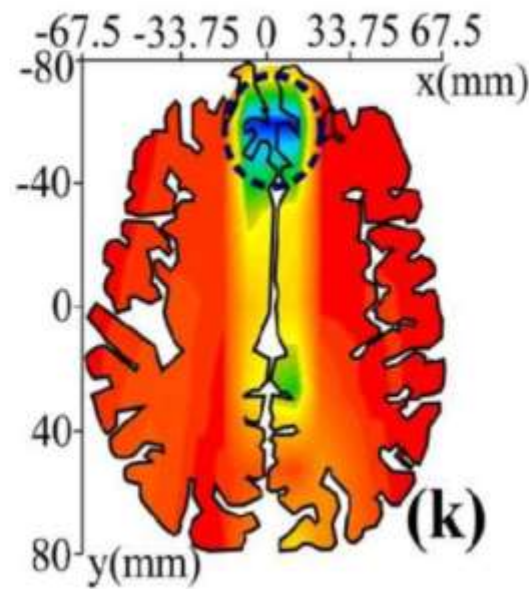
2019-2020



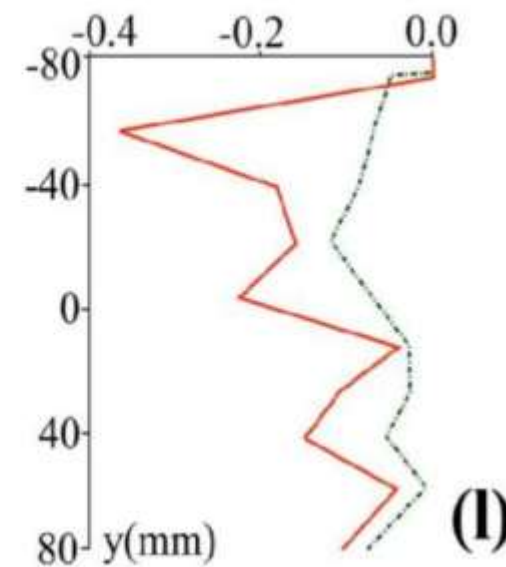
Without Tumor



With Tumor



Signal
Envelope Function





Tomografia por Micro-ondas

Imagens através de Micro-ondas de campo próximo

2018-2021

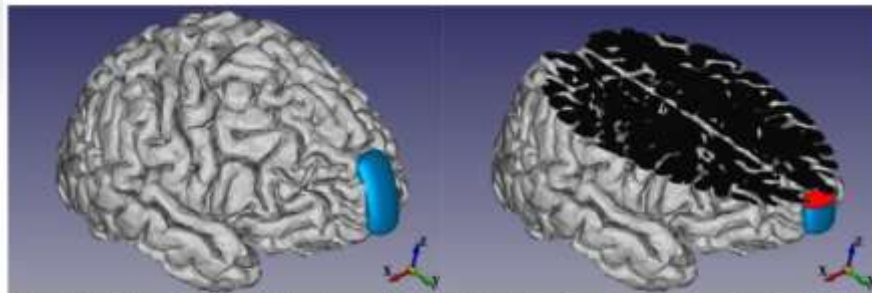


Fig. 10. The 3D digital design of the Infant Brain (gray) was obtained from an MRI and imported into FreeCad 0.16. In detail, the tumor (blue), and the cut of the surface submitted to analysis by microwave image in the proof of concept.

A Fern Antipodal Vivaldi Antenna for Near-Field Microwave Imaging Medical Applications

Alexandre M. de Oliveira, Member, IEEE, Antonio M. de Oliveira, Marcelo B. Perotoni, N. Nurhayati, Member, IEEE, Henri Baudrand, Fellow Member, IEEE, Amaldo de Carvalho Jr., and João F. Justo

Abstract— This investigation presents an oval slot edge (OSE) antipodal Vivaldi antenna (AVA), hereinafter referred to as Fern AVA (FAVA), with an optimized radiation pattern. The use of OSE provided improvements in the antenna characteristics, especially regarding a lower-frequency limit reduction, an increase of the main lobe (ML) gain, and sidelobe level (SLL) reduction. Those contrasting characteristics are simultaneously obtained through the class of the Palm Tree antennas. The proposed FAVA at 1.5 GHz shows an improved gain of 6.66 dB, -12.9 dB of SLL, and 0 degrees of main lobe squint (MLS), in contrast with 4.41 dB of gain, -4.5 dB of SLL, and 4 degrees of MLS in the conventional AVA. For the FAVA, the notches in an elliptical shape, in addition to mitigating the SLL, direct the E-fields distributions towards the main lobe, which categorizes it into the same class as the Palm Tree Vivaldi Antenna. To study the performance of the proposed antenna for medical applications of near-field microwave imaging, a conceptual proof was performed, thus obtaining the microwave image of a Child Head Phantom, homogeneous and semi-realistic, being possible to detect a brain tumor.

Index Terms—ultra-wideband, medical imaging, Directivity Improvement, Palm Tree.

I. INTRODUCTION

The Vivaldi antenna (VA) is an ultra-wideband (UWB) antenna widely used in microwave systems for medical near-field imaging.

board, eliminating the need for connectors and cables [18, 20–22]. However, the Vivaldi antenna has some shortcomings that compromise its classification as a directive device. The regular design, mainly its metal-flat side edges, increases the SLL caused by edge currents, which lessens the antenna directivity. Over the last decade, many antenna designs have been presented, aiming to reduce these influences, through various forms of directors, such as dielectrics, or dielectric lenses (DL), in [4, 15, 23–29], and metamaterials [30, 31] that compromise its main constructive qualities, increasing the final antenna dimensions and making its design more complex.

In order to reduce the SLL of a VA, planar resonant cavities, both in the form of a rectangular slot edge (RSE), and a tapered slot edge (TSE) has been used [3, 5, 9, 10, 12, 13, 23, 25, 26, 28, 29, 32–40] which improved directivity without changing the antenna dimensions, but this technique does not increase the ML gain, and not as efficient to correct the squint in AVA. The slot edge removes side surface currents so that there is an effect in the reduction on the SLL of the VA.

Another very common problem in AVA is the increase in cross-polarization (cross-pol) [41, 42], compared to coplanar VA (CVA) [43–45], and it is intrinsic to its architecture. To reduce this unwanted characteristic, a modification of the conventional AVA in the balanced AVA (BAVA) was proposed by ref. [15], which consists of an AVA composed of layers of substrate, and three or four of copper, which reduces the cross-pol, but not the SLL. Effectively reducing



Instituto Federal de São Paulo
Laboratório Maxwell
 Micro-ondas e Eletromagnetismo Aplicado
 Certificado CNPq nº 5.497.663.866.471.659



LittleMax
 e a luta contra o Câncer
 Cerebral Infantil

Fomento a Pesquisa PRP do
 IFSP via Edital nº. 823/2018



Academia Cearense
 de Matemática - ACM

Tomografia por Micro-ondas

Imagens através de Micro-ondas de campo próximo

LabMat.org

2018-2021

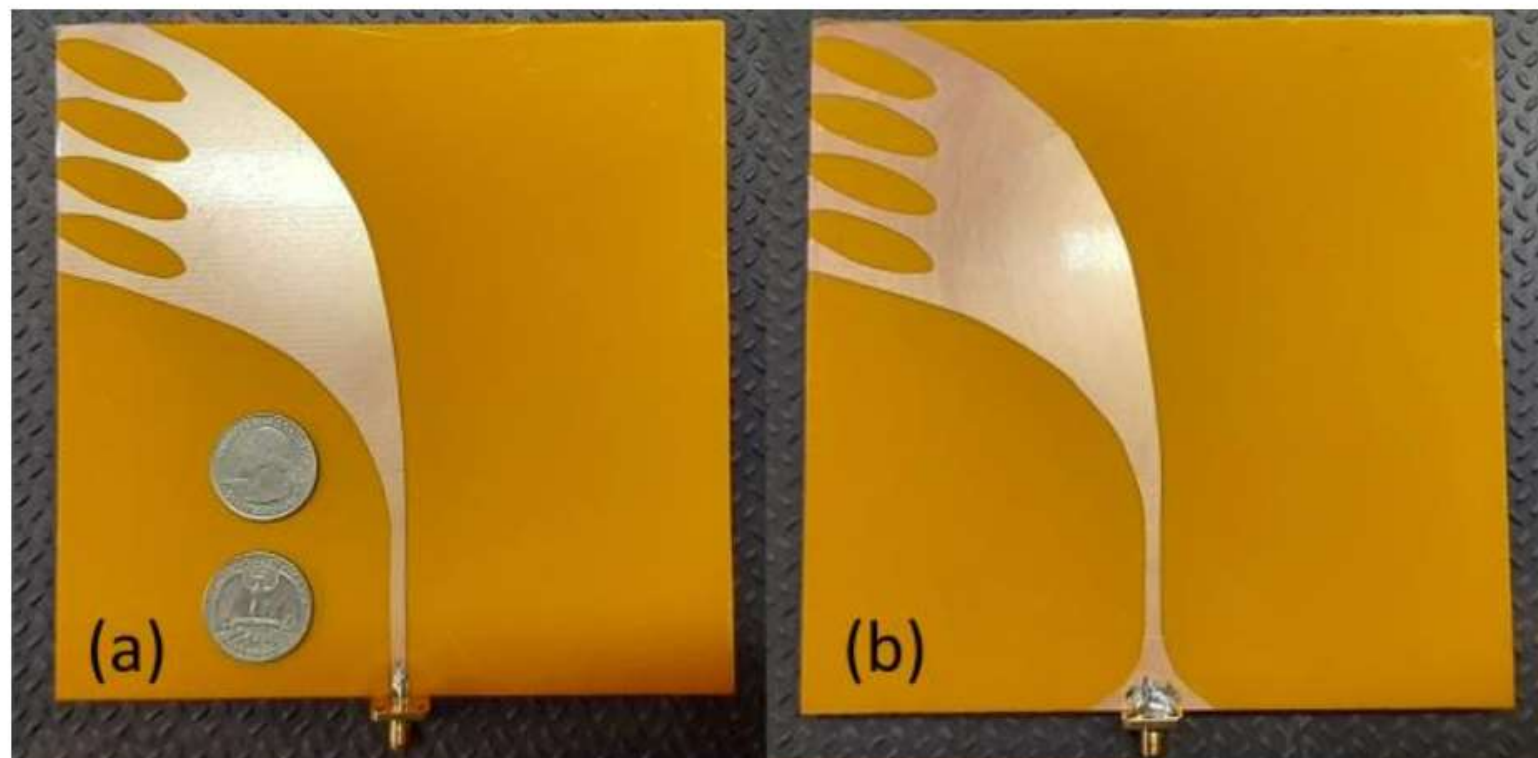
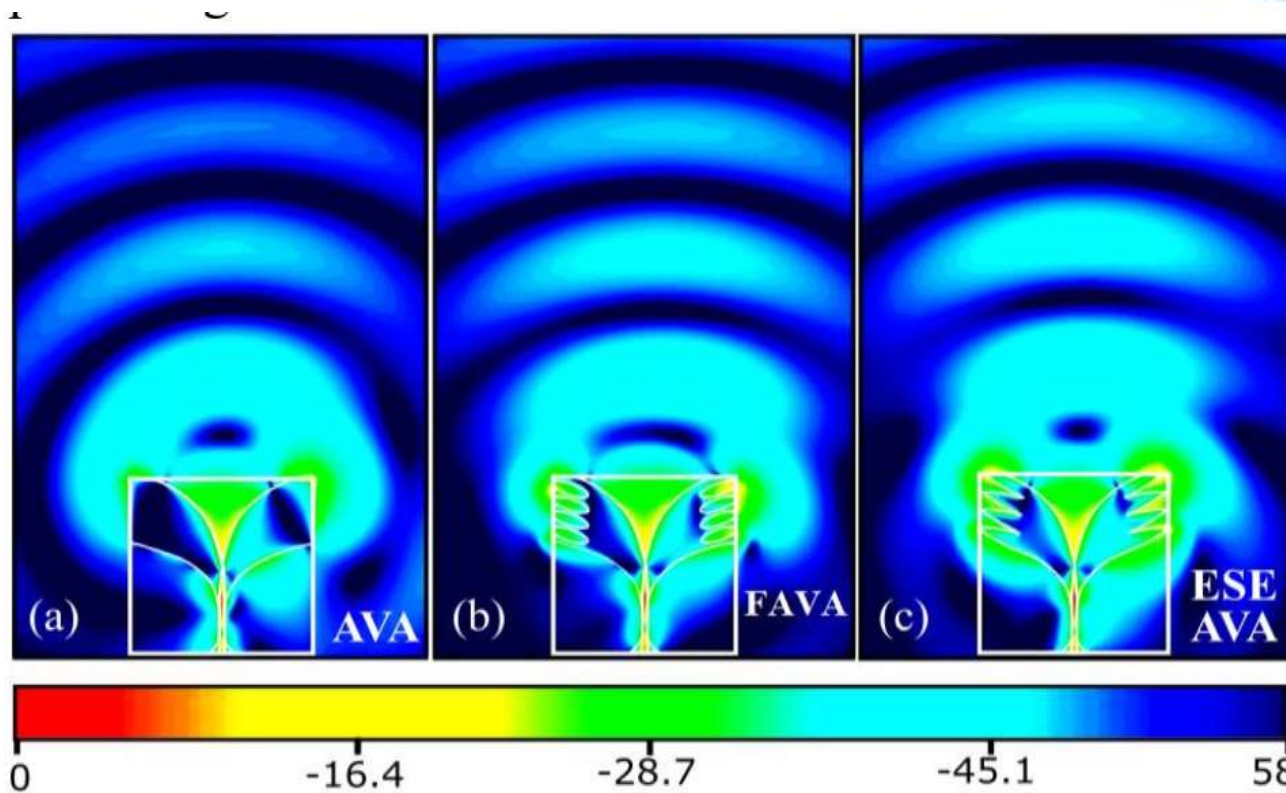


Fig. 2. Fabricated FAVA: (a) top and (b) bottom views.



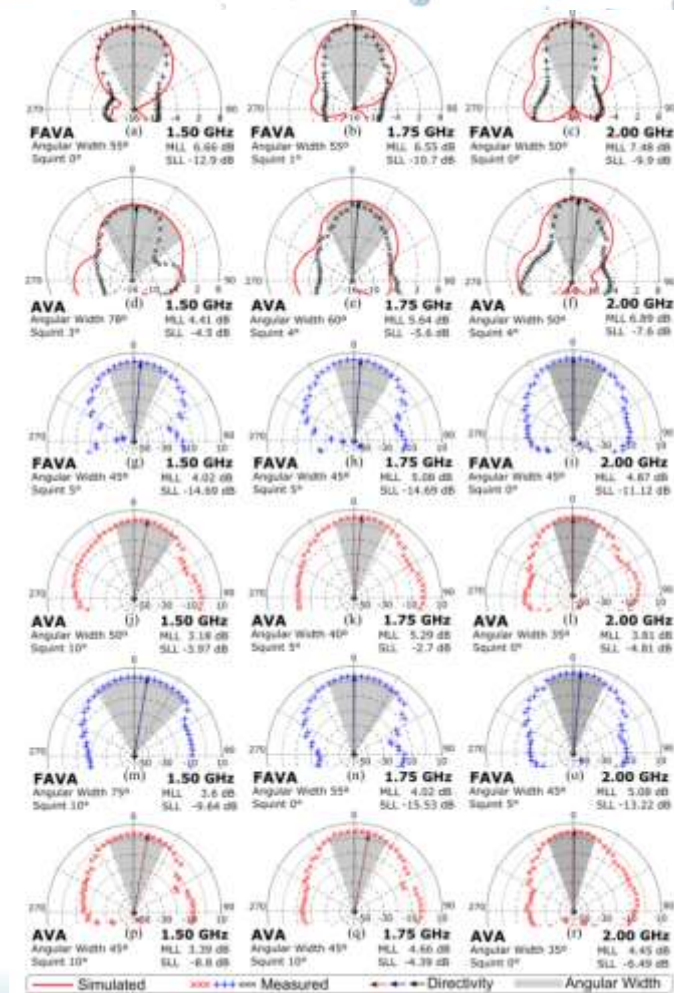
Tomografia por Micro-ondas

Imagens através de Micro-ondas de campo próximo



E-field distribution in dB(V/m)

Fig. 6. E-field distribution in xz -plane at 1.5 GHz for (a) AVA, (b) FAVA, and (c) ESE-AVA at 1.5 GHz.



2018-2021





Tomografia por Micro-ondas

Imagens através de Micro-ondas de campo próximo

www.LabMax.org



Fig. 9. A real-world scenario of the Phantom imaged by the FAVA. (a) Semi realistic and homogeneous infant Phantom. (b) Inside the Head Model, made of Expanded polystyrene (Styrofoam) from Daiso Industries CO., LTD Model YM-18-P6 C028 600 - EPS # 4, Lot # 2009BJ. (c) Infant Brain Model made with a 3D printer technique using conductive filament, composed of ABS and Graphite. (d) The Tumor Model (frontal position) was modeled with a silicone pouch, with walls of 30µm thick, filled with mineral water. (e) Proposed test setup with the Head Phantom on a mobile base controlled by the computer with steps of 1 mm; the FAVA; and the Anritsu Site Master S331B, operating with the DTF function.

2018-2021





Tomografia por Micro-ondas

Imagens através de Micro-ondas de campo próximo

www.LabMax.org

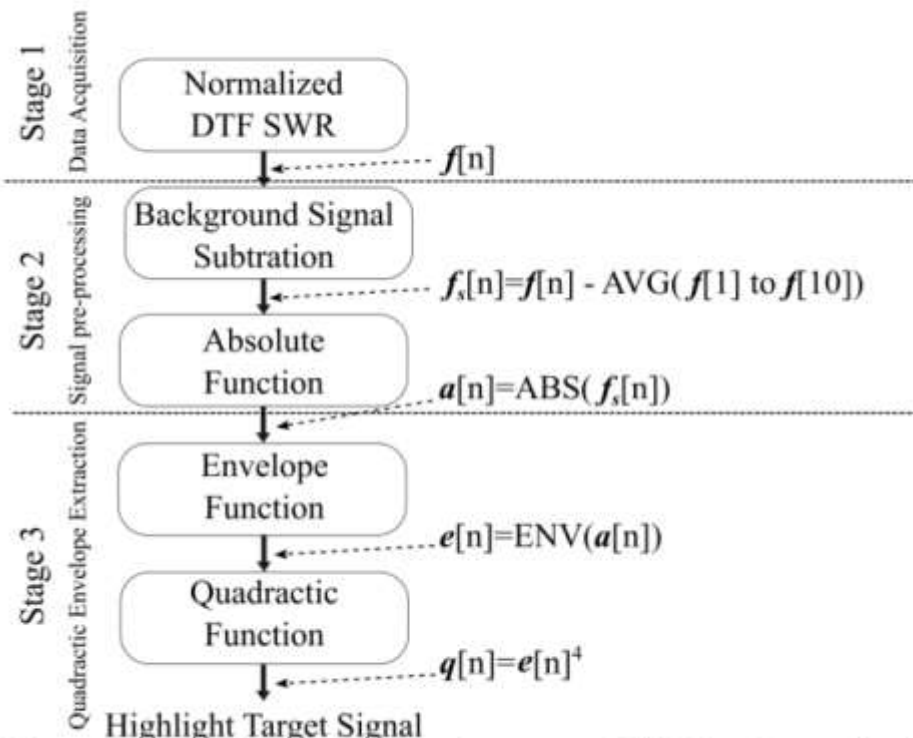
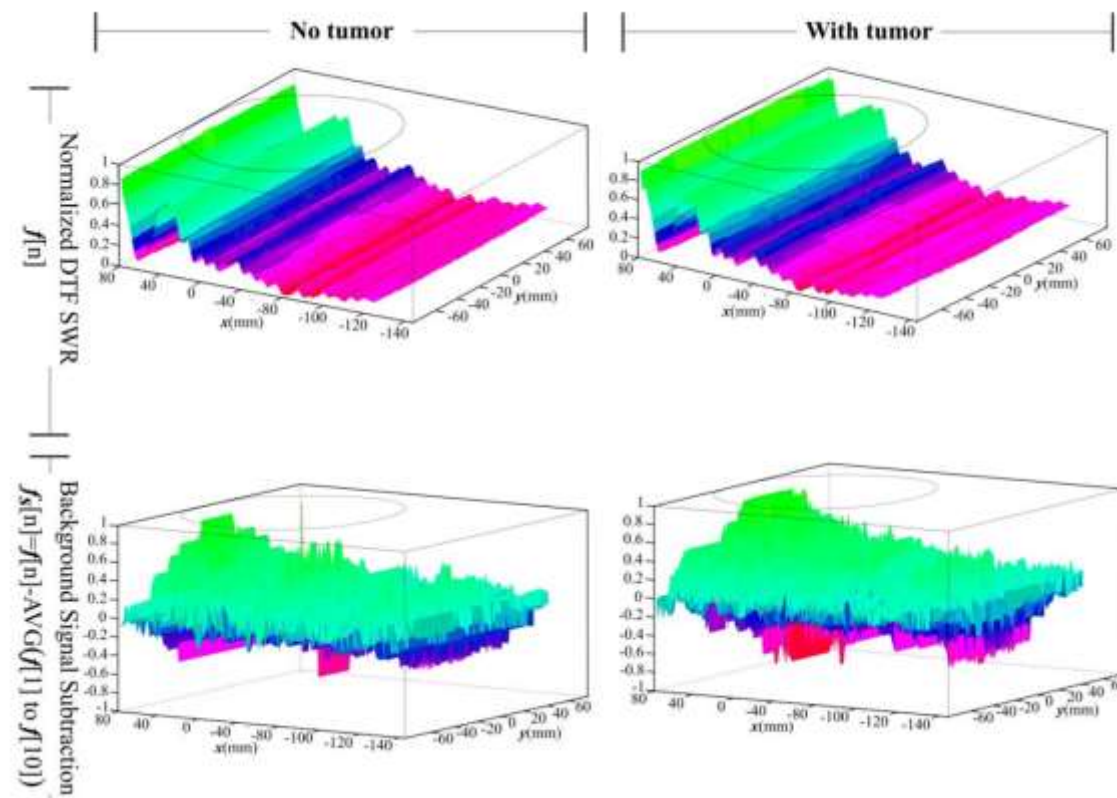


Fig. 11. Block diagram of the three-stage Highlight Target Signal methodology.



2018-2021





Tomografia por Micro-ondas

Imagens através de Micro-ondas de campo próximo

www.LabMax.org

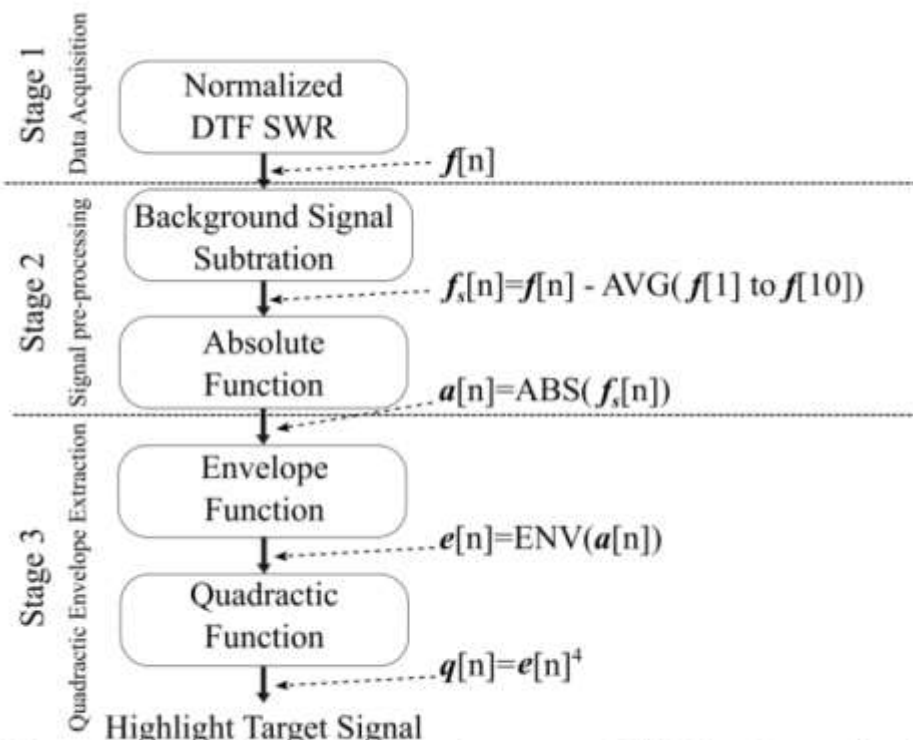
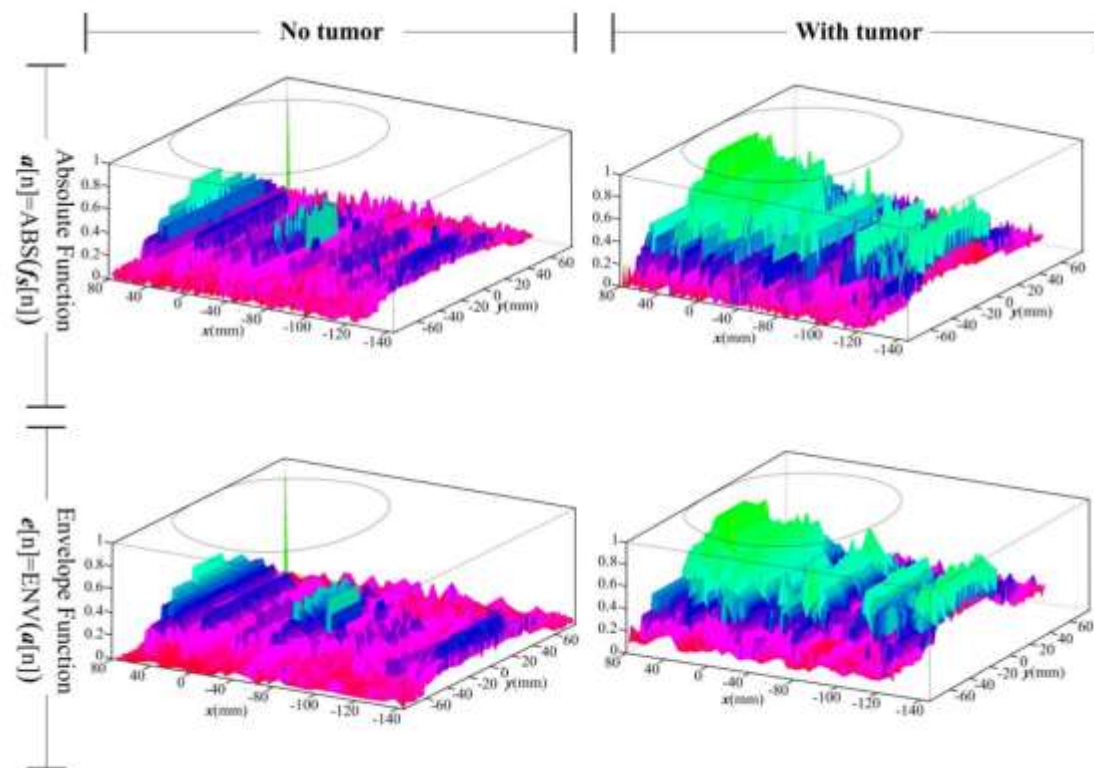


Fig. 11. Block diagram of the three-stage Highlight Target Signal methodology.



2018-2021





Tomografia por Micro-ondas

Imagens através de Micro-ondas de campo próximo

www.LabMax.org

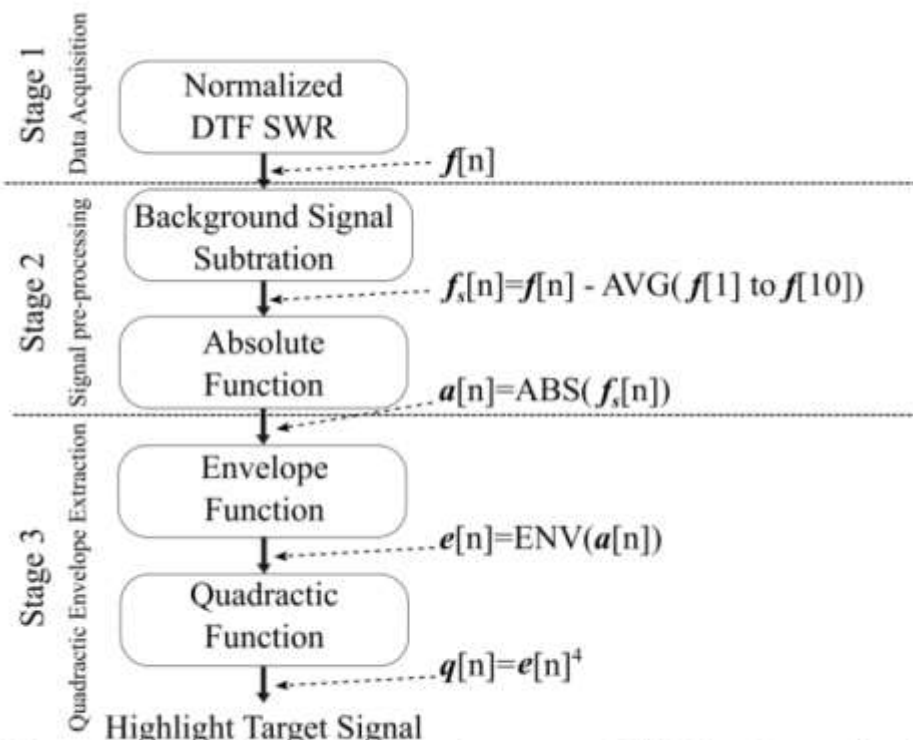
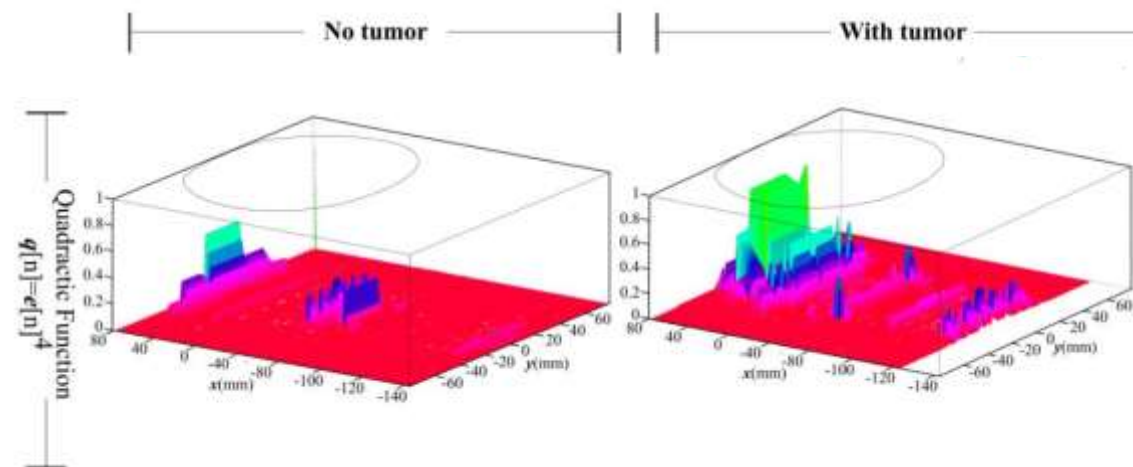


Fig. 11. Block diagram of the three-stage Highlight Target Signal methodology.



2018-2021





Fomento a Pesquisa PRP do
 IFSP via Edital n.º 823/2018

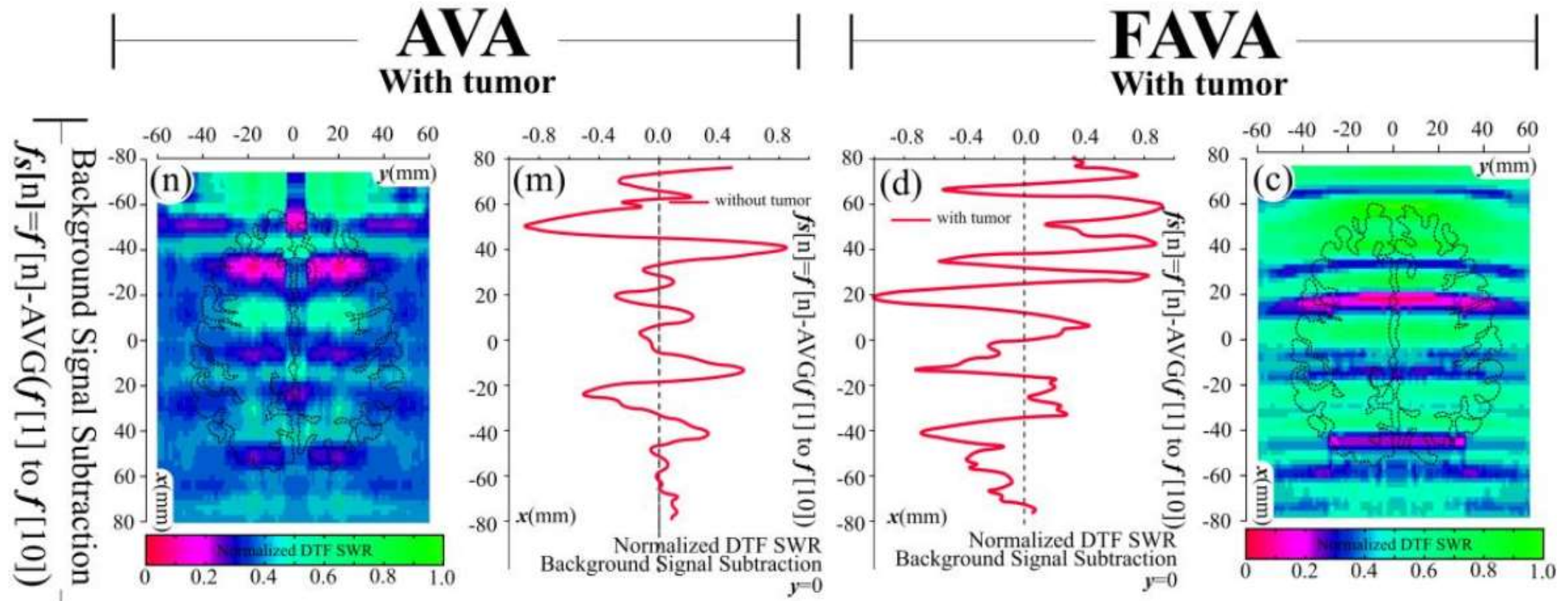


Tomografia por Micro-ondas

Imagens através de Micro-ondas de campo próximo

www.LabMax.org

2018-2021



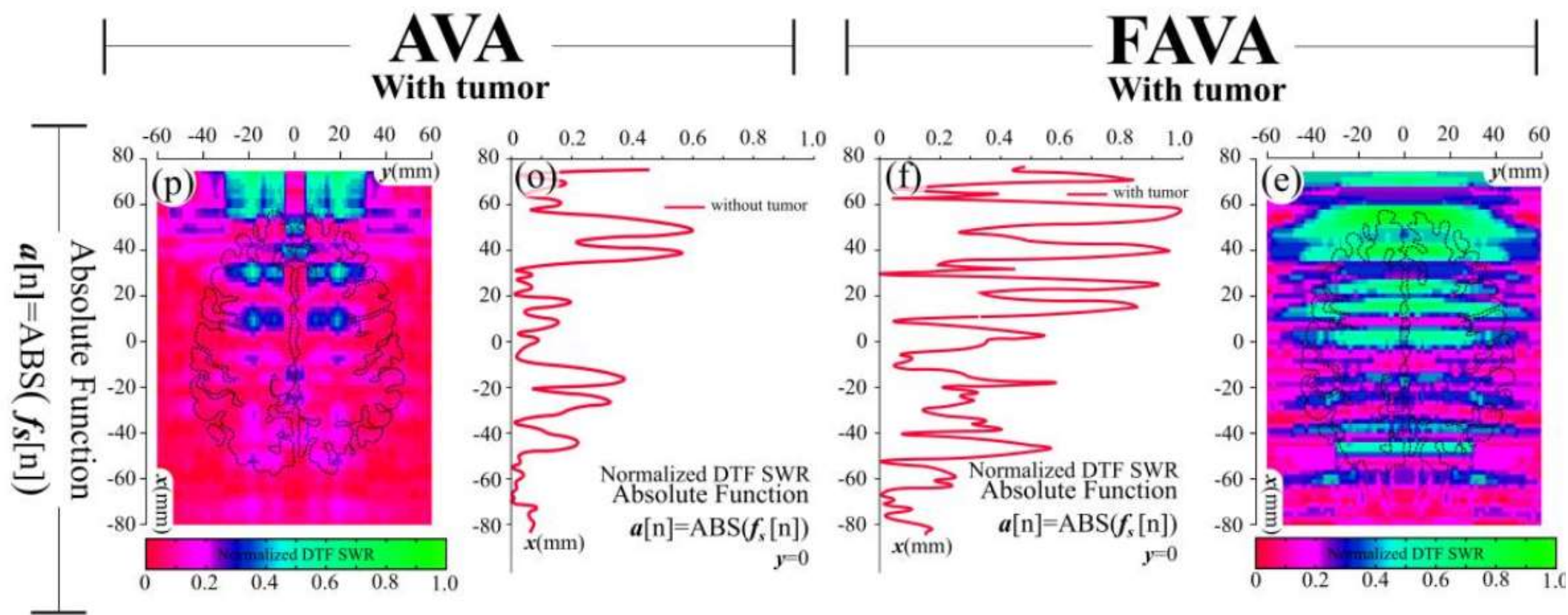


Tomografia por Micro-ondas

Imagens através de Micro-ondas de campo próximo

www.LabMax.org

2018-2021





Fomento a Pesquisa PRP do
 IFSP via Edital n.º 823/2018

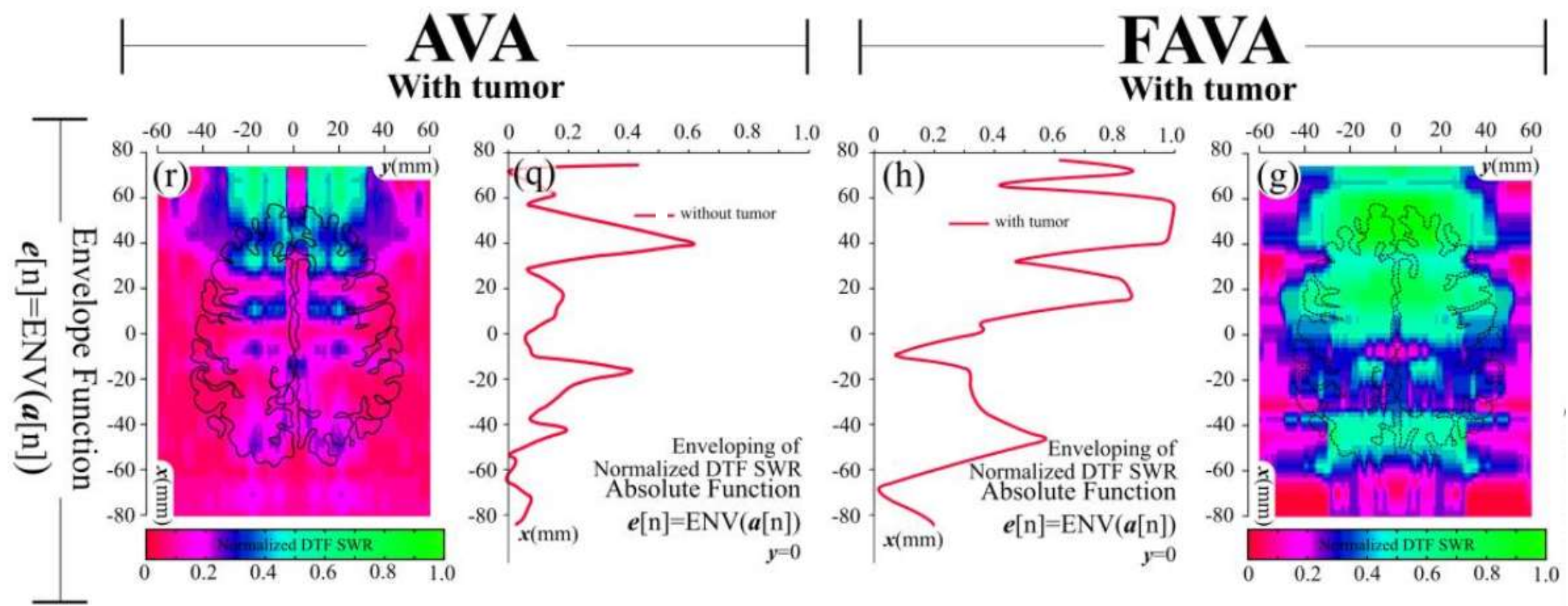


Tomografia por Micro-ondas

Imagens através de Micro-ondas de campo próximo

www.LabMax.org

2018-2021



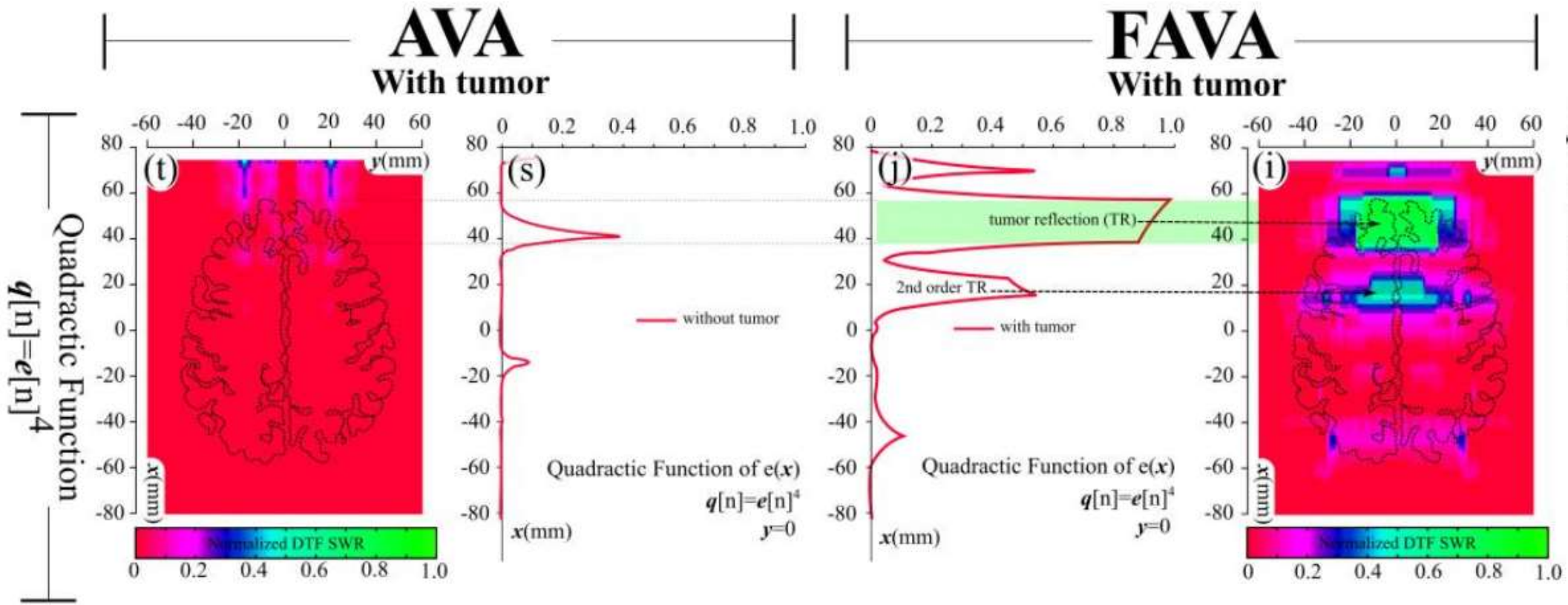


Tomografia por Micro-ondas

Imagens através de Micro-ondas de campo próximo

www.LabMax.org

2018-2021





Tomografia por Micro-ondas

Imagens através de Micro-ondas de campo próximo

www.LabMax.org

2018-2021



Henri Baudrand (SM'90–F'04–LF'14) received the Ph.D. degree in electronics engineering from the National Polytechnic Institute of Toulouse, Toulouse, France, in 1966. He is currently a Professor Emeritus with the National Polytechnic Institute of Toulouse, Toulouse, France. He has authored and co-authored six books. He co-signed more than 110 publications in journals, 4 book chapters, and 250 conference papers.

His research interests include electromagnetic theory, microwaves, antennas, and numerical methods.





Instituto Federal de São Paulo
Laboratório Maxwell
Micro-ondas e Eletromagnetismo Aplicado
Certificado CNPq nº 5.497.663.866.471.659



LittleMax
e a luta contra o Câncer
Cerebral Infantil

Fomento a Pesquisa PRP do
IFSP via Edital nº. 823/2018



Academia Cearense
de Matemática - ACM

Tomografia por Micro-ondas

Imagens através de Micro-ondas de campo próximo

www.LabMax.org



Dr. Alexandre Maniçoba de Oliveira

Pesquisador Sênior e líder do grupo Laboratório Maxwell do Instituto Federal de São Paulo, Campus Cubatão, Rua Maria Cristina, 50 – Jardim Casqueiro – Cubatão – São Paulo – Cep: 11533-160.

Telefone: 13 3346-5300 / Celular: 13 98822-2124.

email: amanicoba@ifsp.edu.br

Site: <https://labmax.org/index.php/pessoas/dralexandre/>